J. Appl. Comput. Mech., 9(1) (2023) 129-167
DOI: 10.22055/jacm.2022.40537.3605

ISSN: 2383-4536
jacm.scu.ac.ir

Shahid Chamran University of Ahvaz

Journal of Applied and Computational Mechanics

Research Paper

Multibody Modeling and Nonlinear Control of a Pantograph Scissor Lift Mechanism

Carmine Maria Pappalardo[1], Rosario La Regina[2], Domenico Guida[3]

[1]Department of Industrial Engineering, University of Salerno, Via Giovanni Paolo II, 132, Fisciano, 84084, Salerno, Italy, Email: cpappalardo@unisa.it

[2]Spin-Off MEID4 s.r.l., University of Salerno, Via Giovanni Paolo II, 132, Fisciano, 84084, Salerno, Italy, Email: r.laregina2@studenti.unisa.it

[3]Department of Industrial Engineering, University of Salerno, Via Giovanni Paolo II, 132, Fisciano, 84084, Salerno, Italy, Email: guida@unisa.it

Received April 13 2022; Revised July 11 2022; Accepted for publication July 12 2022.
Corresponding author: Carmine Maria Pappalardo (cpappalardo@unisa.it)
© 2022 Published by Shahid Chamran University of Ahvaz

Abstract. In this paper, a new strategy for developing effective control policies suitable for guiding the motion of articulated mechanical systems that are described within the framework of multibody system dynamics is proposed. In particular, a scissor lift table having a pantograph topology is analytically modeled as a rigid multibody system by using a Lagrangian formulation. An operational approach is thus introduced in this investigation to design the control system that commands the motion of the lift table. In this vein, two dynamical models are developed in this investigation, namely a minimal coordinate multibody model and a redundant coordinate multibody model. While the minimal coordinate multibody model is used in the paper for the proper design of a high-performing nonlinear controller, the redundant coordinate multibody model is employed to verify both the efficiency and the effectiveness of the control approach adopted in this work, as well as for the refinement of the feedback controller parameters. More specifically, the nonlinear control system devised in this paper is based on the combination of an open-loop control architecture with a closed-loop control strategy. The open-loop control policy is determined by using a nonlinear quasi-static feedforward controller, whereas the closed-loop control action is obtained considering an error-based proportional-derivative feedback controller. With the use of the analytical models of the pantograph scissor lift system developed in this work, several numerical experiments were carried out by employing three multibody programs based on the computational environments relying on MATLAB and SIMSCAPE MULTIBODY, thereby demonstrating the readiness and the effectiveness of the control methodology proposed in this investigation.

Keywords: Multibody System Modeling, Computational Kinematics, Statics, and Dynamics, Nonlinear Regulation and Tracking Control, Quasi-Static Feedforward Controller, Error-Based Proportional-Derivative Feedback Controller, Pantograph Scissor Lift Mechanism.

1. Introduction

1.1 Background information and significance of this research work

This paper deals with the kinematic, static, and dynamic analysis of articulated mechanical systems that can be appropriately modeled within the framework of multibody mechanical systems [1, 2]. From a general perspective, the term multibody system broadly refers to a mechanical system consisting of a set of mechanical components, or simply bodies, connected together by kinematic joints, or simply constraints, in such a way as to have relative motion [3,4]. Thus, a large variety of machines and mechanisms can be modeled under the umbrella of multibody mechanical systems [5–7]. The mass elements of a multibody system can be either rigid or flexible [8,9], while the mechanical devices realizing the geometric connections between them are formed by kinematic pairs which can be perfectly smooth or subjected to contact and friction forces [10–12]. In particular, the mechanical joints composed by the kinematic pairs are specifically designed to allow the relative motion between two elements in certain directions and prevent it in others [13, 14]. In addition to the rigid or flexible bodies and to the kinematic joints that may have clearance and friction, the fundamental items that form a general multibody system are the force elements, the force fields, the time-dependent forcing actions, and the time-dependent imposed motions [15, 16]. In multibody system dynamics, a force element is represented by a relative mechanical action, such as a linear or nonlinear spring-damper force pair, or a linear or nonlinear spring-damper torque pair, applied between two points in the case of a translational force element, or along an axis in the case of a rotational force element [17, 18]. Force elements are, therefore, frequently used to model the typical mechanical components found in industrial structures, aerospace systems, ground vehicles, and railway systems [19,20]. A force field, on the other hand, is used for modeling a distributed field of external forces and/or mechanical moments, such as the gravity force or the effect of the magnetic field, that affect some or all the components of the multibody system [21,22]. The use of force fields is common in modeling several mechanical systems like robots, space structures, aerial vehicles, and biomechanical systems [23–25]. Furthermore, the time-dependent forcing actions can be externally applied forces, mechanical moments, or torques, which are generally associated with the control actions exerted on the mechanical system of interest designed for its proper functioning [26, 27]. Finally, in a multibody model of an articulated mechanical system, the time-dependent imposed motions are often used to simplify the mathematical description of the movement

of some system components that operate in a prescribed transient or stationary regime [28, 29].

Multibody mechanical systems can be modeled by using an analytical formulation and a computational framework that can be developed into a two-dimensional space or into a three-dimensional space [30]. In the former case, the mechanical components are only endowed with a planar motion, whereas, in the latter case, the bodies that form the multibody system perform spatial translations in arbitrary directions and large finite rotations about non-complanar axes [31]. More importantly, as already discussed above, multibody systems are typically formed by mechanical components that can be rigid and/or deformable [32]. Therefore, in the analytical framework and in the computational formulation of the mechanics of multibody systems, it is important to distinguish between the dynamics of rigid multibody systems and the dynamics of flexible multibody systems, since the modeling approaches employed in these two contexts are fundamentally different [33]. The principal methodologies used for modeling rigid multibody mechanical systems are the Reference Point Coordinate Formulation with Euler Angles (RPCF-EA) [34], the Reference Point Coordinate Formulation with Euler Parameters (RPCF-EP) [35], the Natural Coordinate Formulation (NCF) [36], and the Natural Absolute Coordinate Formulation (NACF) [37]. On the other hand, the principal methodologies employed for modeling flexible multibody mechanical systems are the conventional Finite Element Method (FEM) [38], the Nonlinear Finite Element Method (NLFEM) [39], the Floating Frame of Reference Formulation (FFRF) [40], the Absolute Nodal Coordinate Formulation (ANCF) [41], the Rational Absolute Nodal Coordinate Formulation (RANCF) [42], the Consistent Rotation-Based Formulation (CRBF) [43], the Isogeometric Analysis Method (IGAM) [44], the Geometrically Exact Method (GEM) [45], the Incremental Finite Element Method (IFEM) [46], and the Large Rotation Vector Formulation (LRVF) [47]. The case study analyzed in this paper can be properly described as a rigid multibody system. Therefore, the fundamental strategies for modeling rigid multibody systems are briefly recalled and discussed below.

In the reference point coordinate formulation, a geometric point is chosen in a space attached to a given rigid body, and the Cartesian coordinates of this point, which should not necessarily be a material point, are selected as the translational coordinates [48]. On the other hand, the rotational coordinates employed for describing the orientation of a body-fixed reference frame having its origin coincident with the reference point make the difference between the RPCF-EA and the RPCF-EP [49–51]. As the acronyms suggest, the RPCF-EA utilizes the minimal set of the proper Euler angles, or equivalently the Tait-Bryan angles, to represent the spatial orientation of each rigid body, whereas the RPCF-EP employs a redundant set of orientation variables, indeed called Euler parameters, that can be mathematically interpreted as the components of a unit quaternion [52, 53]. Both the RPCF-EA and the RPCF-EP allow for systematically formulating the equations of motion in a differential-algebraic form. In the resulting equations of motion, the differential part inherently concerns the system dynamics, arising from the basic principle of classical mechanics, while the algebraic part is indispensable for the physical modeling of the constraint equations, and indeed is mathematically generated by the use of Lagrange multipliers [54]. In the analytical formulation of the equations of motion in both two-dimensional and three-dimensional spaces, the system mass matrix depends on the general configuration of the multibody system and, in addition to the introduction of the vector of Lagrange multipliers, necessary for describing the constraint generalized force vector, a highly nonlinear vector of inertial quadratic velocity forces is also present in the dynamical model for describing the generalized centrifugal and Coriolis forces [55]. Moreover, it is well-known that every set of three rotational coordinates suffers from the kinematic singularity problem and, therefore, this issue is encountered in the RPCF-EA as well [56]. To solve this issue, particular care should be paid in the computer implementation of the RPCF-EA, since a method for reparameterizing the set of Euler angles during the dynamical simulations should be included for avoiding the singularity points [57]. The RPCF-EP, on the other hand, solves this issue from the outset by using a redundant set of orientation variables that requires an additional set of algebraic constraints called the Euler parameters normalization conditions [58]. This is the main reason why the source code of professional multibody computer software is often based on the use of the RPCF-EP.

Conversely, the NCF is a revolutionary formulation approach in which the choice of the generalized coordinates to be used for modeling the kinematics of a given multibody system is made case by case by following a set of simple rules and reasonable guidelines that facilitate the model construction [36]. To this end, the specific position vectors of the material points and the direction vectors associated with the mechanical joints involved in the kinematic pairs, placed between two rigid bodies, are frequently used as the generalized coordinates, thereby made of Cartesian coordinates in conjunction with direction coordinates, which are necessary for describing the general roto-translational motion of the system components [59]. Unlike the RPCF-EA and the RPCF-EP, the main advantage of the NCF is the formulation of a mechanical model having a constant mass matrix and a zero inertial quadratic velocity vector in which the generalized centrifugal and Coriolis forces disappear [60, 61]. However, its principal drawback is that the criteria for the model construction are hardly generalizable and, therefore, cannot be systematically implemented in a general-purpose multibody code that should be able to handle a wide range of different articulated mechanical systems [62]. The fundamental drawback found in the NCF is completely overcome in the NACF, which represents a modern formulation approach conceived to combine the best advantages of both the RPCF-EP and the NCF [63]. In the NACF, similarly to the RPCF-EP, the Cartesian coordinates of a generic material point belonging to each rigid body are used as the body translational coordinates [64]. Also, to avoid any kinematic singularity problem and to promptly describe the spatial orientation of each body-fixed reference frame, the set of three unit vectors formed by the direction cosines, corresponding to the body frame of reference, is employed as the set of rotational coordinates for univocally identifying the body orientation [65]. Consequently, the NACF inherits the advantages of both the RPCF-EP and the NCF in the sense that this multibody formulation enables the systematic development of the differential-algebraic equations of motion of any complex multibody mechanical system featuring a constant mass matrix and a null vector representing the generalized inertia quadratic velocity forces [66]. As thoroughly discussed in the literature, the drawback associated with the computer implementation of the NACF is the increase of the number of the system generalized coordinates and algebraic constraint equations to be used for its mathematical modeling [67]. Nevertheless, from a computational viewpoint, this drawback does not represent a serious issue since the reduced time expended for the functions calling counterbalances the increase in the model dimensions and leads to fast dynamical simulations [68].

1.2 Formulation of the problem of interest for this study

The control problem formulated in the case of multibody mechanical systems poses several challenges [69]. This is mainly due to the complexity of the mathematical models that serve to describe the dynamic behavior of articulated mechanical systems, which are characterized by highly nonlinear sets of differential-algebraic equations of motion [70]. In general, the nonlinearities of a dynamical system can be broadly subdivided into two groups, namely inherent nonlinearities and intentional nonlinearities [71]. The former class of nonlinearities, also called natural nonlinearities, includes those arising from the regular behavior of the normal components that form the system when modeled without using any simplifying assumptions [72]. The latter class of nonlinearities, on the other hand, are typically referred to as artificial nonlinearities since they are strictly related to the dynamical behavior of the control actuators introduced into the mechanical system by the designer or the control engineer [73]. Some typical examples of inherent nonlinearities found in a general mechanical system are the contact and friction forces, the hysteresis phenomenon, the presence of backlash between the gears of a mechanism, the mechanical actions produced by spring-damper force elements, the resistance torque opposing the shaft rotary motion of rotative machines, and the centrifugal and Coriolis generalized inertia forces generated by the rotational motion that are quadratic with the system generalized velocities [74]. Conversely, common examples

of intentional nonlinearities that can be introduced in a general mechanical system are the active and passive forms of control architectures, which are purposely designed and implemented to exhibit a nonlinear behavior by following prescribed control laws [75]. Moreover, one of the distinguishing features of a multibody mechanical system, which makes their analysis and control more difficult, is the presence of geometric nonlinearities associated with the algebraic equations employed for modeling the kinematic constraints [76,77]. Also, in the case of flexible multibody systems, the presence of considerable displacements, finite rotations, and small/large deformations represents additional sources of geometric nonlinearities to be taken into account in the formulation of a general control problem [78,79]. These kinds of nonlinearities, which can be classified as inherent or natural nonlinearities, are found in addition to those that could be already present in a given mechanical system [80]. Therefore, the presence of hard nonlinearities is the main reason behind the challenging development of a proper nonlinear controller suitable for multibody mechanical systems [81]. Fully addressing and solving this important issue needs advanced methods and nonconventional control strategies applicable to the large family of articulated mechanical systems [82].

As discussed above, the presence of high nonlinearities in the mechanical model of a general multibody system enhances the difficulty of the control problem associated with them [83]. As a result, more complex control strategies are necessary to obtain robust, effective, and efficient control actions adequate for this class of articulated mechanical systems [84]. This is mainly due to the fact that the simple control methods based on the linearization approach, utilized tout court and merely applied to the equations of motion, lead to poor performance of the control system or are entirely not applicable as such [85]. However, some effective control methods that can be adjusted and adapted for the guidance of the dynamic behavior of multibody mechanical systems are available in the literature [86]. For instance, the fundamental equations of constrained motion, based on the new approach to the analytical mechanics originally proposed by Udwadia and Kalaba, define a powerful analytical method capable of computing the generalized acceleration vector and the generalized constraint forces of a given multibody system subjected to both holonomic and nonholonomic constraints [87,88]. In the context of inverse dynamics, the Udwadia-Kalaba equations can be seen as a control design method in which the control requirements are formulated in terms of algebraic constraint equations and, as such, the corresponding generalized control forces are obtained [89,90]. Another general and effective control method that is important to mention, since it has recently found a growing interest in the multibody community, is the adjoint method [91,92]. The adjoint method represents a wide computational framework, rather than a single methodology, in which the regulation and tracking control problems formulated for multibody systems described by differential-algebraic equations of dynamics can be numerically solved by using an iterative optimization procedure necessary to solve the corresponding nonlinear two-point boundary-value problems [93,94]. By doing so, one can effectively determine open-loop and closed-loop control actions that optimally solve the control problem of interest [95]. The single algorithms involved in the elementary building blocks that form the flowchart of the adjoint method are quite complex, but their degree of complexity can be exploited for tuning and calibrating the entire procedure that leads to the determination of the final control actions in a wide range of cases of engineering interest [96,97]. An alternative approach, which is applicable to a vast class of dynamical systems in general, originates from the computational methods of machine learning [98,99]. In this vein, the complex models of an articulated mechanical system can be substituted by a simplified version constructed by using data-driven methods and the tools of neural networks [100]. Similarly, the structure of the controller is designed by defining another neural network representing its behavior [101, 102]. Then, by using the strategy that characterizes the reinforcement learning approach, the system simplified model is used to make predictions on its actual dynamical behavior, while the elements that define the neural network describing controller are iteratively updated in order to learn how to control the system by maximizing a given cumulative reward [103, 104]. To conclude, while the Udwadia-Kalaba equations represent an extension to the domain of nonlinear control of the analytical techniques of classical mechanics, the adjoint method and the reinforcement learning method can be conceptually collocated into two opposite extremes, in which the former represents a fully model-based approach, whereas the latter can be seen as a completely black-box approach with respect to the model of the system to be controlled.

1.3 Literature review

The pantograph lifting mechanism is a device formed by a platform adjustable in height and a symmetric set of crossbars constrained on its frame. The purpose of the bars is to convert a horizontal displacement of the actuator into a vertical displacement of the platform. Usually, the displacement is realized through the use of hydraulic or pneumatic actuators [105]. In some cases, a ball-screw motor arrangement can be used to drive the scissor lift table [106]. Ensuring stability and safety, their use is focused on the elevation of workers, tools, and various materials. Also, these mechanical systems often involve an increase in productivity, thereby sparking the interest of several industrial and academic research groups. For instance, Hongyu and Ziyi proposed the design of a new scissor platform focusing on CAD modeling [107]. In this research work, a calculation is performed to estimate the actuation force required by the control system. In general, since simple geometric modeling cannot make structurally reliable a mechanism intended for industrial use, it is advisable to perform a finite element analysis after the first mechanical modeling to verify the structural strength of the design [108]. The instability of scissor lift tables can indeed cause damage both economically to the goods and physically to the operators [109]. To obtain a reliable system from the point of view of its stability, it is necessary to carry out kinetic simulations by using a reliable mathematical model. In [110], such problem is addressed by resorting to dynamical simulations performed using SIMULINK. Based on the results obtained, the design is then optimized in this work. Therefore, to ensure the stability of a pantograph scissor lift table, the actuation force must be carefully defined to achieve the desired height and have an efficient mechanism. To this end, the dynamic study is significant to modulate the actuation force [111]. Within the study of dynamic stability, several additional factors must be considered, i.e. the clearance present between the parts, the friction forces, and the contact reactions. In this respect, Li et al. addressed these complex issues by using the LuGre model to consider the effect of friction and the Gonthier model for analyzing the contact forces [112].

This paper focuses on the dynamic analysis of the multibody pantograph scissor lift system. The main factors that influence the time evolution of the platform lift to be analyzed in this work are the nonlinearity of the dynamical behavior and the presence of friction forces. To achieve a gradual lifting of the platform in the actual design of this mechanism, the displacement is obtained using an actuator that allows the linear displacement of the body connecting the bar and the frame [113]. If the applied force is too high, the platform will rise too fast, creating instability of the entire system, and also exceeding the safety limit that must not be reached at all. On the other hand, if the force is too low, the platform will fall until it reaches the end of the stroke [114]. One possible and attractive strategy to solve this problem is to control the drive speed of the motor system in such a way as to provide a constant velocity to the platform [115]. Another method to face the problem, very much used, especially in the industrial field, is to include a Proportional-Integral-Derivative (PID) controller such that the scissor system reaches the target despite the presence of different disturbances. This strategy refers to the following logical process, described, for example, in [116]. There is a reference time law for the displacement to follow for the movement of the platform. The control system compares the reference action with the actual behavior exhibited by the system, thereby defining an error signal, and operates accordingly through the calibration of appropriate control parameters. Therefore, in principle, it is possible to derive a controlled force that allows for canceling the trajectory error. However, designing an excellent control strategy to achieve the desired platform displacement requires, as a preliminary step, the development of an accurate multibody model and a detailed kinematic analysis [117]. The definition of a multibody system is related

to the articulated structure of the mechanism of interest, which can be considered as a set of rigid and flexible bodies interconnected by mechanical joints. To define the orientation of a general set of bodies in the three-dimensional space, and then proceed to the subsequent dynamic study, several methods can be employed, as shown in the literature. For this purpose, it is possible to describe the orientation of a generic rigid body using Euler angles, Tait-Bryan angles, or using Euler parameters. In the first two cases, a sequence of three angles is used, while, in the last case, four parameters are used to describe the orientation of the body [118]. In [119], Wang and Chen made a comparison between different control techniques for modulating the speed of the platform. An alternative PID controller is proposed, whose parameters are updated by a backpropagation technique based on neural networks. Using such a controller there is no overshoot at all. This control strategy is very efficient compared to a traditional PID controller or a PID controller with fuzzy logic. Another solution is proposed by Takesue et al. [120]. In this research paper, a Proportional-Derivative (PD) controller is used to regulate the angular displacement of the bar hinged to the frame. The main novelty in the article is a compensation mechanism made using three spring elements.

Another important family of control methods is based on the proper formulation of an optimal control problem. In principle, the optimal control problem for nonlinear dynamical systems requires solving the Hamilton-Jacobi-Bellman equation, a partial differential equation characterized by a terminal condition, which, in general, is challenging to be analytically or numerically solved [121]. On the other hand, a strategy to address the design of a nonlinear controller is to perform a linearization of the system dynamics. However, this operation can compromise the global characteristics of the system, to the extent to create an inefficient or even a harmful controller [122]. Additionally, to obtain stabilized feedback controllers for nonlinear systems, control system designers make use of the Lyapunov function [123]. For example, the method called the Dynamic Sliding Mode Control (DSMC) is based on the Lyapunov function. The DSMC method is a type of controller that exploits the dynamics of the system using it as a nonlinear compensator. This controller tries to augment the system to improve its stability in order to obtain the desired output [124]. From a slightly different perspective, when the robotics literature deals with the control theory, the trajectory tracking problem is often taken into consideration. For example, a hybrid control system is proposed in [125]. In this work, the principle of virtual work is used to obtain the dynamic behavior of the system, and then the actuation forces are optimized using the least-squares method. Having performed this process, the control strategy is established. More specifically, one robot link is controlled considering its position, whereas the subsequent link is dynamically driven by modulating the actuation forces. In [126], Tang et al. proposed a mixed PID/adaptive controller. Such strategy is implemented in a dominant linear second-order model, with a portion of the unmodeled dynamics that can be nonlinear and time-varying. The advantage of the proposed controller is that it can cope with strong nonlinearities in the system while still using a simple PID controller. In [127], Resende et al. developed a fuzzy controller for performing the trajectory tracking. The controller uses two Takagi-Sugeno (TS) fuzzy blocks to generate its control gains. This strategy enables also to limit the velocity and cancel the errors generated by the unwanted system dynamics.

Several other interesting nonlinear control strategies, not fully commented on here because of space limitations, can be found in the literature. These are, for instance, the general control policy based on the control Lyapunov function [128,129], the feedback linearization approach [130,131], the adaptive control method [132,133], the sliding mode control technique [134,135], the backstepping control strategy [136,137], and the state-dependent Riccati equation [138,139]. In this paper, on the other hand, a new approach is proposed for solving the control problem formulated in the case of multibody systems by exploiting the possibility of modeling the system of interest using both a minimal and a redundant coordinate formulation, as well as by extending some straightforward techniques of linear control theory to the nonlinear case [140]. The use of the control method devised in this paper is demonstrated by means of numerical experiments considering an articulated mechanical system of interest in several engineering applications, namely, the scissor mechanism having a pantograph structure that serves to guide the motion of a lift table [141]. In the literature, several control techniques are proposed for this particular lift mechanism. On the other hand, the development of general nonlinear control strategies plays a pivotal role in the scientific community, from the world of bioengineering to robotics, from the automotive sector to aerospace applications. In this paper, a new approach for solving the nonlinear control problem is discussed in detail. Thus, in this short literature survey, an overview of control strategies adopted on multibody systems was provided.

1.4 Scope and contributions of this investigation

This paper is collocated within the research framework of the authors, which has a threefold structure based on the computational mechanics of rigid-flexible multibody systems [142, 143], the nonlinear control problem associated with continuous-time and discrete-time dynamical systems [144,145], and the numerical identification procedures applied to structural systems [146,147]. In this vein, this paper deals with the dynamics and control of articulated mechanical systems modeled as multibody mechanical systems and introduces in this context a new high-performing control strategy, which is thoroughly analyzed through dynamical simulations by addressing the regulation and tracking problems of a pantograph scissor lift mechanism considered as the case study. More specifically, by using the MATLAB and SIMSCAPE MULTIBODY simulation environments, a minimal coordinate multibody model and a redundant coordinate multibody model of the pantograph scissor lift mechanism were analytically developed, whereas the performance of the new control strategy devised and proposed in the paper was tested through extensive numerical experiments. Compared with the excellent studies found in the literature and discussed before, this paper proposes a new control strategy that is general and applicable to a large class of articulated mechanical systems, modeled as rigid multibody systems. The effectiveness of the new methodology proposed in this investigation is demonstrated through numerical experiments performed on the multibody models of a pantograph scissor lift mechanism, which represents the case study considered in this work.

This paper deals with the development of a sound computational approach for the design and the implementation of a new control strategy capable of directing the motion of articulated systems modeled as multibody mechanical systems. Specifically, the paper focuses on the dynamic modeling of an articulated mechanical system commonly employed in industrial applications. For this purpose, the case study considered in this work is a simple scissor lift table having a pantograph structure. The main goal is to design an appropriate model-based control system and verify the effectiveness of a new control policy proposed in this investigation. The pantograph scissor lift mechanism of interest for this investigation is modeled within the rigid multibody dynamic framework, which encompasses only rigid bodies, kinematic joints, force elements, and force fields, leading to two different mathematical models, that is, a minimal coordinate multibody model and a redundant coordinate multibody model. Since the pantograph scissor lift mechanism is composed of a set of several rigid components and mechanical joints but possesses only one degree of freedom, the minimal coordinate multibody model is described by one highly nonlinear ordinary differential equation of motion, while the redundant coordinate multibody model features several generalized coordinates as well as Lagrange multipliers embedded in a nonlinear set of differential-algebraic equations of motion. More importantly, in the paper, the minimal coordinate multibody model is advantageously employed for the design of a nonlinear control strategy, which is suitable for guiding the large displacements and rotations that characterize the rigid motion of the pantograph scissor lift mechanism, whereas the redundant coordinate multibody model serves to validate the controller performance in a more realistic scenario.

In this work, a general and effective method is introduced for the nonlinear control of articulated mechanical systems, and its use is demonstrated for a pantograph scissor lift mechanism modeled as a multibody system. To perform computational analyses that are independent and reliable, as well as to correctly simulate the dynamic behavior of the pantograph scissor lift mechanism,

both the minimal coordinate multibody model and the redundant coordinate multibody model were implemented in MATLAB with the use of a hybrid symbolic-numeric modeling approach. Furthermore, to be able to perform an additional comparison of the numerical results found, the redundant coordinate multibody model was also implemented using the SIMSCAPE MULTIBODY software by employing an object-oriented modeling approach. The main purpose behind the application of a proper control system to the pantograph mechanism is threefold, namely, to guide the motion of the scissor system between two desired configurations, to prevent potentially harmful mechanical oscillations of the lift table when approaching the desired equilibrium configuration, and to maintain the configuration of static equilibrium reached at the end of the system movement. To this end, a new control approach is introduced and tested in this paper. The proposed control approach considers the combination of a quasi-static nonlinear controller, which serves as the modulating feedforward control action, with an error-based proportional-derivative controller, which plays the role of a compensating feedback control action. In order to perform meaningful dynamic analysis through computer simulations, the effectiveness of the nonlinear control policy designed employing the minimal coordinate multibody model and the redundant coordinate multibody model implemented in MATLAB is verified with the use of the redundant coordinate multibody model implemented in SIMSCAPE MULTIBODY. Thus, the numerical experiments performed in this investigation by using the multibody models implemented using the computer codes developed in MATLAB and the programs constructed using SIMSCAPE MULTIBODY demonstrate the effectiveness of the nonlinear control approach devised in this research work.

1.5 Organization of the manuscript

The remaining part of this manuscript is drawn up by following the structure reported below. In Section 2., the control strategy proposed in this paper is described in detail by formulating the control problem in the case of a general articulated mechanical system. Section 3. contains the description of the pantograph scissor lift mechanism considered as the case study of interest for this investigation. While in Section 4. a minimal coordinate multibody model of the articulated system of interest is developed, Section 5. describes a redundant coordinate multibody model for the same mechanical system analyzed in the paper. In Section 6., for corroborating through numerical experiments the efficacy of the nonlinear control policy devised in this investigation, which is applied to the case study considered in the paper, several numerical results obtained using MATLAB and SIMSCAPE MULTIBODY are reported and discussed. Finally, Section 7. contains a summary of the work done, the main conclusions drawn in this paper, and some comments on the directions to be followed in future investigations.

2. Proposed control strategy

2.1 Multibody equations of motion

In this section, the control strategy introduced in this research work is described in a general form to clarify the subsequent application to the case study analyzed below. For this purpose, consider the dynamic model of a multibody mechanical system whose kinematic structure is described by using a minimal coordinate formulation, that is, a set of generalized coordinates whose total number denoted with n_q is equal to the number of the system degrees of freedom denoted with n_f. In this broad scenario, the multibody equations of motion assume the following general form:

$$\boldsymbol{M}\ddot{\boldsymbol{q}} = \boldsymbol{Q}_{\mathrm{b}} + \boldsymbol{Q}_{\mathrm{c}} \tag{1}$$

where $\boldsymbol{q} \equiv \boldsymbol{q}(t)$ is a vector having dimension n_q representing the system Lagrangian coordinates, $\boldsymbol{M} \equiv \boldsymbol{M}(\boldsymbol{q}, t)$ is a matrix of dimensions $n_q \times n_q$ representing the system mass matrix, $\boldsymbol{Q}_{\mathrm{b}} \equiv \boldsymbol{Q}_{\mathrm{b}}(\boldsymbol{q}, \dot{\boldsymbol{q}}, t)$ is a vector having dimension n_q representing the system total body generalized force vector, $\boldsymbol{Q}_{\mathrm{c}} \equiv \boldsymbol{Q}_{\mathrm{c}}(\boldsymbol{q}, \dot{\boldsymbol{q}}, t)$ is a vector having dimension n_q representing the control generalized force vector applied to the multibody system, and the dot symbols indicate the derivatives taken with respect to the time denoted with t. To further clarify the meaning of the analytical terms that appear in the general set of dynamical equations introduced above, the system total body generalized force vector, as well as the system control generalized force vector, can be rewritten in a more explicit form. To this end, the system total body generalized force vector can be expressed as follows:

$$\boldsymbol{Q}_{\mathrm{b}} = \boldsymbol{Q}_{\mathrm{v}} + \boldsymbol{Q}_{\mathrm{e}} \tag{2}$$

where $\boldsymbol{Q}_{\mathrm{v}} \equiv \boldsymbol{Q}_{\mathrm{v}}(\boldsymbol{q}, \dot{\boldsymbol{q}}, t)$ is a vector having dimension n_q representing the system inertia quadratic velocity generalized force vector, absorbing all the terms that are quadratic in generalized velocities, and $\boldsymbol{Q}_{\mathrm{e}} \equiv \boldsymbol{Q}_{\mathrm{e}}(\boldsymbol{q}, \dot{\boldsymbol{q}}, t)$ is a vector having dimension n_q representing the system total external generalized force vector, including both the conservative and nonconservative terms. The system control generalized force vector can be expressed as follows:

$$\boldsymbol{Q}_{\mathrm{c}} = \boldsymbol{B}_{\mathrm{a}}\boldsymbol{u}_{\mathrm{c}} \tag{3}$$

where the number of control actions is denoted with n_u, while $\boldsymbol{B}_{\mathrm{a}} \equiv \boldsymbol{B}_{\mathrm{a}}(\boldsymbol{q}, t)$ is a matrix of dimensions $n_q \times n_u$ representing the system actuator collocation matrix, and $\boldsymbol{u}_{\mathrm{c}} \equiv \boldsymbol{u}_{\mathrm{c}}(\boldsymbol{q}, \dot{\boldsymbol{q}}, t)$ is a vector having dimension n_u representing the nonlinear vector of control actions acting on the multibody system. As a fundamental hypothesis for the development of the control strategy proposed in this investigation, it is assumed that the multibody mechanical system to be controlled is fully actuated. Essentially, this hypothesis means that the number of control actions n_u, assumed all independently manipulable, is equal to the number of the system degrees of freedom n_f. More importantly, since a minimal coordinate formulation is employed for the derivation of the multibody dynamical model, this, in turn, implies that the number of control actions n_u is also equal to the number of Lagrangian coordinates n_q used in the kinematic description. Consequently, it is assumed that the system actuator collocation matrix $\boldsymbol{B}_{\mathrm{a}}$ is a square matrix having a full rank given by $r_a = n_q$. Since Equation (3) represents a well-posed system of algebraic equations, this fundamental assumption allows for univocally computing the vector of control inputs $\boldsymbol{u}_{\mathrm{c}}$ corresponding to a given vector of control generalized forces $\boldsymbol{Q}_{\mathrm{c}}$ and vice versa. On the other hand, Equation (1) represents a nonlinear set of ordinary differential equations that govern the dynamic behavior of the multibody system associated with them. As a special case, these differential equations also describe the static equilibrium of the multibody system. In this special case, the system equations of motion become the system static equations and assume the following particular form:

$$\boldsymbol{Q}_{\mathrm{e}} + \boldsymbol{B}_{\mathrm{a}}\boldsymbol{u}_{\mathrm{c}} = \boldsymbol{0} \tag{4}$$

where the analytical terms associated with the generalized velocities and accelerations vanish in any configuration of static equilibrium. Equation (4) represents a nonlinear set of algebraic equations that allows for identifying the configurations of static equilibrium ensured by the presence of a constant set of control actions. Furthermore, as mentioned before, Equation (1) forms a highly nonlinear set of ordinary differential equations describing the motion in large of the multibody system of interest, namely, the system dynamic behavior when its components undergo large displacements and large finite rotations. However, if one is interested in describing only small perturbations of the system motion around a given equilibrium configuration, determined by solving Equation

(4), a linearized version of the multibody equations of motion can be found by performing a Taylor series expansion truncated at the first order. By doing so, one obtains:

$$\bar{\boldsymbol{M}}_e\ddot{\bar{\boldsymbol{q}}} + \bar{\boldsymbol{R}}_e\dot{\bar{\boldsymbol{q}}} + \bar{\boldsymbol{K}}_e\bar{\boldsymbol{q}} = \bar{\boldsymbol{B}}_{\mathrm{a},e}\bar{\boldsymbol{u}}_{\mathrm{c}} \tag{5}$$

where:

$$\boldsymbol{q} = \boldsymbol{q}_e + \bar{\boldsymbol{q}}, \quad \boldsymbol{u}_{\mathrm{c}} = \boldsymbol{u}_{\mathrm{c},e} + \bar{\boldsymbol{u}}_{\mathrm{c}} \tag{6}$$

where $\boldsymbol{q}_e$ is a constant vector of dimension n_q representing a configuration of static equilibrium, $\boldsymbol{u}_{\mathrm{c},e}$ is a constant vector of dimension n_u representing the control actions necessary for attaining and keeping the static equilibrium, $\bar{\boldsymbol{q}} \equiv \bar{\boldsymbol{q}}(t)$ is a vector of dimension n_q representing the perturbation of the system configuration from the static equilibrium, $\bar{\boldsymbol{u}}_{\mathrm{c}} \equiv \bar{\boldsymbol{u}}_{\mathrm{c}}(t)$ is a vector of dimension n_u representing the perturbation of the control actions from those that guarantee the static equilibrium, while $\bar{\boldsymbol{M}}_e$, $\bar{\boldsymbol{R}}_e$, and $\bar{\boldsymbol{K}}_e$ are constant matrix having dimensions $n_q \times n_q$ that respectively identify the system linearized mass, damping, and stiffness matrices, whereas $\bar{\boldsymbol{B}}_{\mathrm{a},e}$ is a constant matrix having dimensions $n_q \times n_u$ representing the system linearized input collocation matrix. Additionally, since Equation (4) represents a set of algebraic equations that is nonlinear as well, more than one configuration of static equilibrium can be found by analytically or numerically solving them. This is a key point that is used as the basic concept for developing the control policy proposed in the present paper. More specifically, a combination of a feedforward control strategy with a feedback control approach is devised herein, leading to the following general form of the vector of control actions:

$$\boldsymbol{u}_{\mathrm{c}} = \boldsymbol{u}_{\mathrm{c,FF}} + \boldsymbol{u}_{\mathrm{c,FB}} \tag{7}$$

where $\boldsymbol{u}_{\mathrm{c,FF}} \equiv \boldsymbol{u}_{\mathrm{c,FF}}(t)$ is a vector of dimension n_u representing the feedforward control actions and $\boldsymbol{u}_{\mathrm{c,FB}} \equiv \boldsymbol{u}_{\mathrm{c,FB}}(\boldsymbol{q}, \dot{\boldsymbol{q}}, t)$ is a vector of dimension n_u representing the feedback control actions. Finally, it is noteworthy to emphasize that the control strategy proposed in this work allows for separately defining the structure of both the feedforward and feedback controllers. This goal is achieved through the use of a time-dependent quasi-static control technique in combination with an error-based proportional-derivative control method. The analytical formulation and the parameter tuning of the proposed feedforward plus feedback control strategy are discussed in detail below.

2.2 Time-dependent quasi-static feedforward controller

The feedforward controller proposed in this paper is designed using a quasi-static control approach. To this end, two configurations of static equilibrium are first determined by solving Equation (4). By respectively denoting with the vectors $\boldsymbol{q}_0$ and $\boldsymbol{q}_e$ having dimension n_q the two configurations of static equilibrium thereby identified, where $\boldsymbol{q}_0$ represents the system initial configuration and $\boldsymbol{q}_e$ identifies the desired configuration of static equilibrium, to be reached by the multibody system through the action of the feedforward controller, one can accordingly find two constant vectors of control actions respectively denoted with $\boldsymbol{u}_{\mathrm{c},0}$ and $\boldsymbol{u}_{\mathrm{c},e}$ of dimension n_u that enforce the two corresponding configurations of static equilibrium introduced before. According to the previous assumptions, the key idea, on which the quasi-static control method proposed here is based, is to introduce a smooth interpolating function that allows for reaching the final vector of control actions $\boldsymbol{u}_{\mathrm{c},e}$, associated with the desired static equilibrium configuration $\boldsymbol{q}_e$, starting from the initial vector of control actions $\boldsymbol{u}_{\mathrm{c},0}$, associated with the system initial configuration $\boldsymbol{q}_0$. For this purpose, one can effectively employ the following interpolating function:

$$\tau = \frac{t}{T_a}, \quad f_u = \begin{cases} 3\tau^2 - 2\tau^3, & 0 \leq \tau < 1 \\ 1, & \tau \geq 1 \end{cases} \tag{8}$$

where t is the time variable, T_a represents the actuation time, $\tau \equiv \tau(t)$ identifies the dimensionless time variable, and $f_u \equiv f_u(t)$ denotes the interpolating function of interest. Finally, the feedforward controller based on the quasi-static control strategy can be written as follows:

$$\boldsymbol{u}_{\mathrm{c,FF}} = \boldsymbol{u}_{\mathrm{c},0} + f_u\Delta\boldsymbol{u}_{\mathrm{c},e} \tag{9}$$

being:

$$\Delta\boldsymbol{u}_{\mathrm{c},e} = \boldsymbol{u}_{\mathrm{c},e} - \boldsymbol{u}_{\mathrm{c},0} \tag{10}$$

where $\Delta\boldsymbol{u}_{\mathrm{c},e}$ is a constant vector of dimension n_u representing the difference between the final vector of equilibrium control actions $\boldsymbol{u}_{\mathrm{c},e}$ and the initial vector of equilibrium control actions $\boldsymbol{u}_{\mathrm{c},0}$. To conclude the description of the feedforward controller obtained through the implementation of the quasi-static control strategy, it is important to note that the time interpolating function given by Equation (8) allows for reaching the final input vector $\boldsymbol{u}_{\mathrm{c},e}$ with a constant slope in time starting from the initial input vector $\boldsymbol{u}_{\mathrm{c},0}$ with a zero time derivative, thereby avoiding sharp variations in the resulting vector of feedforward control actions.

2.3 Error-based proportional-derivative feedback controller

The feedback controller proposed in this paper is designed using a proportional-derivative control approach. In order to achieve this goal, a fundamental preliminary step is represented by the introduction of a control function denoted with $\boldsymbol{g}_{\mathrm{c}}$, where $\boldsymbol{g}_{\mathrm{c}} \equiv \boldsymbol{g}_{\mathrm{c}}(\boldsymbol{q}, \dot{\boldsymbol{q}}, t)$ identifies a nonlinear vector function of dimension n_u that must be suitably chosen for the definition of a proper feedback control vector capable of ensuring the system stability around the required equilibrium configuration. In particular, in the design of the feedback controller based on the proportional-derivative control strategy proposed herein, the desired configuration of static equilibrium denoted with $\boldsymbol{q}_e$ is adopted as the reference configuration vector. By doing so, one can readily define the following control error vector:

$$\boldsymbol{e}_{\mathrm{c}} = \boldsymbol{g}_{\mathrm{c}} - \boldsymbol{g}_{\mathrm{c},e} \tag{11}$$

being:

$$\boldsymbol{g}_{\mathrm{c},e} = \boldsymbol{g}_{\mathrm{c}}(\boldsymbol{q} = \boldsymbol{q}_e, \dot{\boldsymbol{q}} = \boldsymbol{0}, t = T_a) \tag{12}$$

where $\boldsymbol{g}_{\mathrm{c},e}$ is a constant vector of dimension n_u identifying the control function evaluated in correspondence of the desired configuration of static equilibrium and $\boldsymbol{e}_{\mathrm{c}} \equiv \boldsymbol{e}_{\mathrm{c}}(\boldsymbol{q}, \dot{\boldsymbol{q}}, t)$ is a vector having dimension n_u representing the control error vector evaluated in a general configuration of the multibody system to be controlled. Subsequently, the feedback controller based on the proportional-derivative control approach is, therefore, simply defined as follows:

$$\boldsymbol{u}_{\mathrm{c,FB}} = -\boldsymbol{K}_{\mathrm{c}}\boldsymbol{e}_{\mathrm{c}} - \boldsymbol{R}_{\mathrm{c}}\dot{\boldsymbol{e}}_{\mathrm{c}} \tag{13}$$

where $\boldsymbol{K}_{\mathrm{c}}$ is a constant matrix of dimensions $n_u \times n_u$ containing the controller proportional coefficients and $\boldsymbol{R}_{\mathrm{c}}$ is a constant matrix of dimensions $n_u \times n_u$ containing the controller derivative coefficients. By introducing the definition of the proportional-derivative

feedback controller given by Equation (13) into the multibody system equations of motion given by Equation (1), and performing a linearization process identical to the one discussed in detail above, the following linearized model is obtained:

$$\bar{\boldsymbol{M}}_e \ddot{\bar{\boldsymbol{q}}} + \left(\bar{\boldsymbol{R}}_e + \bar{\boldsymbol{R}}_{\mathrm{c},e}\right) \dot{\bar{\boldsymbol{q}}} + \left(\bar{\boldsymbol{K}}_e + \bar{\boldsymbol{K}}_{\mathrm{c},e}\right) \bar{\boldsymbol{q}} = \boldsymbol{0} \tag{14}$$

being:

$$\bar{\boldsymbol{K}}_{\mathrm{c},e} = \boldsymbol{B}_{\mathrm{a}} \boldsymbol{K}_{\mathrm{c}} \boldsymbol{P}_{\mathrm{c},e} = \boldsymbol{B}_{\mathrm{a}} \boldsymbol{K}_{\mathrm{c}} \boldsymbol{E}_{\mathrm{c},e}, \quad \bar{\boldsymbol{R}}_{\mathrm{c},e} = \boldsymbol{B}_{\mathrm{a}} \boldsymbol{R}_{\mathrm{c}} \boldsymbol{V}_{\mathrm{c},e} = \boldsymbol{B}_{\mathrm{a}} \boldsymbol{R}_{\mathrm{c}} \boldsymbol{E}_{\mathrm{c},e} \tag{15}$$

and

$$\begin{cases} \boldsymbol{P}_{\mathrm{c},e} = \frac{\partial \boldsymbol{e}_{\mathrm{c}}}{\partial \boldsymbol{q}}(\boldsymbol{q} = \boldsymbol{q}_e, \dot{\boldsymbol{q}} = \boldsymbol{0}, t = T_a) = \boldsymbol{E}_{\mathrm{c},e} \\ \boldsymbol{V}_{\mathrm{c},e} = \frac{\partial \dot{\boldsymbol{e}}_{\mathrm{c}}}{\partial \dot{\boldsymbol{q}}}(\boldsymbol{q} = \boldsymbol{q}_e, \dot{\boldsymbol{q}} = \boldsymbol{0}, t = T_a) = \boldsymbol{E}_{\mathrm{c},e} \end{cases} \tag{16}$$

where $\bar{\boldsymbol{M}}_e$, $\bar{\boldsymbol{R}}_e$, and $\bar{\boldsymbol{K}}_e$ are constant matrix having dimensions $n_q \times n_q$ that respectively identify the system linearized mass, damping, and stiffness matrices, whereas $\boldsymbol{P}_{\mathrm{c}} \equiv \boldsymbol{P}_{\mathrm{c}}(\boldsymbol{q}, \dot{\boldsymbol{q}}, t)$ is a matrix of dimensions $n_u \times n_q$ arising from the linearization of the control error vector $\boldsymbol{e}_{\mathrm{c}}$ with respect to the system generalized coordinate vector $\boldsymbol{q}$, $\boldsymbol{V}_{\mathrm{c}} \equiv \boldsymbol{V}_{\mathrm{c}}(\boldsymbol{q}, \dot{\boldsymbol{q}}, t)$ is a matrix of dimensions $n_u \times n_q$ arising from the linearization of the time derivative of the control error vector $\dot{\boldsymbol{e}}_{\mathrm{c}}$ with respect to the system generalized velocity vector $\dot{\boldsymbol{q}}$, $\boldsymbol{E}_{\mathrm{c}} \equiv \boldsymbol{E}_{\mathrm{c}}(\boldsymbol{q}, \dot{\boldsymbol{q}}, t)$ is a matrix of dimensions $n_u \times n_q$ arising from the linearization process, while $\bar{\boldsymbol{K}}_{\mathrm{c},e}$ is a constant matrix of dimensions $n_q \times n_q$ representing the equivalent stiffness matrix induced by the feedback controller, and $\bar{\boldsymbol{R}}_{\mathrm{c},e}$ is a constant matrix of dimensions $n_q \times n_q$ representing the equivalent damping matrix induced by the feedback controller. Since the equations of motion that describe the system small perturbations around the desired configuration of static equilibrium denoted with $\boldsymbol{q}_e$ form a linear set of ordinary differential equations, the equivalent control stiffness matrix $\bar{\boldsymbol{K}}_{\mathrm{c},e}$ and the equivalent control damping matrix $\bar{\boldsymbol{R}}_{\mathrm{c},e}$ can be computed by using the conventional methods of the classic control theory. More specifically, one can adopt the pole placement method, also called the full state feedback control method in the classical control system theory, to assign the eigenstructure of the linearized mechanical model and obtain the equivalent control stiffness and damping matrices $\bar{\boldsymbol{K}}_{\mathrm{c},e}$ and $\bar{\boldsymbol{R}}_{\mathrm{c},e}$, from which the corresponding matrices $\boldsymbol{K}_{\mathrm{c}}$ and $\boldsymbol{R}_{\mathrm{c}}$ containing the controller proportional and derivative coefficients can be readily extracted. Therefore, the pole placement method, which can be effectively used to place the closed-loop eigenvalues of a linear dynamical system in predetermined locations of the complex plane, represents the fundamental technique employed in this paper for the definition of the feedback controller based on the proportional-derivative control architecture. However, in practical applications, the feedback control parameters, originally found using the pole placement method mentioned herein, require an additional iterative process of refinement through numerical experiments, and this process should be carried out by assessing the controller performance in terms of a set of proper quantitative metrics, such as the rise time, the maximum overshoot, the settling time, and the steady-state error considered in this paper. As a final remark, the control method proposed here represents a general strategy applicable to both linear and nonlinear mechanical systems. In this investigation, as discussed below, this method is used for solving the control problem of an articulated mechanical system forming a pantograph scissor lift mechanism.

3. Description of the case study

3.1 System geometric properties

The articulated mechanical system considered in this investigation as the case study is a scissor lift table with a pantograph closed-chain layout. This mechanism is used in industrial and civil applications as the base device of scissor lifts for handling heavy loads. A simplified CAD model of this mechanism is shown in Figure 1.

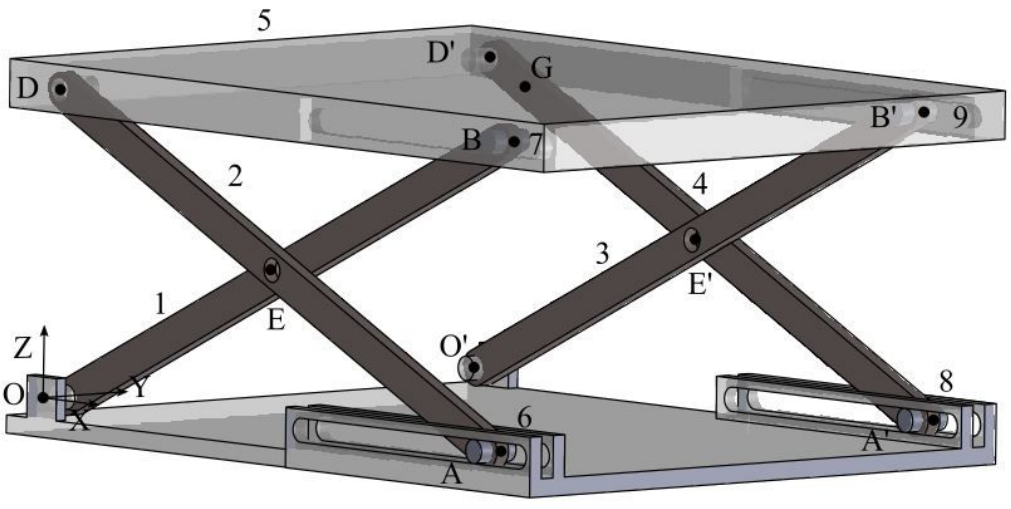

Figure 1. *CAD model of the pantograph scissor lift mechanism.*

In this paper, the pantograph scissor lift mechanism represented in Figure 1 is modeled as a rigid multibody mechanical system. This multibody system is composed of $N_b = 9$ rigid bodies, excluding the ground, and $N_{c,\Psi} = 14$ kinematic joints representing the set of extrinsic constraints, excluding the $N_{c,\Phi} = N_b = 9$ normalization conditions that will be subsequently employed in the redundant coordinate multibody model as the algebraic equations for the regularization of the sets of Euler parameters used as orientation parameters. From the first to the last, the rigid bodies that form the mechanical model of the mechanism under consideration are the front left bar placed in OB (body number $i = 1$), the front right bar placed in AD (body number $i = 2$), the rear left bar placed in $O'B'$ (body number $i = 3$), the rear right bar placed in $A'D'$ (body number $i = 4$), the table platform deployed in

$BB'D'D$ (body number $i = 5$), the front bottom roller collocated in A (body number $i = 6$), the front top roller collocated in B (body number $i = 7$), the rear bottom roller collocated in A' (body number $i = 8$), and the rear top roller collocated in B' (body number $i = 9$). The fundamental geometric parameters necessary for the description of the closed-chain multibody model of the pantograph scissor lift mechanism, namely, the length L_i, the thickness H_i, the width W_i, and the diameter D_i of each rigid body i, whenever they represent appropriate geometric dimensions, are reported in Table 1.

Table 1. Geometric parameters of the pantograph scissor lift mechanism.

Descriptions	Symbols	Data (units)
Characteristic length	$L = L_b$	1.2 (m)
Characteristic thickness	$H = H_p$	0.08 (m)
Characteristic width	$W = W_p$	1 (m)
Characteristic diameter	$D = D_r$	0.04 (m)
First body length	$L_1 = L_b$	1.2 (m)
First body thickness	$H_1 = H_b$	0.06 (m)
First body width	$W_1 = W_b$	0.025 (m)
Second body length	$L_2 = L_b$	1.2 (m)
Second body thickness	$H_2 = H_b$	0.06 (m)
Second body width	$W_2 = W_b$	0.025 (m)
Third body length	$L_3 = L_b$	1.2 (m)
Third body thickness	$H_3 = H_b$	0.06 (m)
Third body width	$W_3 = W_b$	0.025 (m)
Fourth body length	$L_4 = L_b$	1.2 (m)
Fourth body thickness	$H_4 = H_b$	0.06 (m)
Fourth body width	$W_4 = W_b$	0.025 (m)
Fifth body length	$L_5 = L_p$	1.35 (m)
Fifth body thickness	$H_5 = H_p$	0.08 (m)
Fifth body width	$W_5 = W_p$	1 (m)
Sixth body diameter	$D_6 = D_r$	0.04 (m)
Sixth body width	$W_6 = W_r$	0.075 (m)
Seventh body diameter	$D_7 = D_r$	0.04 (m)
Seventh body width	$W_7 = W_r$	0.075 (m)
Eighth body diameter	$D_8 = D_r$	0.04 (m)
Eighth body width	$W_8 = W_r$	0.075 (m)
Ninth body diameter	$D_9 = D_r$	0.04 (m)
Ninth body width	$W_9 = W_r$	0.075 (m)

Also, the geometric quantities denoted with L, H, W, and D reported in Table 1 represents some characteristic geometric dimensions of the pantograph scissor lift mechanism.

3.2 System mechanical properties

The inertial parameters associated with the rigid bodies which form the multibody model of the pantograph scissor lift mechanism, that is, the mass m_i of each body and the principal mass moments of inertia $I_{xx,i}$, $I_{yy,i}$, and $I_{zz,i}$ referred to the centroid G_i of each body, are reported in Table 2.

On the other hand, as discussed more in detail below, the kinematic joints that connect the rigid body of the mechanism under study are, from the first to the last, a revolute joint collocated in O (joint number $k = 1$), a revolute joint collocated in A (joint number $k = 2$), a prismatic joint collocated in A (joint number $k = 3$), a revolute joint collocated in B (joint number $k = 4$), a prismatic joint collocated in B (joint number $k = 5$), a revolute joint collocated in D (joint number $k = 6$), a revolute joint collocated in E (joint number $k = 7$), a revolute joint collocated in O' (joint number $k = 8$), a revolute joint collocated in A' (joint number $k = 9$), a prismatic joint collocated in A' (joint number $k = 10$), a revolute joint collocated in B' (joint number $k = 11$), a prismatic joint collocated in B' (joint number $k = 12$), a revolute joint collocated in D' (joint number $k = 13$), and a revolute joint collocated in E' (joint number $k = 14$). The pantograph scissor lift mechanism undergoes the action of a constant gravitational field featuring a gravity acceleration equal to g, which is aligned with the vertical direction of the global frame of reference (Z-axis), whose origin is placed at the point O and is shown in Figure 1. The presence of dry friction forces acting on the rollers is also taken into consideration. For simplicity, the friction effects are modeled as $N_a = 4$ linear viscous forces having a constant coefficient equal to σ. More precisely, the dry friction forces at the interface of the guides of the prismatic joints in which the rollers slide are modeled considering a force element characterized by a linear viscous force having constant damping equal to σ. Thus, from the first to the last, the force elements taken into account are a linear viscous force element collocated at the point A acting between the front bottom roller and the ground (force element number $h = 1$), a linear viscous force element collocated at the point B acting between the front top roller and the platform (force element number $h = 2$), a linear viscous force element collocated at the point A' acting between the rear bottom roller and the ground (force element number $h = 3$), and a linear viscous force element collocated at the point B' acting between the rear top roller and the platform (force element number $h = 4$). Furthermore, it is assumed that a control device collocated at point A of Figure 1 is capable of producing a control force field denoted with F_c and directed along the horizontal direction of the global frame of reference (X-axis). Thus, the manipulable control force denoted with F_c counteracts the external action of the gravity force denoted with F_g, since this second force field affects the entire mechanism and represents the principal external load applied on the mechanical system. Although the mechanical model of the pantograph scissor lift mechanism is formed by several rigid bodies and kinematic joints, it can be easily proved that this multibody system features only $n_f = 1$ degree of freedom. Consequently, in general, one can derive a multibody model of this mechanical system by following two different approaches, namely, considering a minimal coordinate formulation, in which the number of generalized coordinates n_q is equal to the number of the system degrees of freedom n_f, or employing a redundant coordinate formulation, in which the number of generalized coordinates n_q is larger than the

Table 2. Inertial parameters of the pantograph scissor lift mechanism.

Descriptions	Symbols	Data (units)
Load mass	m_l	2000 (kg)
First body mass	$m_1 = m_b$	14.148 (kg)
First body first moment of inertia	$I_{xx,1} = I_{xx,b}$	$4.981 \cdot 10^{-3}$ (kg $\times$ m^2)
First body second moment of inertia	$I_{yy,1} = I_{yy,b}$	1.698 (kg $\times$ m^2)
First body third moment of inertia	$I_{zz,1} = I_{zz,b}$	1.702 (kg $\times$ m^2)
Second body mass	$m_2 = m_b$	14.148 (kg)
Second body first moment of inertia	$I_{xx,2} = I_{xx,b}$	$4.981 \cdot 10^{-3}$ (kg $\times$ m^2)
Second body second moment of inertia	$I_{yy,2} = I_{yy,b}$	1.698 (kg $\times$ m^2)
Second body third moment of inertia	$I_{zz,2} = I_{zz,b}$	1.702 (kg $\times$ m^2)
Third body mass	$m_3 = m_b$	14.148 (kg)
Third body first moment of inertia	$I_{xx,3} = I_{xx,b}$	$4.981 \cdot 10^{-3}$ (kg $\times$ m^2)
Third body second moment of inertia	$I_{yy,3} = I_{yy,b}$	1.698 (kg $\times$ m^2)
Third body third moment of inertia	$I_{zz,3} = I_{zz,b}$	1.702 (kg $\times$ m^2)
Fourth body mass	$m_4 = m_b$	14.148 (kg)
Fourth body first moment of inertia	$I_{xx,4} = I_{xx,b}$	$4.981 \cdot 10^{-3}$ (kg $\times$ m^2)
Fourth body second moment of inertia	$I_{yy,4} = I_{yy,b}$	1.698 (kg $\times$ m^2)
Fourth body third moment of inertia	$I_{zz,4} = I_{zz,b}$	1.702 (kg $\times$ m^2)
Fifth body mass	$m_5 = m_p$	848.88 (kg)
Fifth body first moment of inertia	$I_{xx,5} = I_{xx,p}$	71.193 (kg $\times$ m^2)
Fifth body second moment of inertia	$I_{yy,5} = I_{yy,p}$	$1.997 \cdot 10^2$ (kg $\times$ m^2)
Fifth body third moment of inertia	$I_{zz,5} = I_{zz,p}$	$1.294 \cdot 10^2$ (kg $\times$ m^2)
Sixth body mass	$m_6 = m_r$	0.741 (kg)
Sixth body first moment of inertia	$I_{xx,6} = I_{xx,r}$	$1.482 \cdot 10^{-4}$ (kg $\times$ m^2)
Sixth body second moment of inertia	$I_{yy,6} = I_{yy,r}$	$4.213 \cdot 10^{-4}$ (kg $\times$ m^2)
Sixth body third moment of inertia	$I_{zz,6} = I_{zz,r}$	$1.482 \cdot 10^{-4}$ (kg $\times$ m^2)
Seventh body mass	$m_7 = m_r$	0.741 (kg)
Seventh body first moment of inertia	$I_{xx,7} = I_{xx,r}$	$1.482 \cdot 10^{-4}$ (kg $\times$ m^2)
Seventh body second moment of inertia	$I_{yy,7} = I_{yy,r}$	$4.213 \cdot 10^{-4}$ (kg $\times$ m^2)
Seventh body third moment of inertia	$I_{zz,7} = I_{zz,r}$	$1.482 \cdot 10^{-4}$ (kg $\times$ m^2)
Eighth body mass	$m_8 = m_r$	0.741 (kg)
Eighth body first moment of inertia	$I_{xx,8} = I_{xx,r}$	$1.482 \cdot 10^{-4}$ (kg $\times$ m^2)
Eighth body second moment of inertia	$I_{yy,8} = I_{yy,r}$	$4.213 \cdot 10^{-4}$ (kg $\times$ m^2)
Eighth body third moment of inertia	$I_{zz,8} = I_{zz,r}$	$1.482 \cdot 10^{-4}$ (kg $\times$ m^2)
Ninth body mass	$m_9 = m_r$	0.741 (kg)
Ninth body first moment of inertia	$I_{xx,9} = I_{xx,r}$	$1.482 \cdot 10^{-4}$ (kg $\times$ m^2)
Ninth body second moment of inertia	$I_{yy,9} = I_{yy,r}$	$4.213 \cdot 10^{-4}$ (kg $\times$ m^2)
Ninth body third moment of inertia	$I_{zz,9} = I_{zz,r}$	$1.482 \cdot 10^{-4}$ (kg $\times$ m^2)

number of the system degrees of freedom n_f. While the latter strategy allows for the systematic development of a multibody model in a differential-algebraic form that is readily applicable in a computational environment, the former methodology requires the implementation of a hybrid symbolic-numeric programming paradigm, leading to a compact nonlinear set of ordinary differential equations capable of describing complex systems such as the pantograph scissor lift mechanism considered herein. A detailed list of all the physical parameters relevant for constructing both the minimal coordinate multibody model and the redundant coordinate multibody model of the pantograph scissor lift mechanism is reported in Table 3.

Table 3. Physical parameters of the pantograph scissor lift mechanism.

Descriptions	Symbols	Data (units)
Platform initial vertical displacement	h_0	0.3 (m)
Bar initial angular displacement	θ_0	0.253 (rad)
Roller initial horizontal displacement	s_0	1.162 (m)
Platform final vertical displacement	h_e	1 (m)
Bar final angular displacement	θ_e	0.985 (rad)
Roller final horizontal displacement	s_e	0.663 (m)
Gravity acceleration	g	9.807 (m/s^2)
Viscous damping coefficient	σ	100 (N $\times$ s/m)
Feedforward controller actuation time	T_a	2.5 (s)
Desired natural frequency	$\bar{f}_{n,d}$	5 (Hz)
Desired damping ratio	$\bar{\xi}_d$	2 $(-)$
Feedback controller proportional coefficient	k_c	$1.308 \cdot 10^6$ (N/m)
Feedback controller derivative coefficient	σ_c	$1.610 \cdot 10^5$ (N $\times$ s/m)

As discussed in detail below, in this paper, a minimal coordinate multibody model is developed first for the design of an appropriate nonlinear control strategy for guiding the motion of the platform of the scissor lift table, whereas a redundant coordinate multibody model is subsequently derived for verifying the effectiveness of the control policy devised before.

4. Minimal coordinate multibody model

4.1 Kinematic modeling

For the sake of simplicity, the pantograph scissor lift mechanism is considered herein as a rigid multibody mechanical system modeled in a Euclidean space of dimension $d = 2$. A schematic representation of the two-dimensional multibody model of the pantograph scissor lift mechanism based on a minimal set of Lagrangian coordinates is shown in Figure 2.

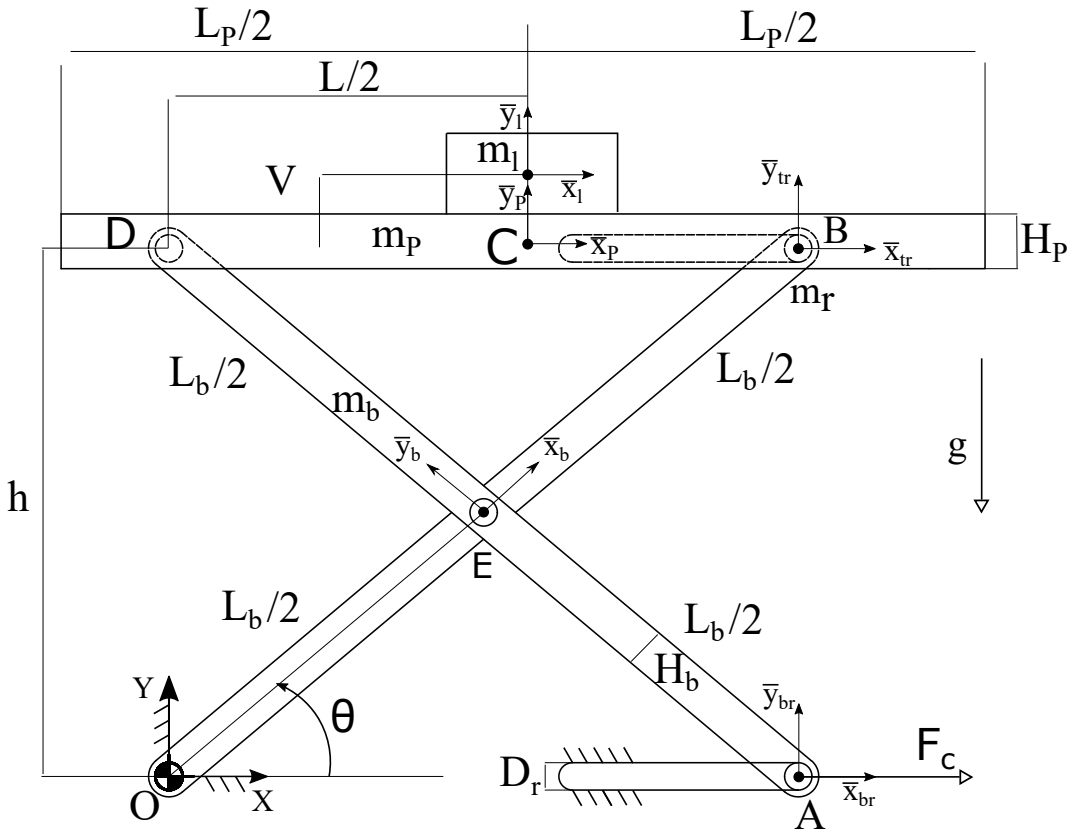

Figure 2. *Two-dimensional scheme for the minimal coordinate multibody model of the pantograph scissor lift mechanism.*

Considering a minimal coordinate formulation approach, the dimension n_q of the system generalized coordinate vector is equal to the number of the system degrees of freedom n_f. In particular, the pantograph scissor lift mechanism has only $n_f = 1$ degree of freedom. In this case, by following the minimal coordinate formulation approach, the system generalized coordinate vector contains only $n_q = n_f = 1$ Lagrangian coordinate. It is, therefore, assumed that the angular displacement of the front left bar denoted with $\theta \equiv \theta(t)$ is used as the system generalized coordinate denoted with $q \equiv q(t)$, where t denotes the independent variable describing the time. As shown in Figure 2, the two-dimensional multibody model of the pantograph scissor lift mechanism based on a minimal set of Lagrangian coordinates presents a set of geometric points of interest denoted with O, A, B, C, D, and E. Thus, the absolute position vectors of the points of interest belonging to the multibody system model developed here can be explicitly written in terms of the system Lagrangian coordinate as follows:

$$\boldsymbol{r}_O = \begin{bmatrix} x_O \\ y_O \end{bmatrix} = \begin{bmatrix} 0 \\ 0 \end{bmatrix}, \quad \boldsymbol{r}_A = \begin{bmatrix} x_A \\ y_A \end{bmatrix} = \begin{bmatrix} L\cos(\theta) \\ 0 \end{bmatrix} \tag{17}$$

$$\boldsymbol{r}_B = \begin{bmatrix} x_B \\ y_B \end{bmatrix} = \begin{bmatrix} L\cos(\theta) \\ L\sin(\theta) \end{bmatrix}, \quad \boldsymbol{r}_C = \begin{bmatrix} x_C \\ y_C \end{bmatrix} = \begin{bmatrix} \frac{L}{2} \\ L\sin(\theta) \end{bmatrix} \tag{18}$$

$$\boldsymbol{r}_D = \begin{bmatrix} x_D \\ y_D \end{bmatrix} = \begin{bmatrix} 0 \\ L\sin(\theta) \end{bmatrix}, \quad \boldsymbol{r}_E = \begin{bmatrix} x_E \\ y_E \end{bmatrix} = \begin{bmatrix} \frac{L}{2}\cos(\theta) \\ \frac{L}{2}\sin(\theta) \end{bmatrix} \tag{19}$$

where L represents the length of the bars, while the vectors $\boldsymbol{r}_O \equiv \boldsymbol{r}_O(\theta, t)$, $\boldsymbol{r}_A \equiv \boldsymbol{r}_A(\theta, t)$, $\boldsymbol{r}_B \equiv \boldsymbol{r}_B(\theta, t)$, $\boldsymbol{r}_C \equiv \boldsymbol{r}_C(\theta, t)$, $\boldsymbol{r}_D \equiv \boldsymbol{r}_D(\theta, t)$, and $\boldsymbol{r}_E \equiv \boldsymbol{r}_E(\theta, t)$ having dimension d respectively represent the absolute position vectors of the geometric points of interest identified as O, A, B, C, D, and E. Similarly, the absolute velocity vectors of the geometric points of interest can be expressed as follows:

$$\dot{\boldsymbol{r}}_O = \begin{bmatrix} \dot{x}_O \\ \dot{y}_O \end{bmatrix} = \begin{bmatrix} 0 \\ 0 \end{bmatrix}, \quad \dot{\boldsymbol{r}}_A = \begin{bmatrix} \dot{x}_A \\ \dot{y}_A \end{bmatrix} = \begin{bmatrix} -L\sin(\theta)\dot{\theta} \\ 0 \end{bmatrix} \tag{20}$$

$$\dot{\boldsymbol{r}}_B = \begin{bmatrix} \dot{x}_B \\ \dot{y}_B \end{bmatrix} = \begin{bmatrix} -L\sin(\theta)\dot{\theta} \\ L\cos(\theta)\dot{\theta} \end{bmatrix}, \quad \dot{\boldsymbol{r}}_C = \begin{bmatrix} \dot{x}_C \\ \dot{y}_C \end{bmatrix} = \begin{bmatrix} 0 \\ L\cos(\theta)\dot{\theta} \end{bmatrix} \tag{21}$$

$$\dot{\boldsymbol{r}}_D = \begin{bmatrix} \dot{x}_D \\ \dot{y}_D \end{bmatrix} = \begin{bmatrix} 0 \\ L\cos(\theta)\dot{\theta} \end{bmatrix}, \quad \dot{\boldsymbol{r}}_E = \begin{bmatrix} \dot{x}_E \\ \dot{y}_E \end{bmatrix} = \begin{bmatrix} -\frac{L}{2}\sin(\theta)\dot{\theta} \\ \frac{L}{2}\cos(\theta)\dot{\theta} \end{bmatrix} \tag{22}$$

where the vectors $\dot{\boldsymbol{r}}_O \equiv \dot{\boldsymbol{r}}_O(\theta,\dot{\theta},t)$, $\dot{\boldsymbol{r}}_A \equiv \dot{\boldsymbol{r}}_A(\theta,\dot{\theta},t)$, $\dot{\boldsymbol{r}}_B \equiv \dot{\boldsymbol{r}}_B(\theta,\dot{\theta},t)$, $\dot{\boldsymbol{r}}_C \equiv \dot{\boldsymbol{r}}_C(\theta,\dot{\theta},t)$, $\dot{\boldsymbol{r}}_D \equiv \dot{\boldsymbol{r}}_D(\theta,\dot{\theta},t)$, and $\dot{\boldsymbol{r}}_E \equiv \dot{\boldsymbol{r}}_E(\theta,\dot{\theta},t)$ having dimension d respectively represent the absolute velocity vectors of the geometric points of interest identified as O, A, B, C, D, and E. As mentioned before, the pantograph scissor lift mechanism is formed by $N_b = 9$ rigid bodies. However, considering a simplified kinematic description that exploits the system planar motion, only five categories of rigid bodies are relevant for developing a minimal coordinate multibody model. These are the platform (first body category labeled with the subscript p), the load (second body category labeled with the subscript l), the bar (third body category labeled with the subscript b), the bottom roller (fourth body category labeled with the subscript br), and the top roller (fifth body category labeled with the subscript tr). The body category identified as the platform includes only the lift table (body number $i = 5$). The body category identified as the load includes only a rigid body attached to the lift table (body number $i = 5$). The body category identified as the bar includes the front left bar (body number $i = 1$), the front right bar (body number $i = 2$), the rear left bar (body number $i = 3$), and the rear right bar (body number $i = 4$). The body category identified as the bottom roller includes the front bottom roller (body number $i = 6$) and the rear bottom roller (body number $i = 8$). The body category identified as the top roller includes the front top roller (body number $i = 7$) and the rear top roller (body number $i = 9$). Considering the body categories thereby defined, and taking into account the analytical description of the points of interest belonging to the planar mechanism, one can readily identify the kinematic quantities necessary for the formulation of the dynamic model of the pantograph scissor lift multibody system. To this end, considering the absolute position vectors of the reference points introduced above, one can write:

$$h_p = y_C = L\sin(\theta), \quad h_l = y_C + V = L\sin(\theta) + V \tag{23}$$

$$h_b = y_E = \frac{L}{2}\sin(\theta), \quad h_{br} = y_A = 0, \quad h_{tr} = y_B = L\sin(\theta) \tag{24}$$

where the constant geometric quantity denoted with V represents the height of the load with respect to the platform shown in Figure 2, while $h_p \equiv h_p(\theta,t)$, $h_l \equiv h_l(\theta,t)$, $h_b \equiv h_b(\theta,t)$, $h_{br} \equiv h_{br}(\theta,t)$, and $h_{tr} \equiv h_{tr}(\theta,t)$ respectively represent the centroid altitudes in relation to the ground level of the five categories of rigid bodies identified as the platform, the load, the bar, the bottom roller, and the top roller. By adopting the same approach, considering the absolute velocity vectors of the reference points, one can also write:

$$v_p = \sqrt{\dot{x}_C^2 + \dot{y}_C^2} = L\cos(\theta)\dot{\theta} \tag{25}$$

$$v_l = \sqrt{\dot{x}_C^2 + \dot{y}_C^2} = L\cos(\theta)\dot{\theta} \tag{26}$$

$$v_b = \sqrt{\dot{x}_E^2 + \dot{y}_E^2} = \frac{L}{2}\dot{\theta} \tag{27}$$

$$v_{br} = \sqrt{\dot{x}_A^2 + \dot{y}_A^2} = L\sin(\theta)\dot{\theta}, \quad v_{tr} = \sqrt{\dot{x}_B^2 + \dot{y}_B^2} = L\dot{\theta} \tag{28}$$

where $v_p \equiv v_p(\theta,\dot{\theta},t)$, $v_l \equiv v_l(\theta,\dot{\theta},t)$, $v_b \equiv v_b(\theta,\dot{\theta},t)$, $v_{br} \equiv v_{br}(\theta,\dot{\theta},t)$, and $v_{tr} \equiv v_{tr}(\theta,\dot{\theta},t)$ respectively represent the magnitudes of the centroid linear velocities of the five categories of rigid bodies identified as the platform, the load, the bar, the bottom roller, and the top roller. Furthermore, it can be easily proved that the following equations hold:

$$\omega_p = 0, \quad \omega_l = 0, \quad \omega_b = \dot{\theta}, \quad \omega_{br} = 0, \quad \omega_{tr} = 0 \tag{29}$$

where $\omega_p \equiv \omega_p(\dot{\theta},t)$, $\omega_l \equiv \omega_l(\dot{\theta},t)$, $\omega_b \equiv \omega_b(\dot{\theta},t)$, $\omega_{br} \equiv \omega_{br}(\dot{\theta},t)$, and $\omega_{tr} \equiv \omega_{tr}(\dot{\theta},t)$ respectively represent the magnitudes of the angular velocities of the five categories of rigid bodies identified as the platform, the load, the bar, the bottom roller, and the top roller. In fact, considering a frame of reference attached to each body as shown in Figure 2, it is apparent that the only rigid bodies that rotate are the bars, while the other rigid bodies carry out only a translational motion. Finally, the velocity functions necessary for modeling the presence of velocity-proportional frictional forces that affect the translational motion of the rollers are given by:

$$\dot{\Delta}_{br} = \dot{x}_A = -L\sin(\theta)\dot{\theta}, \quad \dot{\Delta}_{tr} = \dot{x}_B = -L\sin(\theta)\dot{\theta} \tag{30}$$

where $\dot{\Delta}_{br} \equiv \dot{\Delta}_{br}(\theta,\dot{\theta},t)$ and $\dot{\Delta}_{tr} \equiv \dot{\Delta}_{tr}(\theta,\dot{\theta},t)$ respectively represent the velocity functions relative to the viscous friction forces acting on the bottom roller and on the top roller.

4.2 Static analysis

In order to identify the equilibrium configuration assumed by the pantograph scissor lift mechanism when a given constant control action is applied to it, a static analysis is required first. To effectively perform this task, one can readily employ the stationary version of the Lagrange equations of the second kind. To this end, it is necessary to derive the total potential energy of the mechanical system, as well as the total virtual work of the external nonconservative forces acting on it. In the kinematic modeling of the pantograph scissor lift mechanism, five categories of rigid bodies are recognized, namely the platform, the load, the bar, the bottom roller, and the top roller. Thus, the gravitational potential energies associated with the five categories of rigid bodies mentioned before can be computed as follows:

$$U_p = m_p g h_p = m_p g L\sin(\theta), \quad U_l = m_l g h_l = m_l g L\sin(\theta) + m_l g V \tag{31}$$

$$U_b = m_b g h_b = m_b g \frac{L}{2}\sin(\theta) \tag{32}$$

$$U_{br} = m_r g h_{br} = 0, \quad U_{tr} = m_r g h_{tr} = m_r g L\sin(\theta) \tag{33}$$

where g is the gravity acceleration, m_p is the platform mass, m_l is the load mass, m_b is the bar mass, m_r is the roller mass, whereas $U_p \equiv U_p(\theta,t)$ is the platform potential energy, $U_l \equiv U_l(\theta,t)$ is the load potential energy, $U_b \equiv U_b(\theta,t)$ is the bar potential energy, $U_{br} \equiv U_{br}(\theta,t)$ is the bottom roller potential energy, and $U_{tr} \equiv U_{tr}(\theta,t)$ is the top roller potential energy. Consequently, the total potential energy of the mechanical system is given by:

$$U = U_p + U_l + 4U_b + 2U_{br} + 2U_{tr} = m_e g L\sin(\theta) + m_l g V \tag{34}$$

where:

$$m_e = m_p + m_l + 2m_b + 2m_r \tag{35}$$

where m_e is the equivalent mass associated with the gravitational potential energy and $U \equiv U(\theta, t)$ is the system total potential energy. On the other hand, the virtual work of the control force F_c applied to the left bottom roller collocated at the point A of the pantograph scissor lift mechanism can be computed as follows:

$$\delta W_c = F_c \delta x_A = -F_c L \sin(\theta) \delta\theta \tag{36}$$

where $\delta W_c \equiv \delta W_c(\theta, \delta\theta, t)$ represents the virtual work of the external control action. For the pantograph scissor lift mechanism, the stationary version of the Lagrange equations of the second kind assumes the following particular form:

$$\frac{\partial U}{\partial \theta} = \frac{\delta W_c}{\delta \theta} \tag{37}$$

which leads to:

$$m_e g L \cos(\theta) = -F_c L \sin(\theta) \tag{38}$$

or equivalently:

$$F_c = -m_e g \cot(\theta) \tag{39}$$

From Equation (39), one can determine the external control force identified as F_e necessary for obtaining a given angular displacement of static equilibrium denoted with θ_e. For instance, assuming that θ_0 represents the initial angular displacement of the pantograph scissor lift mechanism considered at the rest configuration, the external control force necessary for guaranteeing the state of static equilibrium is denoted with F_0 and can be readily obtained from Equation (39). As will be shown in detail in the following subsections of the paper, the explicit computation of the equilibrium control forces, to be applied to the pantograph scissor lift mechanism for obtaining a preassigned set of equilibrium configurations, represents a fundamental preliminary step in the design of the control system for the implementation of a quasi-static control strategy.

4.3 Dynamic analysis

For the problem under consideration, the dynamic analysis is necessary for describing the time evolution of the pantograph scissor lift mechanism when a given time law of the external control action is considered, as well as for the proper design of an effective control policy. For this purpose, the analytical derivation of the system equation of motion is required. To carry out this task, one can directly use the complete version of the Lagrange equations of the second kind, which preliminarily requires the analytical determination of the total kinetic and potential energies of the multibody system, the computation of the total Rayleigh dissipation function associated with the linear viscous forces, and the total virtual work of the external nonconservative actions applied to it. In the kinematic modeling of the pantograph scissor lift mechanism, five categories of rigid bodies are recognized, namely the platform, the load, the bar, the bottom roller, and the top roller. Therefore, the kinetic energies associated with the five categories of rigid bodies mentioned before can be computed as follows:

$$T_p = \frac{1}{2} m_p v_p^2 + \frac{1}{2} I_{zz,p} \omega_p^2 = \frac{1}{2} I_{e,p} \dot{\theta}^2 \tag{40}$$

$$T_l = \frac{1}{2} m_l v_l^2 + \frac{1}{2} I_{zz,l} \omega_l^2 = \frac{1}{2} I_{e,l} \dot{\theta}^2 \tag{41}$$

$$T_b = \frac{1}{2} m_b v_b^2 + \frac{1}{2} I_{zz,b} \omega_b^2 = \frac{1}{2} I_{e,b} \dot{\theta}^2 \tag{42}$$

$$T_{br} = \frac{1}{2} m_r v_{br}^2 + \frac{1}{2} I_{zz,r} \omega_{br}^2 = \frac{1}{2} I_{e,br} \dot{\theta}^2 \tag{43}$$

$$T_{tr} = \frac{1}{2} m_r v_{tr}^2 + \frac{1}{2} I_{zz,r} \omega_{tr}^2 = \frac{1}{2} I_{e,tr} \dot{\theta}^2 \tag{44}$$

where:

$$I_{e,p} = m_p L^2 \cos^2(\theta), \quad I_{e,l} = m_l L^2 \cos^2(\theta) \tag{45}$$

and

$$I_{e,b} = \frac{1}{4} m_b L^2 + I_{zz,b}, \quad I_{e,br} = m_r L^2 \sin^2(\theta), \quad I_{e,tr} = m_r L^2 \tag{46}$$

where m_p is the platform mass, m_l is the load mass, m_b is the bar mass, m_r is the roller mass, $I_{zz,p}$ is the platform mass moment of inertia, $I_{zz,l}$ is the load mass moment of inertia, $I_{zz,b}$ is the bar mass moment of inertia, $I_{zz,r}$ is the roller mass moment of inertia, while $T_p \equiv T_p(\theta, \dot{\theta}, t)$ is the platform kinetic energy, $T_l \equiv T_l(\theta, \dot{\theta}, t)$ is the load kinetic energy, $T_b \equiv T_b(\theta, \dot{\theta}, t)$ is the bar kinetic energy, $T_{br} \equiv T_{br}(\theta, \dot{\theta}, t)$ is the bottom roller kinetic energy, $T_{tr} \equiv T_{tr}(\theta, \dot{\theta}, t)$ is the top roller kinetic energy, whereas $I_{e,p} \equiv I_{e,p}(\theta, t)$ is the platform equivalent mass moment of inertia, $I_{e,l} \equiv I_{e,l}(\theta, t)$ is the load equivalent mass moment of inertia, $I_{e,b} \equiv I_{e,b}(\theta, t)$ is the bar equivalent mass moment of inertia, $I_{e,br} \equiv I_{e,br}(\theta, t)$ is the bottom roller equivalent mass moment of inertia, and $I_{e,tr} \equiv I_{e,tr}(\theta, t)$ is the top roller equivalent mass moment of inertia. Thus, the total kinetic energy of the mechanical system is given by:

$$T = T_p + T_l + 4T_b + 2T_{br} + 2T_{tr} = \frac{1}{2} I_e \dot{\theta}^2 \tag{47}$$

where:

$$\begin{aligned} I_e &= I_{e,p} + I_{e,l} + 4I_{e,b} + 2I_{e,br} + 2I_{e,tr} \\ &= m_w L^2 \cos^2(\theta) + m_b L^2 + 4I_{zz,b} + 2m_r L^2 \sin^2(\theta) + 2m_r L^2 \end{aligned} \tag{48}$$

and

$$m_w = m_p + m_l \tag{49}$$

where m_w is the equivalent mass associated with the kinetic energy of the platform and the load, $I_e \equiv I_e(\theta, t)$ is the system total equivalent mass moment of inertia, and $T = T(\theta, \dot{\theta}, t)$ is the system total kinetic energy. On the other hand, it is assumed that frictional forces modeled as viscous damping act on the rollers of the pantograph scissor lift mechanism. Therefore, the Rayleigh dissipation functions corresponding to the viscous friction forces applied on the rollers can be calculated as follows:

$$R_{br} = \frac{1}{2}\sigma\dot{\Delta}_{br}^2 = \frac{1}{2}\sigma L^2 \sin^2(\theta)\dot{\theta}^2, \quad R_{tr} = \frac{1}{2}\sigma\dot{\Delta}_{tr}^2 = \frac{1}{2}\sigma L^2 \sin^2(\theta)\dot{\theta}^2 \tag{50}$$

where σ represents the viscous damping coefficient necessary for analytically modeling the friction forces in the rollers employing a simplified formulation. Thus, the total Rayleigh dissipation function of the mechanical system is given by:

$$R = 2R_{br} + 2R_{tr} = \frac{1}{2}\left(\sigma_e L^2 \sin^2(\theta)\right)\dot{\theta}^2 \tag{51}$$

where:

$$\sigma_e = 4\sigma \tag{52}$$

where σ_e is the equivalent viscous coefficient associated with the Rayleigh dissipation function of the rollers. For the pantograph scissor lift mechanism, the complete version of the Lagrange equations of the second kind is given by the following particular form:

$$\frac{d}{dt}\frac{\partial T}{\partial \dot{\theta}} - \frac{\partial T}{\partial \theta} + \frac{\partial R}{\partial \dot{\theta}} + \frac{\partial U}{\partial \theta} = \frac{\delta W_c}{\delta \theta} \tag{53}$$

After some simple mathematical manipulations, Equation (53) leads to:

$$\begin{gathered}\left(m_w L^2 \cos^2(\theta) + m_b L^2 + 4I_{zz,b} + 2m_r L^2 \sin^2(\theta) + 2m_r L^2\right)\ddot{\theta} = \\ -m_v L^2 \sin(2\theta)\dot{\theta}^2 - m_e g L \cos(\theta) - \sigma_e L^2 \sin^2(\theta)\dot{\theta} - F_c L \sin(\theta)\end{gathered} \tag{54}$$

or equivalently:

$$I_e \ddot{\theta} = f_e \tag{55}$$

where:

$$f_e = -m_v L^2 \sin(2\theta)\dot{\theta}^2 - m_e g L \cos(\theta) - \sigma_e L^2 \sin^2(\theta)\dot{\theta} - F_c L \sin(\theta) \tag{56}$$

and

$$m_v = m_r - \frac{1}{2}m_w \tag{57}$$

where m_v is the equivalent mass of the inertia generalized quadratic velocity forces associated with the rollers, the platform, and the load, whereas I_e is the system total equivalent mass moment of inertia defined in Equation (48), and $f_e \equiv f_e(\theta, \dot{\theta}, t)$ is a highly nonlinear function which describes the total generalized forces that affect the mechanical system, including the quadratic inertia terms, the conservative external terms, and the nonconservative external terms. Finally, to further clarify the mathematical structure of the dynamic equation that governs the motion of the pantograph scissor lift mechanism, Equation (55) can be rewritten as:

$$I_e \ddot{\theta} = f_b + f_c \tag{58}$$

where:

$$f_b = -m_v L^2 \sin(2\theta)\dot{\theta}^2 - m_e g L \cos(\theta) - \sigma_e L^2 \sin^2(\theta)\dot{\theta}, \quad f_c = -F_c L \sin(\theta) \tag{59}$$

where $f_b \equiv f_b(\theta, \dot{\theta}, t)$ represents the nonlinear generalized force field that describes all the uncontrollable forces acting on the system, while $f_c \equiv f_c(\theta, \dot{\theta}, t)$ identifies another nonlinear generalized force field that models the system external forces which can be arbitrarily controlled. As mentioned before, the system equation of motion assumes a highly nonlinear form because of the presence of the generalized inertial, gravitational, viscous, and control force terms. As a consequence, for performing time simulations of the dynamical behavior of the pantograph scissor lift mechanism, it is necessary to adopt a numerical integration strategy that leads to a numerical approximation of the system evolution in time. This can be done, for example, by solving a forward dynamics problem and determining the system time response to a given time law designed for its external control action. On the other hand, knowing the analytical form of the system equation of motion is also vital for constructing an effective control strategy, as thoroughly discussed below.

4.4 Controller design

As demonstrated before, although the pantograph scissor lift mechanism considered as the case study has only one degree of freedom, the dynamic behavior of this mechanical system is highly nonlinear. Therefore, it is necessary to adopt a suitable nonlinear control strategy to properly guide the motion of this articulated mechanical system. To achieve this goal, a combination of a feedforward controller plus a feedback control action is considered for the actuator force, which can be written as:

$$F_c = F_{c,FF} + F_{c,FB} \tag{60}$$

where $F_c \equiv F_c(\theta, \dot{\theta}, t)$ denotes the force field representing the total control action, $F_{c,FF} \equiv F_{c,FF}(t)$ denotes the forcing function associated with the feedforward control action, and $F_{c,FB} \equiv F_{c,FB}(\theta, \dot{\theta}, t)$ denotes the force field describing the feedback control action. The key idea devised in this paper for the design of an effective nonlinear controller suitable for the pantograph scissor lift mechanism is to adopt a quasi-static control strategy for the synthesis of the feedforward controller and a proportional-derivative control strategy for the synthesis of the feedback controller. Before carrying out the design of the control system by following the proposed approach, some fundamental analytical quantities are recalled and introduced. First, since θ represents the angular displacement of the front left bar chosen as the system degree of freedom, it is assumed that the pantograph scissor lift mechanism starts its motion from an initial rest configuration in which $\theta(t = 0) = \theta_0$ and ends its movement into a final equilibrium configuration in which $\theta(t = T_s) = \theta_e$, where θ_0 denotes the initial equilibrium angular displacement, θ_e denotes the final equilibrium angular displacement, and T_s is the constant time span in which the entire motion occurs. Furthermore, for simplicity, and considering

the same conditions, it is assumed that the time function $h \equiv h(t)$ represents the platform vertical displacement, whereas the time function $s \equiv s(t)$ represents the horizontal displacement of the front bottom roller, to which the external control action F_c is applied. In particular, it is apparent that these quantities can be analytically computed in terms of the system generalized coordinate θ as $h = L\sin(\theta)$ and $s = L\cos(\theta)$. Thus, one can easily realize that, when the system is in the initial equilibrium configuration identified by the angular displacement θ_0, then the platform vertical displacement is equal to h_0 since a constant equilibrium force F_0 is applied to the roller and its horizontal displacement is equal to s_0. Similarly, when the system is in the final equilibrium configuration identified by the angular displacement θ_e, then the platform vertical displacement is equal to h_e since a constant equilibrium force F_e is applied to the roller and its horizontal displacement is equal to s_e. These considerations immediately suggest that a quasi-static controller can be employed as the feedforward control action $F_{c,FF}$ by adopting the following time law:

$$F_{c,FF} = F_a, \quad F_a = \begin{cases} F_0 + \left(3\tau^2 - 2\tau^3\right)\Delta F_{e,0}, & t < T_a \\ F_e, & t \geq T_a \end{cases} \tag{61}$$

where:

$$\tau = \frac{t}{T_a}, \quad \Delta F_{e,0} = F_e - F_0 \tag{62}$$

where $F_a \equiv F_a(t)$ is the time law of the quasi-static control strategy, $\tau \equiv \tau(t)$ is a dimensionless time variable, T_a is the constant actuation time representing the time span in which the quasi-static controller operates, and $\Delta F_{e,0}$ is the constant variation between the two control forces corresponding to the desired equilibrium configurations. In particular, to prevent any shocks of the lift table of the pantograph mechanism, the time law F_a considered as the quasi-static control action is obtained as a cubic polynomial in terms of the time variable t, which guarantees that the control action starts from the initial value F_0 with a horizontal slope and ends to the final value F_e again with a horizontal tangent line. In theory, it is sufficient to use the explicit time law F_a based on the quasi-static control strategy as the feedforward control action $F_{c,FF}$ for guaranteeing a smooth motion of the table platform between the two desired equilibrium configurations. However, in practice, it is well known that any feedforward controllers alone do not represent a robust solution for controlling an articulated mechanical system, especially in the case of a nonlinear dynamical system. This is particularly relevant even in the case of computer simulations, in which no external disturbances are present, but where the numerical integration errors associated with the approximate solution of the equations of motion play the role of unpredictable external perturbations. This is the reason behind the introduction of an additional controller having a feedback architecture denoted with $F_{c,FB}$. For this purpose, a proportional-derivative feedback controller is adopted in this paper, leading to the following mathematical structure of the feedback control action:

$$F_{c,FB} = F_b, \quad F_b = -k_c\delta - \sigma_c\dot{\delta} \tag{63}$$

where:

$$\delta = s - s_e = L\cos(\theta) - s_e, \quad \dot{\delta} = \dot{s} - \dot{s}_e = -L\sin(\theta)\dot{\theta} \tag{64}$$

where $F_b \equiv F_b(\theta, \dot{\theta}, t)$ represents the particular proportional-derivative control architecture assumed for the feedback control action, $\delta \equiv \delta(\theta, t)$ identifies the deviation of the roller horizontal position from the final configuration of static equilibrium, whereas k_c and σ_c are two control constants to be properly determined for tuning the feedback controller. Therefore, while the design of a suitable feedforward controller requires the proper selection of the actuation time parameter T_a, the synthesis of an effective feedback controller reduces to the determination of the constant parameters k_c and σ_c that characterize the proportional-derivative control scheme. For the selection of the feedforward actuation time T_a, a trial-and-error strategy is necessary. Conversely, the definition of the feedback control parameters k_c and σ_c can be methodologically performed by analyzing the linear version of the system equation of motion perturbed around the desired final configuration of static equilibrium. To carry out this task, the first step is to derive the analytical form assumed by the nonlinear control action F_c, as well as by the nonlinear control force field f_c, when the combination of the quasi-static controller with the proportional-derivative controller is used. To this end, one can write:

$$F_c = F_{c,FF} + F_{c,FB} = F_a + F_b = F_a - k_c\left(L\cos(\theta) - s_e\right) + \sigma_c L\sin(\theta)\dot{\theta} \tag{65}$$

which leads to:

$$\begin{aligned} f_c &= -F_c L\sin(\theta) \\ &= -F_a L\sin(\theta) + k_c\left(L\cos(\theta) - s_e\right)L\sin(\theta) - \sigma_c L^2\sin^2(\theta)\dot{\theta} \end{aligned} \tag{66}$$

Subsequently, to obtain the linear version of the system equation of motion expressed in the equivalent form given by Equation (58), one needs to linearize both the left and right-hand sides of this dynamic equation. To achieve this goal, consider the following perturbation functions:

$$\bar{\theta} = \theta - \theta_e, \quad \dot{\bar{\theta}} = \dot{\theta}, \quad \ddot{\bar{\theta}} = \ddot{\theta} \tag{67}$$

where $\bar{\theta}$ represents the angular displacement of the front left bar perturbed from its equilibrium configuration θ_e, whereas $\dot{\bar{\theta}}$ and $\ddot{\bar{\theta}}$ respectively denote the first and second time derivatives of the same analytical function. The linearization process is based on a Taylor expansion of the system equation of motion truncated at the first order, which leads to the following linearized dynamic model:

$$\bar{I}_e\ddot{\bar{\theta}} + \bar{\sigma}_e\dot{\bar{\theta}} + \bar{k}_e\bar{\theta} = 0 \tag{68}$$

where $\bar{I}_e$, $\bar{\sigma}_e$, and $\bar{k}_e$ respectively denote the constant coefficients associated with the equivalent inertia, damping, and stiffness terms of the linearized system. The equivalent inertia coefficient denoted with $\bar{I}_e$ that appears in the linearized dynamic model is readily defined as follows:

$$\begin{aligned} \bar{I}_e &= I_e(\theta = \theta_e, t = T_s) \\ &= m_w L^2\cos^2(\theta_e) + m_b L^2 + 4I_{zz,b} + 2m_r L^2\sin^2(\theta_e) + 2m_r L^2 \end{aligned} \tag{69}$$

On the other hand, the equivalent damping and stiffness coefficients respectively denoted with $\bar{\sigma}_e$ and $\bar{k}_e$ that appears in the linearized dynamic model can be analytically computed by linearizing the uncontrollable force field denoted with f_b and the controllable force field denoted with f_c as follows:

$$\begin{aligned}\bar{\sigma}_e &= -\frac{\partial f_b}{\partial \dot{\theta}}(\theta=\theta_e,\dot{\theta}=0,t=T_s) - \frac{\partial f_c}{\partial \dot{\theta}}(\theta=\theta_e,\dot{\theta}=0,t=T_s) \\ &= (\sigma_e+\sigma_c)\,L^2\sin^2(\theta_e)\end{aligned} \tag{70}$$

and

$$\begin{aligned}\bar{k}_e &= -\frac{\partial f_b}{\partial \theta}(\theta=\theta_e,\dot{\theta}=0,t=T_s) - \frac{\partial f_c}{\partial \theta}(\theta=\theta_e,\dot{\theta}=0,t=T_s) \\ &= -m_e g L\,(\sin(\theta_e)+\cot(\theta_e)\cos(\theta_e)) + k_c L^2\sin^2(\theta_e)\end{aligned} \tag{71}$$

It is, therefore, apparent that the equivalent stiffness and damping coefficients respectively denoted with $\bar{k}_e$ and $\bar{\sigma}_e$ depend on the proportional and derivative coefficients of the feedback controller respectively denoted with k_c and σ_c, while the other constant parameters that appear in Equations (70) and (71) assume known values. Thus, if the linearized stiffness and damping coefficients $\bar{k}_e$ and $\bar{\sigma}_e$ are known, one can determine the proportional and derivative coefficients k_c and σ_c that define the feedback control action by using the following inverse formulas:

$$k_c = \frac{\bar{k}_e}{L^2}\csc^2(\theta_e) + \frac{m_e g}{L}\csc(\theta_e)\left(1+\cot^2(\theta_e)\right) \tag{72}$$

and

$$\sigma_c = \frac{\bar{\sigma}_e}{L^2}\csc^2(\theta_e) - \sigma_e \tag{73}$$

To be able to effectively use Equations (72) and (73) for a proper design of the parameters that characterize the feedback control action, the following strategy is employed. First, one needs to define the desired natural frequency denoted with $\bar{f}_{n,d}$ and the desired damping ratio denoted with $\bar{\xi}_d$ for the linearized dynamical model of the pantograph system. Then, one can readily compute the linearized stiffness and damping coefficients $\bar{k}_e$ and $\bar{\sigma}_e$ of the linearized equation of motion in terms of the desired natural frequency and the desired damping ratio. The implementation of this analytical method leads to the following equations:

$$\left\{\begin{array}{l}\bar{f}_n = \frac{1}{2\pi}\sqrt{\frac{\bar{k}_e}{\bar{I}_e}} \\ \bar{f}_n = \bar{f}_{n,d}\end{array}\right. \quad \Rightarrow \quad \bar{k}_e = 4\pi^2\bar{I}_e\bar{f}_{n,d}^2 \tag{74}$$

and

$$\left\{\begin{array}{l}\bar{\xi} = \frac{\bar{\sigma}_e}{2\sqrt{\bar{k}_e\bar{I}_e}} \\ \bar{\xi} = \bar{\xi}_d\end{array}\right. \quad \Rightarrow \quad \bar{\sigma}_e = 2\sqrt{\bar{k}_e\bar{I}_e}\bar{\xi}_d \tag{75}$$

In conclusion, the use of Equations (74) and (75), necessary for the computation of the linearized stiffness and damping coefficients $\bar{k}_e$ and $\bar{\sigma}_e$, in conjunction with Equations (72) and (73), allows for the determination of the proportional and derivative coefficients k_c and σ_c of the feedback controller that guarantee the desired natural frequency and damping ratio $\bar{f}_{n,d}$ and $\bar{\xi}_d$ of the linearized dynamical model. The numerical values of the proportional and derivative coefficients k_c and σ_c obtained by implementing this method in correspondence of a given set of desired natural frequency and damping ratio $\bar{f}_{n,d}$ and $\bar{\xi}_d$ are provided in Table 3. It is important to note that the computational procedure shown herein for the determination of the proportional and derivative coefficients of the feedback controller provides analytical results that are fully consistent with those obtained from the direct application of the pole placement method considered in the control methodology proposed in the paper. As a final remark, the control strategy designed herein is composed of the combination of a feedforward controller based on a quasi-static strategy with a feedback controller based on a proportional-derivative architecture. As demonstrated through the use of numerical experiments, while the feedforward controller serves to guide the motion in large of the lift table towards the desired equilibrium configuration, the feedback controller is necessary for compensating the trajectory errors in the neighborhood of the final equilibrium configuration.

4.5 State-space representation

To be able to perform dynamical simulations using the minimal coordinate multibody model of the pantograph scissor lift mechanism, the nonlinear version of the system equation of motion given by Equation (55) must be transformed from the configuration space to the state space. Because of the presence of strong geometric nonlinearities, this transformation is necessary to enable the use of standard numerical integration procedures for the determination of an approximate solution of the system equation of motion. This simple process starts with the following definition of the system state vector:

$$\boldsymbol{z} = \left[\begin{array}{c} z_1 \\ z_2 \end{array}\right] = \left[\begin{array}{c} \theta \\ \dot{\theta} \end{array}\right] \tag{76}$$

where $\boldsymbol{z} \equiv \boldsymbol{z}(t)$ represents the state vector of the minimal coordinate multibody model having dimension $n_z = 2n_q = 2$. Consequently, the system state function obtained form the use of the minimal coordinate formulation is given by:

$$\boldsymbol{f} = \left[\begin{array}{c} f_1 \\ f_2 \end{array}\right] = \left[\begin{array}{c} \dot{\theta} \\ \ddot{\theta} \end{array}\right] = \left[\begin{array}{c} \dot{\theta} \\ \frac{f_e}{I_e} \end{array}\right] \tag{77}$$

where $\boldsymbol{f} \equiv \boldsymbol{f}(\boldsymbol{z},t)$ is the nonlinear state function having dimension n_z that describes the dynamics of the pantograph scissor lift mechanism in the space of states. Considering the previous definitions, the state-space form of the equation of motion arising from the minimal coordinate multibody formulation is given by:

$$\left\{\begin{array}{l}\dot{\boldsymbol{z}} = \boldsymbol{f} \\ \boldsymbol{z}(t=0) = \boldsymbol{z}_0\end{array}\right. \tag{78}$$

where $\boldsymbol{z}_0$ represents the vector of initial conditions defined as:

$$\boldsymbol{z}_0 = \begin{bmatrix} \theta_0 \\ 0 \end{bmatrix} \tag{79}$$

As mentioned before, the analytical formulation of the state-space model corresponding to the minimal coordinate multibody model of the pantograph scissor lift mechanism allows for readily performing dynamical simulations through the computer implementation of the dynamic model. This strategy allows for performing numerous numerical experiments on the time response of the pantograph scissor lift mechanism corresponding to the designed control policy, as shown in the numerical results section of the paper.

5. Redundant coordinate multibody model

5.1 Kinematic modeling

For the sake of completeness, the pantograph scissor lift mechanism is considered herein as a rigid multibody mechanical system modeled in a Euclidean space of dimension $d = 3$. A schematic representation of the three-dimensional multibody model of the pantograph scissor lift mechanism based on a redundant set of Lagrangian coordinates is shown in Figure 3.

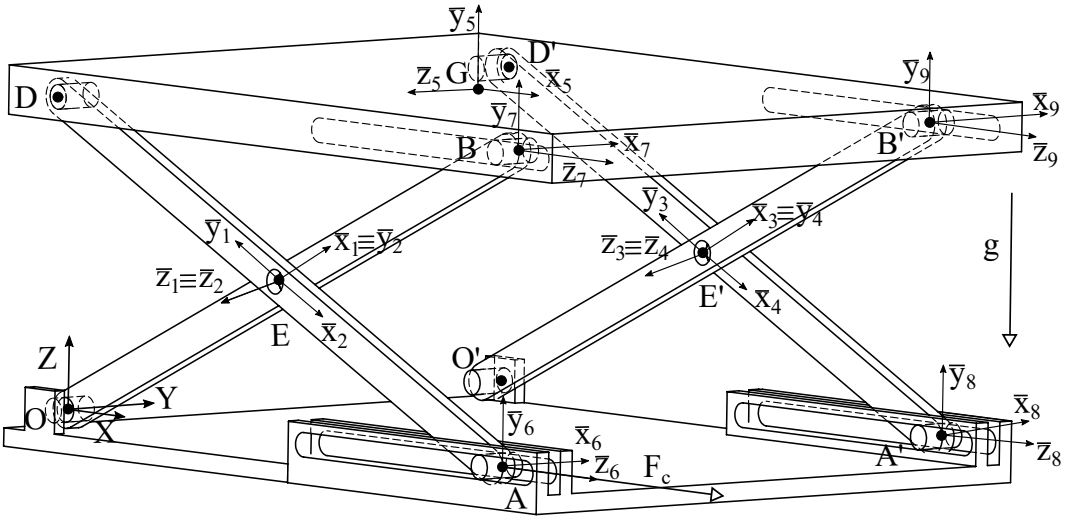

Figure 3. *Three-dimensional scheme for the redundant coordinate multibody model of the pantograph scissor lift mechanism.*

Considering a redundant coordinate formulation approach, the dimension n_q of the system generalized coordinate vector denoted with $\boldsymbol{q} \equiv \boldsymbol{q}(t)$ is larger than the number of the system degrees of freedom n_f. In particular, the pantograph scissor lift mechanism is composed of $N_b = 9$ rigid bodies and each body is described by a set of $n_b = n_d + n_p = 7$ generalized coordinates, where $n_d = d = 3$ represents the number of the body translational coordinates and $n_p = 4$ represents the number of the body rotational coordinates. Furthermore, to simplify the development of the redundant coordinate multibody model of the pantograph scissor lift mechanism, the inertial effects of the load are taken into account by considering an additional mass attached to the lift platform, that is, the body labeled with the integer $i = 5$, thereby avoiding the unnecessary introduction of an additional rigid body into the multibody model. In this case, by following the redundant coordinate formulation approach, the system generalized coordinate vector contains $n_q = N_b n_b = 63$ Lagrangian coordinates and is defined as follows:

$$\boldsymbol{q} = \begin{bmatrix} \boldsymbol{q}_1 \\ \boldsymbol{q}_2 \\ \vdots \\ \boldsymbol{q}_{N_b} \end{bmatrix} \tag{80}$$

where $\boldsymbol{q}_i \equiv \boldsymbol{q}_i(t)$ is a vector having dimension n_b representing the generalized coordinate vector of the generic rigid body labeled with the integer number i. It is, therefore, assumed that the set of Cartesian coordinates of the body centroid denoted with $\boldsymbol{R}_i \equiv \boldsymbol{R}_i(t)$ having dimension d is employed for representing the spatial position of each rigid body, whereas the set of Euler parameters denoted with $\boldsymbol{\theta}_i \equiv \boldsymbol{\theta}_i(t)$ having dimension n_p is used for representing the spatial orientation of each rigid body, where the subscript i identifies the body number. The previous vector quantities are respectively given by:

$$\boldsymbol{q}_i = \begin{bmatrix} \boldsymbol{R}_i \\ \boldsymbol{\theta}_i \end{bmatrix}, \quad i = 1, 2, \ldots, N_b \tag{81}$$

where:

$$\boldsymbol{R}_i = \begin{bmatrix} x_i \\ y_i \\ z_i \end{bmatrix}, \quad i = 1, 2, \ldots, N_b \tag{82}$$

and

$$\boldsymbol{p}_i = \begin{bmatrix} p_{1,i} \\ p_{2,i} \\ p_{3,i} \end{bmatrix}, \quad \boldsymbol{\theta}_i = \begin{bmatrix} p_{0,i} \\ \boldsymbol{p}_i \end{bmatrix}, \quad i = 1, 2, \ldots, N_b \tag{83}$$

where $x_i \equiv x_i(t)$, $y_i \equiv y_i(t)$, and $z_i \equiv z_i(t)$ denote the Cartesian coordinates describing the absolute position of the reference point chosen on each rigid body i, $\boldsymbol{p}_i \equiv \boldsymbol{p}_i(t)$ is a time-dependent vector of dimension $n_p - 1$, while $p_{0,i} \equiv p_{0,i}(t)$, $p_{1,i} \equiv p_{1,i}(t)$, $p_{2,i} \equiv p_{2,i}(t)$, and $p_{3,i} \equiv p_{3,i}(t)$ identify the set of Euler parameters describing the absolute orientation of each body-fixed reference frame. Assuming the set of Euler parameters as the body orientation coordinates, the rotation matrix of a generic rigid body i can be immediately constructed as follows:

$$\boldsymbol{A}_i = \boldsymbol{E}_i \bar{\boldsymbol{E}}_i^T, \quad i = 1, 2, \ldots, N_b \tag{84}$$

where:

$$\boldsymbol{E}_i = \begin{bmatrix} -\boldsymbol{p}_i & p_{0,i}\boldsymbol{I} + \tilde{\boldsymbol{p}}_i \end{bmatrix}, \quad \bar{\boldsymbol{E}}_i = \begin{bmatrix} -\boldsymbol{p}_i & p_{0,i}\boldsymbol{I} - \tilde{\boldsymbol{p}}_i \end{bmatrix}, \quad i = 1, 2, \ldots, N_b \tag{85}$$

and

$$\tilde{\boldsymbol{p}}_i = \begin{bmatrix} 0 & -p_{3,i} & p_{2,i} \\ p_{3,i} & 0 & -p_{1,i} \\ -p_{2,i} & p_{1,i} & 0 \end{bmatrix}, \quad i = 1, 2, \ldots, N_b \tag{86}$$

where $\boldsymbol{A}_i \equiv \boldsymbol{A}_i(\boldsymbol{\theta}_i, t)$ is the rotation matrix of the generic body i having dimensions $d \times d$, $\boldsymbol{E}_i \equiv \boldsymbol{E}_i(\boldsymbol{\theta}_i, t)$ and $\bar{\boldsymbol{E}}_i \equiv \bar{\boldsymbol{E}}_i(\boldsymbol{\theta}_i, t)$ are two time-dependent rectangular matrices of dimensions $d \times n_p$, $\boldsymbol{I}$ is the identity matrix having dimensions $d \times d$, and $\tilde{\boldsymbol{p}}_i \equiv \tilde{\boldsymbol{p}}_i(t)$ denotes a skew-symmetric matrix of dimensions $d \times d$ associated with the vector $\boldsymbol{p}_i$. Although the mathematical model of the pantograph scissor lift mechanism is constructed employing a redundant coordinate multibody approach based on the use of the set of Euler parameters as rotational coordinates, for the definition of the initial configuration of each body of the multibody model, and, in particular, for readily identifying the body initial orientation, it is more convenient to adopt as orientation parameters the set of Euler angles and then convert them into the equivalent set of Euler parameters. For this purpose, one can directly exploit the X, Y, Z sequence of Euler angles embedded in the following vector of rotational coordinates:

$$\boldsymbol{e}_i = \begin{bmatrix} \alpha_i \\ \beta_i \\ \gamma_i \end{bmatrix}, \quad i = 1, 2, \ldots, N_b \tag{87}$$

where $\boldsymbol{e}_i \equiv \boldsymbol{e}_i(t)$ is a time-dependent vector of dimension d containing the set of Euler angles, while $\alpha_i \equiv \alpha_i(t)$, $\beta_i \equiv \beta_i(t)$, and $\gamma_i \equiv \gamma_i(t)$ respectively denote the successive angular displacements performed about the current X, Y, and Z axes, carried out in order to transform the absolute frame of reference into the local reference system of the generic rigid body i. By doing so, one can obtain an equivalent form of the rotation matrix of each body as follows:

$$\boldsymbol{A}_i = \boldsymbol{A}_{x,i}\boldsymbol{A}_{y,i}\boldsymbol{A}_{z,i} = \begin{bmatrix} \boldsymbol{a}_i & \boldsymbol{b}_i & \boldsymbol{c}_i \end{bmatrix}, \quad i = 1, 2, \ldots, N_b \tag{88}$$

where:

$$\boldsymbol{A}_{x,i} = \begin{bmatrix} 1 & 0 & 0 \\ 0 & \cos(\alpha_i) & -\sin(\alpha_i) \\ 0 & \sin(\alpha_i) & \cos(\alpha_i) \end{bmatrix}, \quad i = 1, 2, \ldots, N_b \tag{89}$$

$$\boldsymbol{A}_{y,i} = \begin{bmatrix} \cos(\beta_i) & 0 & \sin(\beta_i) \\ 0 & 1 & 0 \\ -\sin(\beta_i) & 0 & \cos(\beta_i) \end{bmatrix}, \quad i = 1, 2, \ldots, N_b \tag{90}$$

$$\boldsymbol{A}_{z,i} = \begin{bmatrix} \cos(\gamma_i) & -\sin(\gamma_i) & 0 \\ \sin(\gamma_i) & \cos(\gamma_i) & 0 \\ 0 & 0 & 1 \end{bmatrix}, \quad i = 1, 2, \ldots, N_b \tag{91}$$

and

$$\boldsymbol{a}_i = \begin{bmatrix} a_{1,i} \\ a_{2,i} \\ a_{3,i} \end{bmatrix} = \begin{bmatrix} \cos(\beta_i)\cos(\gamma_i) \\ \sin(\alpha_i)\sin(\beta_i)\cos(\gamma_i) + \cos(\alpha_i)\sin(\gamma_i) \\ -\cos(\alpha_i)\sin(\beta_i)\cos(\gamma_i) + \sin(\alpha_i)\sin(\gamma_i) \end{bmatrix}, \quad i = 1, 2, \ldots, N_b \tag{92}$$

$$\boldsymbol{b}_i = \begin{bmatrix} b_{1,i} \\ b_{2,i} \\ b_{3,i} \end{bmatrix} = \begin{bmatrix} -\cos(\beta_i)\sin(\gamma_i) \\ \cos(\alpha_i)\cos(\gamma_i) - \sin(\alpha_i)\sin(\beta_i)\sin(\gamma_i) \\ \sin(\alpha_i)\cos(\gamma_i) + \cos(\alpha_i)\sin(\beta_i)\sin(\gamma_i) \end{bmatrix}, \quad i = 1, 2, \ldots, N_b \tag{93}$$

$$\boldsymbol{c}_i = \begin{bmatrix} c_{1,i} \\ c_{2,i} \\ c_{3,i} \end{bmatrix} = \begin{bmatrix} \sin(\beta_i) \\ -\sin(\alpha_i)\cos(\beta_i) \\ \cos(\alpha_i)\cos(\beta_i) \end{bmatrix}, \quad i = 1, 2, \ldots, N_b \tag{94}$$

where $\boldsymbol{A}_{x,i} \equiv \boldsymbol{A}_{x,i}(\boldsymbol{e}_i, t)$, $\boldsymbol{A}_{y,i} \equiv \boldsymbol{A}_{y,i}(\boldsymbol{e}_i, t)$, and $\boldsymbol{A}_{z,i} \equiv \boldsymbol{A}_{z,i}(\boldsymbol{e}_i, t)$ respectively represent three elemental rotation matrices obtained considering the three fundamental rotations about the axes X, Y, and Z, whereas $\boldsymbol{a}_i \equiv \boldsymbol{a}_i(\boldsymbol{e}_i, t)$, $\boldsymbol{b}_i \equiv \boldsymbol{b}_i(\boldsymbol{e}_i, t)$, and $\boldsymbol{c}_i \equiv \boldsymbol{c}_i(\boldsymbol{e}_i, t)$ denote three unit vectors associated with the X, Y, and Z axes of the body-fixed frame of reference pertaining to the generic rigid body i. To derive the particular set of Euler parameters $\boldsymbol{\theta}_i$ that corresponds to a given set of Euler angles $\boldsymbol{e}_i$, the first task to be performed is the computation of the trace of the rotation matrix $\boldsymbol{A}_i$ constructed by using the set of Euler angles as rotational coordinates. To this end, one can write:

$$\tau_i = \mathrm{tr}(\boldsymbol{A}_i) = a_{1,i} + b_{2,i} + c_{3,i}, \quad i = 1, 2, \ldots, N_b \tag{95}$$

where $\tau_i \equiv \tau_i(\boldsymbol{e}_i, t)$ is the trace of the rotation matrix $\boldsymbol{A}_i$ expressed by using the set of Euler angles $\boldsymbol{e}_i$ for a given rigid body i. Subsequently, one can readily calculate the first Euler parameter $p_{0,i}$ as follows:

$$p_{0,i} = \frac{1}{2}\sqrt{1+\tau_i}, \quad i = 1, 2, \ldots, N_b \tag{96}$$

Finally, the remaining three Euler parameters $p_{1,i}$, $p_{2,i}$, and $p_{3,i}$ can be determined employing one of the two sets of formulas reported below:

$$p_{0,i} \neq 0 \quad \Rightarrow \quad \begin{cases} p_{1,i} = \frac{b_{3,i} - c_{2,i}}{4p_{0,i}} \\ p_{2,i} = \frac{c_{1,i} - a_{3,i}}{4p_{0,i}} \\ p_{3,i} = \frac{a_{2,i} - b_{1,i}}{4p_{0,i}} \end{cases}, \quad i = 1, 2, \ldots, N_b \tag{97}$$

or

$$p_{0,i} = 0 \quad \Rightarrow \quad \begin{cases} p_{1,i} = \sqrt{\frac{1}{4}\left(1 + 2a_{1,i} - \tau_i\right)} \\ p_{2,i} = \sqrt{\frac{1}{4}\left(1 + 2b_{2,i} - \tau_i\right)} \\ p_{3,i} = \sqrt{\frac{1}{4}\left(1 + 2c_{3,i} - \tau_i\right)} \end{cases}, \quad i = 1, 2, \ldots, N_b \tag{98}$$

where the first set of formulas must be used when the first Euler parameter $p_{0,i}$ is different from zero, whereas the second set of formulas must be employed when the first Euler parameter $p_{0,i}$ is equal to zero. By adopting the strategy mentioned above for conveniently describing the orientation of each rigid body belonging to the redundant coordinate multibody model of the pantograph scissor lift mechanism, and taking into account the particular closed-chain structure of this articulated mechanical system, one can readily identify the initial configuration of each rigid body that forms the multibody system, namely, the initial position of the body reference point, assumed coincident with its centroid, and the initial orientation of the body-fixed reference system. This process leads to the systematic construction of the position and orientation vectors reported in Table 4.

Table 4. Initial configuration parameters of the pantograph scissor lift mechanism.

Rigid body number	Initial translational coordinate vector	Initial rotational coordinate vector
i	$\boldsymbol{R}_{i,0} = \left[\begin{array}{ccc} x_{i,0} & y_{i,0} & z_{i,0} \end{array}\right]^T$	$\boldsymbol{e}_{i,0} = \left[\begin{array}{ccc} \alpha_{i,0} & \beta_{i,0} & \gamma_{i,0} \end{array}\right]^T$
1	$\boldsymbol{R}_{1,0} = \left[\begin{array}{ccc} \frac{s_0}{2} & 0 & \frac{h_0}{2} \end{array}\right]^T$	$\boldsymbol{e}_{1,0} = \left[\begin{array}{ccc} \frac{\pi}{2} & 0 & \theta_0 \end{array}\right]^T$
2	$\boldsymbol{R}_{2,0} = \left[\begin{array}{ccc} \frac{s_0}{2} & 0 & \frac{h_0}{2} \end{array}\right]^T$	$\boldsymbol{e}_{2,0} = \left[\begin{array}{ccc} \frac{\pi}{2} & 0 & -\theta_0 \end{array}\right]^T$
3	$\boldsymbol{R}_{3,0} = \left[\begin{array}{ccc} \frac{s_0}{2} & W_p & \frac{h_0}{2} \end{array}\right]^T$	$\boldsymbol{e}_{3,0} = \left[\begin{array}{ccc} \frac{\pi}{2} & 0 & \theta_0 \end{array}\right]^T$
4	$\boldsymbol{R}_{4,0} = \left[\begin{array}{ccc} \frac{s_0}{2} & W_p & \frac{h_0}{2} \end{array}\right]^T$	$\boldsymbol{e}_{4,0} = \left[\begin{array}{ccc} \frac{\pi}{2} & 0 & -\theta_0 \end{array}\right]^T$
5	$\boldsymbol{R}_{5,0} = \left[\begin{array}{ccc} \frac{L_b}{2} & \frac{W_p}{2} & h_0 \end{array}\right]^T$	$\boldsymbol{e}_{5,0} = \left[\begin{array}{ccc} \frac{\pi}{2} & 0 & 0 \end{array}\right]^T$
6	$\boldsymbol{R}_{6,0} = \left[\begin{array}{ccc} s_0 & 0 & 0 \end{array}\right]^T$	$\boldsymbol{e}_{6,0} = \left[\begin{array}{ccc} \frac{\pi}{2} & \frac{\pi}{2} & 0 \end{array}\right]^T$
7	$\boldsymbol{R}_{7,0} = \left[\begin{array}{ccc} s_0 & 0 & h_0 \end{array}\right]^T$	$\boldsymbol{e}_{7,0} = \left[\begin{array}{ccc} \frac{\pi}{2} & \frac{\pi}{2} & 0 \end{array}\right]^T$
8	$\boldsymbol{R}_{8,0} = \left[\begin{array}{ccc} s_0 & W_p & 0 \end{array}\right]^T$	$\boldsymbol{e}_{8,0} = \left[\begin{array}{ccc} \frac{\pi}{2} & \frac{\pi}{2} & 0 \end{array}\right]^T$
9	$\boldsymbol{R}_{9,0} = \left[\begin{array}{ccc} s_0 & W_p & h_0 \end{array}\right]^T$	$\boldsymbol{e}_{9,0} = \left[\begin{array}{ccc} \frac{\pi}{2} & \frac{\pi}{2} & 0 \end{array}\right]^T$

Furthermore, it is assumed that the pantograph scissor lift mechanism starts its motion from a rest configuration of static equilibrium in which one has $\dot{\boldsymbol{R}}_i(t=0) = \boldsymbol{0}$ and $\dot{\boldsymbol{\theta}}_i(t=0) = \boldsymbol{0}$ for each body i of the multibody system, which altogether leads to $\dot{\boldsymbol{q}}(t=0) = \boldsymbol{0}$. To complete the kinematic description of the redundant coordinate multibody model of the pantograph scissor lift mechanism, one needs to analytically define the position field of each rigid body i and its first and second derivatives with respect to the time variable. Considering a generic material point P_i pertaining to the rigid body i, the position field of the generic rigid body i can be written as:

$$\boldsymbol{r}_i = \boldsymbol{R}_i + \boldsymbol{A}_i \bar{\boldsymbol{u}}_i, \quad i = 1, 2, \ldots, N_b \tag{99}$$

being:

$$\bar{\boldsymbol{u}}_i = \begin{bmatrix} \bar{x}_i \\ \bar{y}_i \\ \bar{z}_i \end{bmatrix}, \quad i = 1, 2, \ldots, N_b \tag{100}$$

where $\bar{\boldsymbol{u}}_i \equiv \bar{\boldsymbol{u}}_i(P_i)$ is a vector of dimension d representing the local position vector of the material point P_i belonging to the rigid body i, while $\bar{x}_i \equiv \bar{x}_i(P_i)$, $\bar{y}_i \equiv \bar{y}_i(P_i)$, and $\bar{z}_i \equiv \bar{z}_i(P_i)$ are the Cartesian coordinates of the point P_i that form the local position vector $\bar{\boldsymbol{u}}_i$, whereas $\boldsymbol{r}_i \equiv \boldsymbol{r}_i(P_i, \boldsymbol{q}_i, t)$ is a vector of dimension d representing the global position vector of the same material point P_i. Operating in the same analytical framework and by using a systematic multibody approach, the virtual displacement field of a generic rigid body i can be explicitly calculated as follows:

$$\delta \boldsymbol{r}_i = \boldsymbol{L}_i \delta \boldsymbol{q}_i, \quad i = 1, 2, \ldots, N_b \tag{101}$$

where:

$$\boldsymbol{L}_i = \begin{bmatrix} \boldsymbol{I} & \boldsymbol{A}_i \tilde{\bar{\boldsymbol{u}}}_i^T \bar{\boldsymbol{G}}_i \end{bmatrix}, \quad i = 1, 2, \ldots, N_b \tag{102}$$

and

$$\bar{\boldsymbol{G}}_i = 2\bar{\boldsymbol{E}}_i = 2 \begin{bmatrix} -\boldsymbol{p}_i & p_{0,i}\boldsymbol{I} - \tilde{\boldsymbol{p}}_i \end{bmatrix}, \quad i = 1, 2, \ldots, N_b \tag{103}$$

where $\delta \boldsymbol{r}_i \equiv \delta \boldsymbol{r}_i(P_i, \boldsymbol{q}_i, \delta \boldsymbol{q}_i, t)$ is a vector of dimension d representing the virtual displacement field of the rigid body i, $\delta \boldsymbol{q}_i \equiv \delta \boldsymbol{q}_i(t)$ denotes a vector of dimension n_b that identifies a virtual change in the generalized coordinates of the body i, $\boldsymbol{L}_i \equiv \boldsymbol{L}_i(P_i, \boldsymbol{q}_i, t)$ identifies a rectangular matrix having dimensions $d \times n_b$ representing the position field Jacobian matrix associated with the rigid body i, $\tilde{\bar{\boldsymbol{u}}}_i \equiv \tilde{\bar{\boldsymbol{u}}}_i(P_i)$ is a skew-symmetric matrix of dimensions $d \times d$ associated with the local position vector $\bar{\boldsymbol{u}}_i$ which has the same structure of the skew symmetric matrix reported in Equation (86), and $\bar{\boldsymbol{G}}_i \equiv \bar{\boldsymbol{G}}_i(\boldsymbol{q}_i, t)$ is a rectangular matrix having dimensions $d \times n_p$. In particular, $\bar{\boldsymbol{G}}_i$ is a transformation matrix that allows for computing the local angular velocity vector of the generic rigid body i as a linear combination of the Euler parameters derived with respect to time as follows:

$$\bar{\boldsymbol{\omega}}_i = \bar{\boldsymbol{G}}_i \dot{\boldsymbol{\theta}}_i = \bar{\boldsymbol{W}}_i \dot{\boldsymbol{q}}_i, \quad i = 1, 2, \ldots, N_b \tag{104}$$

being:

$$\bar{\boldsymbol{W}}_i = \begin{bmatrix} \boldsymbol{O} & \bar{\boldsymbol{G}}_i \end{bmatrix}, \quad i = 1, 2, \ldots, N_b \tag{105}$$

where $\boldsymbol{O}$ is a zero matrix having dimensions $d \times n_d$ and $\bar{\boldsymbol{\omega}}_i \equiv \bar{\boldsymbol{\omega}}_i(\boldsymbol{q}_i, \dot{\boldsymbol{q}}_i, t)$ is a vector of dimension d describing the local angular velocity vector of the rigid body i, and $\bar{\boldsymbol{W}}_i \equiv \bar{\boldsymbol{W}}_i(\boldsymbol{q}_i, t)$ is another local transformation matrix of dimensions $d \times n_b$ which allows for computing the local angular velocity vector of the generic rigid body i as a linear combination of the components of the body generalized velocity vector. Finally, to conclude the kinematic modeling of the redundant coordinate multibody model developed for describing the pantograph scissor lift mechanism, the following velocity and acceleration fields need to be considered:

$$\dot{\boldsymbol{r}}_i = \boldsymbol{L}_i \dot{\boldsymbol{q}}_i, \quad i = 1, 2, \ldots, N_b \tag{106}$$

and

$$\ddot{\boldsymbol{r}}_i = \boldsymbol{L}_i \ddot{\boldsymbol{q}}_i + \dot{\boldsymbol{L}}_i \dot{\boldsymbol{q}}_i, \quad i = 1, 2, \ldots, N_b \tag{107}$$

where:

$$\dot{\boldsymbol{L}}_i = \begin{bmatrix} \boldsymbol{O} & \boldsymbol{A}_i \tilde{\bar{\boldsymbol{\omega}}}_i \tilde{\bar{\boldsymbol{u}}}_i^T \bar{\boldsymbol{G}}_i + \boldsymbol{A}_i \tilde{\bar{\boldsymbol{u}}}_i^T \dot{\bar{\boldsymbol{G}}}_i \end{bmatrix}, \quad i = 1, 2, \ldots, N_b \tag{108}$$

and

$$\dot{\bar{\boldsymbol{G}}}_i = 2 \begin{bmatrix} -\dot{\boldsymbol{p}}_i & \dot{p}_{0,i}\boldsymbol{I} - \dot{\tilde{\boldsymbol{p}}}_i \end{bmatrix}, \quad i = 1, 2, \ldots, N_b \tag{109}$$

where $\dot{\boldsymbol{r}}_i \equiv \dot{\boldsymbol{r}}_i(P_i, \boldsymbol{q}_i, \dot{\boldsymbol{q}}_i, t)$ is a vector of dimension d representing the velocity field of the rigid body i, $\ddot{\boldsymbol{r}}_i \equiv \ddot{\boldsymbol{r}}_i(P_i, \boldsymbol{q}_i, \dot{\boldsymbol{q}}_i, \ddot{\boldsymbol{q}}_i, t)$ is a vector of dimension d representing the acceleration field of the rigid body i, and $\tilde{\bar{\boldsymbol{\omega}}}_i \equiv \tilde{\bar{\boldsymbol{\omega}}}_i(\boldsymbol{q}_i, \dot{\boldsymbol{q}}_i, t)$ is a skew-symmetric matrix of dimensions $d \times d$ associated with the local angular velocity vector $\bar{\boldsymbol{\omega}}_i$ which has the same structure of the skew symmetric matrix reported in Equation (86). The kinematic analysis of the redundant coordinate multibody model of the pantograph scissor lift mechanism allows for describing the global position, velocity, and acceleration vectors of an arbitrary point P_i selected on a given rigid body i that form this articulated mechanical system, as well as to define the local angular velocity vectors of all the bodies belonging to the multibody systems. As discussed in detail below, this is fundamental geometric information necessary for identifying the force elements and force fields acting on all the components of this mechanical system, to be able to carry out a comprehensive dynamic analysis of the system behavior through the derivation of its differential-algebraic equations governing the motion, and for the systematic formulation of the constraint equations representing the combined set of the intrinsic normalization conditions and the extrinsic kinematic joints.

5.2 Force fields and force elements identification

In the redundant coordinate multibody model of the pantograph scissor lift mechanism, both force fields and force elements are present and active. More precisely, only one category of force field affects this articulated mechanism, that is, the gravity force field. Similarly, only one type of force element is considered for modeling the friction forces acting on the sliding motion of the rollers, namely, a linear viscous force element aligned with the direction of the prismatic joints. To simplify the model description, a direct Lagrangian approach is used for modeling both the force fields and the force elements to be considered in the redundant coordinate multibody model. In this respect, and leveraging on the kinematic description of the multibody model, one can readily identify the altitudes in the gravitational field of the centroid of each rigid body as follows:

$$h_i = z_i, \quad i = 1, 2, \ldots, N_b \tag{110}$$

where $h_i \equiv h_i(\boldsymbol{q}_i, t)$ is the centroid altitude of the generic rigid body i necessary for the determination of the body potential energy. Thus, the gravitational potential energy of the generic rigid body i is given by:

$$U_i = m_i g h_i, \quad i = 1, 2, \ldots, N_b \tag{111}$$

where $U_i \equiv U_i(\boldsymbol{q}_i, t)$ denotes the gravitational potential energy of the generic body i and represents the only form of potential energy associated with the multibody system under study. The total potential energy of the mechanical system is denoted with $U \equiv U(\boldsymbol{q}, t)$ and is given by:

$$U = \sum_{i=1}^{N_b} U_i \tag{112}$$

The explicit determination of the total potential energy of the pantograph scissor lift mechanism allows for analytically determining the system total conservative generalized external force vector as follows:

$$\boldsymbol{Q}_{\mathrm{e,c}} = -\left(\frac{\partial U}{\partial \boldsymbol{q}}\right)^T = \sum_{i=1}^{N_b} \boldsymbol{B}_i^T \boldsymbol{Q}_{\mathrm{e,c},i} \tag{113}$$

where:

$$\boldsymbol{g} = \begin{bmatrix} 0 \\ 0 \\ g \end{bmatrix}, \quad \boldsymbol{Q}_{\mathrm{e,c},i} = \begin{bmatrix} -m_i \boldsymbol{g} \\ \boldsymbol{0} \end{bmatrix}, \quad i = 1, 2, \ldots, N_b \tag{114}$$

and

$$\boldsymbol{q}_i = \boldsymbol{B}_i \boldsymbol{q}, \quad i = 1, 2, \ldots, N_b \tag{115}$$

where $\boldsymbol{Q}_{\mathrm{e,c}} \equiv \boldsymbol{Q}_{\mathrm{e,c}}(\boldsymbol{q}, t)$ is a vector of dimension n_q representing the system total conservative generalized external force vector, $\boldsymbol{Q}_{\mathrm{e,c},i} \equiv \boldsymbol{Q}_{\mathrm{e,c},i}(\boldsymbol{q}_i, t)$ is a vector of dimension n_b representing the conservative generalized external force vector relative to the generic rigid body i, $\boldsymbol{g}$ is the constant gravity force vector having dimension d, and $\boldsymbol{B}_i$ is a constant Boolean matrix having dimensions $n_b \times n_q$ that allows for recovering the generalized coordinate vector of a given body i from the system vector of Lagrangian coordinates. On the other hand, as already introduced above, the presence of dry friction forces affecting the linear motion of the rollers along the direction of the prismatic joints in which they translate is modeled through the use of N_a force elements characterized by linear viscous forces having a constant damping coefficient equal to σ. Detailed information regarding the type and the collocation of the force elements used for modeling the system dissipative effects is reported in Table 5.

Table 5. Type and collocation of the force elements.

Force element number	Force element type	First body number	Second body number	First body location point	Second body location point
h	Name	i_h	j_h	$\bar{\boldsymbol{u}}_{i_h} = \begin{bmatrix} \bar{x}_{i_h} & \bar{y}_{i_h} & \bar{z}_{i_h} \end{bmatrix}^T$	$\bar{\boldsymbol{u}}_{j_h} = \begin{bmatrix} \bar{x}_{j_h} & \bar{y}_{j_h} & \bar{z}_{j_h} \end{bmatrix}^T$
1	Damper	6	0	$\bar{\boldsymbol{u}}_6 = \begin{bmatrix} 0 & 0 & 0 \end{bmatrix}^T$	$\bar{\boldsymbol{u}}_0 = \begin{bmatrix} L & 0 & 0 \end{bmatrix}^T$
2	Damper	7	5	$\bar{\boldsymbol{u}}_7 = \begin{bmatrix} 0 & 0 & 0 \end{bmatrix}^T$	$\bar{\boldsymbol{u}}_5 = \begin{bmatrix} \frac{L_5}{2} & 0 & \frac{W_5}{2} \end{bmatrix}^T$
3	Damper	8	0	$\bar{\boldsymbol{u}}_8 = \begin{bmatrix} 0 & 0 & 0 \end{bmatrix}^T$	$\bar{\boldsymbol{u}}_0 = \begin{bmatrix} L & W & 0 \end{bmatrix}^T$
4	Damper	9	5	$\bar{\boldsymbol{u}}_9 = \begin{bmatrix} 0 & 0 & 0 \end{bmatrix}^T$	$\bar{\boldsymbol{u}}_5 = \begin{bmatrix} \frac{L_5}{2} & 0 & -\frac{W_5}{2} \end{bmatrix}^T$

In Table 5, the number h of each force element is specified together with its physical structure. The two bodies connected by the generic force element h are also identified in Table 5 using the integer numbers i_h and j_h, the ground body is identified with the integer 0, while the local position vectors having dimension d relative to the collocation points P_{i_h} and P_{j_h} are respectively indicated with $\bar{\boldsymbol{u}}_{i_h} \equiv \bar{\boldsymbol{u}}_{i_h}(P_{i_h})$ and $\bar{\boldsymbol{u}}_{j_h} \equiv \bar{\boldsymbol{u}}_{j_h}(P_{j_h})$. To derive the nonconservative generalized force vector associated with each force element h, the following approach is adopted. First, the global position vectors of the two geometric points P_{i_h} and P_{j_h}, between which each linear force element acts, are identified as follows:

$$\boldsymbol{r}_{i_h} = \boldsymbol{R}_{i_h} + \boldsymbol{A}_{i_h} \bar{\boldsymbol{u}}_{i_h}, \quad \boldsymbol{r}_{j_h} = \boldsymbol{R}_{j_h} + \boldsymbol{A}_{j_h} \bar{\boldsymbol{u}}_{j_h}, \quad h = 1, 2, \ldots, N_a \tag{116}$$

where $\boldsymbol{r}_{i_h} \equiv \boldsymbol{r}_{i_h}(P_{i_h}, \boldsymbol{q}_{i_h}, t)$ is a vector of dimension d representing the global position vector of the first geometric point involved in the generic force element h, while $\boldsymbol{r}_{j_h} \equiv \boldsymbol{r}_{j_h}(P_{j_h}, \boldsymbol{q}_{j_h}, t)$ is a vector of dimension d representing the global position vector of the second geometric point considered in the same force element. Then, one can easily determine the linear elongation vector associated to the force element at hand as follows:

$$\boldsymbol{l}_h = \boldsymbol{r}_{i_h} - \boldsymbol{r}_{j_h}, \quad h = 1, 2, \ldots, N_a \tag{117}$$

where $\boldsymbol{l}_h \equiv \boldsymbol{l}_h(P_{i_h}, P_{j_h}, \boldsymbol{q}_{i_h}, \boldsymbol{q}_{j_h}, t)$ is a vector of dimension d representing the geometric elongation vector of the generic force element h. Once this fundamental geometric quantity is calculated for each force element h, one can go ahead with the analytical determination of the magnitude of the force element elongation vector and its time derivative as follows:

$$l_h = \sqrt{\boldsymbol{l}_h^T \boldsymbol{l}_h}, \quad \dot{l}_h = \frac{\boldsymbol{l}_h^T \dot{\boldsymbol{l}}_h}{l_h}, \quad h = 1, 2, \ldots, N_a \tag{118}$$

where $l_h \equiv l_h(P_{i_h}, P_{j_h}, \boldsymbol{q}_{i_h}, \boldsymbol{q}_{j_h}, t)$ denotes the magnitude of the force element elongation vector h. Finally, the geometric deformation associated with the generic force element h, as well as its time derivative, are respectively given as follows:

$$\Delta_h = l_h - l_{0,h}, \quad \dot{\Delta}_h = \dot{l}_h, \quad h = 1, 2, \ldots, N_a \tag{119}$$

where $\Delta_h \equiv \Delta_h(P_{i_h}, P_{j_h}, \boldsymbol{q}_{i_h}, \boldsymbol{q}_{j_h}, t)$ denotes the geometric deformation of the force element labeled with the integer h and the constant quantity $l_{0,h} \equiv l_{0,h}(P_{i_h}, P_{j_h})$ identifies the undeformed length of the same force element. Consequently, the Rayleigh dissipation function associated with the viscous damping of the generic force element h can be readily obtained as:

$$R_h = \frac{1}{2}\sigma\dot{\Delta}_h^2, \quad h = 1, 2, \ldots, N_a \tag{120}$$

where $R_h \equiv R_h(\boldsymbol{q}_{i_h}, \boldsymbol{q}_{j_h}, \dot{\boldsymbol{q}}_{i_h}, \dot{\boldsymbol{q}}_{j_h}, t)$ denotes the Rayleigh dissipation function of the generic force element h, which represents the only form of dissipated power associated with the multibody system under consideration, and it is assumed that the same viscous coefficient σ represents the constant damping acting on all the rollers. The total Rayleigh dissipation function of the mechanical system is denoted with $R \equiv R(\boldsymbol{q}, \dot{\boldsymbol{q}}, t)$ and is given by:

$$R = \sum_{h=1}^{N_a} R_h \tag{121}$$

The explicit determination of the total Rayleigh dissipation function of the pantograph scissor lift mechanism allows for analytically determining the system total nonconservative generalized external force vector as follows:

$$\boldsymbol{Q}_{\mathrm{e,nc}} = -\left(\frac{\partial R}{\partial \dot{\boldsymbol{q}}}\right)^T = \sum_{h=1}^{N_a}\left(\boldsymbol{B}_{i_h}^T\boldsymbol{Q}_{\mathrm{e,nc},i_h} - \boldsymbol{B}_{j_h}^T\boldsymbol{Q}_{\mathrm{e,nc},j_h}\right) \tag{122}$$

where:

$$\boldsymbol{F}_h = -\sigma\frac{\dot{\Delta}_h}{l_h}\boldsymbol{l}_h, \quad \begin{cases} \boldsymbol{Q}_{\mathrm{e,nc},i_h} = \boldsymbol{L}_{i_h}^T\boldsymbol{F}_h \\ \\ \boldsymbol{Q}_{\mathrm{e,nc},j_h} = \boldsymbol{L}_{j_h}^T\boldsymbol{F}_h \end{cases}, \quad h = 1, 2, \ldots, N_a \tag{123}$$

and

$$\boldsymbol{q}_{i_h} = \boldsymbol{B}_{i_h}\boldsymbol{q}, \quad \boldsymbol{q}_{j_h} = \boldsymbol{B}_{j_h}\boldsymbol{q}, \quad h = 1, 2, \ldots, N_a \tag{124}$$

where $\boldsymbol{Q}_{\mathrm{e,nc}} \equiv \boldsymbol{Q}_{\mathrm{e,nc}}(\boldsymbol{q}, \dot{\boldsymbol{q}}, t)$ is a vector of dimension n_q representing the system total nonconservative generalized external force vector, $\boldsymbol{Q}_{\mathrm{e,nc},i_h} \equiv \boldsymbol{Q}_{\mathrm{e,nc},i_h}(\boldsymbol{q}_{i_h}, \boldsymbol{q}_{j_h}, \dot{\boldsymbol{q}}_{i_h}, \dot{\boldsymbol{q}}_{j_h}, t)$ and $\boldsymbol{Q}_{\mathrm{e,nc},j_h} \equiv \boldsymbol{Q}_{\mathrm{e,nc},j_h}(\boldsymbol{q}_{i_h}, \boldsymbol{q}_{j_h}, \dot{\boldsymbol{q}}_{i_h}, \dot{\boldsymbol{q}}_{j_h}, t)$ are two vector of dimension n_b representing the total nonconservative generalized external force vectors relative to the generic force element h, $\boldsymbol{F}_h \equiv \boldsymbol{F}_h(\boldsymbol{q}_{i_h}, \boldsymbol{q}_{j_h}, \dot{\boldsymbol{q}}_{i_h}, \dot{\boldsymbol{q}}_{j_h}, t)$ is a force vector having dimension d representing the linear viscous effects, whereas $\boldsymbol{L}_{i_h} \equiv \boldsymbol{L}_{i_h}(P_{i_h}, \boldsymbol{q}_{i_h}, t)$ and $\boldsymbol{L}_{j_h} \equiv \boldsymbol{L}_{j_h}(P_{j_h}, \boldsymbol{q}_{j_h}, t)$ are the Jacobian matrices of the rigid bodies i_h and j_h affected by the generic force element h and particularized in their application points P_{i_h} and P_{j_h}, while $\boldsymbol{B}_{i_h}$ and $\boldsymbol{B}_{j_h}$ are constant Boolean matrices having dimensions $n_b \times n_q$ that allow for recovering from the system vector of Lagrangian coordinates the generalized coordinate vectors of the rigid bodies labeled with i_h and j_h. Finally, one can simply obtain the system total external generalized force vector as:

$$\boldsymbol{Q}_{\mathrm{e}} = \boldsymbol{Q}_{\mathrm{e,c}} + \boldsymbol{Q}_{\mathrm{e,nc}} \tag{125}$$

where $\boldsymbol{Q}_{\mathrm{e}} \equiv \boldsymbol{Q}_{\mathrm{e}}(\boldsymbol{q}, \dot{\boldsymbol{q}}, t)$ represents a highly nonlinear vector of generalized external forces having dimension n_q which takes into account all the conservative and nonconservative effects arising from all the force fields and the force elements acting on the pantograph scissor lift mechanism.

5.3 Dynamic analysis

To accomplish the systematic formulation of the differential part of the redundant coordinate multibody model developed herein for the pantograph scissor lift mechanism, the last fundamental step is to take into account the inertial effects and the control action relevant for performing a consistent dynamic analysis. To this end, a Lagrangian approach can be effectively employed. Thus, one needs to obtain first the kinetic energy of the generic rigid body i by using the following form of the Konig theorem:

$$T_i = \frac{1}{2}m_i\dot{\boldsymbol{R}}_i^T\dot{\boldsymbol{R}}_i + \frac{1}{2}\bar{\boldsymbol{\omega}}_i^T\bar{\boldsymbol{I}}_{G_i}\bar{\boldsymbol{\omega}}_i, \quad i = 1, 2, \ldots, N_b \tag{126}$$

being:

$$\bar{\boldsymbol{I}}_{G_i} = \mathrm{diag}(I_{xx,i}, I_{yy,i}, I_{zz,i}) \tag{127}$$

where m_i is the mass of the generic rigid body i, while $I_{xx,i}$, $I_{yy,i}$, and $I_{zz,i}$ are the principal mass moments of inertia of the rigid body i referred to the body center of mass G_i, whereas $\bar{\boldsymbol{I}}_{G_i}$ is a constant diagonal matrix of dimensions $d \times d$ containing the principal moments of inertia of the rigid body i, and $T_i \equiv T_i(\boldsymbol{q}_i, \dot{\boldsymbol{q}}_i, t)$ is the total roto-translational kinetic energy of the body i. Note that one can use the form of the Konig theorem given by Equation (126) because, in the kinematic model of the articulated mechanical system under consideration, it is assumed that the local frame of reference pertaining to each rigid body i is a central reference system, that is, its origin $\bar{O}_i$ coincides with the body i center of mass G_i and its axes are aligned with the body principal directions. The total kinetic energy of the mechanical system is, therefore, denoted with $T \equiv T(\boldsymbol{q}, \dot{\boldsymbol{q}}, t)$ and is given by:

$$T = \sum_{i=1}^{N_b} T_i \tag{128}$$

The explicit determination of the total kinetic energy of the pantograph scissor lift mechanism allows for analytically determining the system total generalized inertia force vector as follows:

$$\boldsymbol{Q}_{\mathrm{i}} = -\frac{d}{dt}\left(\frac{\partial T}{\partial \dot{\boldsymbol{q}}}\right)^T + \left(\frac{\partial T}{\partial \boldsymbol{q}}\right)^T = \boldsymbol{Q}_{\mathrm{v}} - \boldsymbol{M}\ddot{\boldsymbol{q}} \tag{129}$$

where $\boldsymbol{Q}_{\mathrm{i}} \equiv \boldsymbol{Q}_{\mathrm{i}}(\boldsymbol{q}, \dot{\boldsymbol{q}}, t)$ is a vector of dimension n_q representing the system total generalized inertia force vector, $\boldsymbol{M} \equiv \boldsymbol{M}(\boldsymbol{q}, t)$ is a matrix of dimensions $n_q \times n_q$ representing the system total mass matrix, and $\boldsymbol{Q}_{\mathrm{v}} \equiv \boldsymbol{Q}_{\mathrm{v}}(\boldsymbol{q}, \dot{\boldsymbol{q}}, t)$ is a vector of dimension n_q representing the system total generalized inertia quadratic velocity force vector. The total mass matrix of the redundant coordinate multibody model can be analytically determined as:

$$\boldsymbol{M} = -\frac{\partial \boldsymbol{Q}_{\mathrm{i}}}{\partial \ddot{\boldsymbol{q}}} = \sum_{i=1}^{N_b} \boldsymbol{B}_i^T \boldsymbol{M}_i \boldsymbol{B}_i \tag{130}$$

where:

$$\boldsymbol{M}_i = \begin{bmatrix} m_i \boldsymbol{I} & \boldsymbol{O} \\ \boldsymbol{O}^T & \bar{\boldsymbol{G}}_i^T \bar{\boldsymbol{I}}_{G_i} \bar{\boldsymbol{G}}_i \end{bmatrix} \tag{131}$$

where $\boldsymbol{O}$ is a zero matrix having dimensions $n_d \times n_p$, $\boldsymbol{M}_i \equiv \boldsymbol{M}_i(\boldsymbol{q}_i, t)$ denotes a matrix having dimensions $n_b \times n_b$ that identifies the mass matrix of the generic rigid body i obtained assuming that the body-fixed reference point $\bar{O}_i$ coincides with the body centroid G_i, and $\boldsymbol{B}_i$ is a constant Boolean matrix of dimensions $n_b \times n_q$ that allows for deriving the generalized coordinate vector of the generic rigid body i from the vector of the system Lagrangian coordinates. Similarly, the system total generalized inertia quadratic velocity force vector of the redundant coordinate multibody model can be analytically determined as:

$$\boldsymbol{Q}_{\mathrm{v}} = \boldsymbol{Q}_{\mathrm{i}} + \boldsymbol{M}\ddot{\boldsymbol{q}} = \sum_{i=1}^{N_b} \boldsymbol{B}_i^T \boldsymbol{Q}_{\mathrm{v},i} \tag{132}$$

where:

$$\boldsymbol{Q}_{\mathrm{v},i} = \begin{bmatrix} \boldsymbol{0} \\ -\bar{\boldsymbol{G}}_i^T \tilde{\bar{\boldsymbol{\omega}}}_i \bar{\boldsymbol{I}}_{G_i} \bar{\boldsymbol{\omega}}_i \end{bmatrix} \tag{133}$$

where $\boldsymbol{Q}_{\mathrm{v},i} \equiv \boldsymbol{Q}_{\mathrm{v},i}(\boldsymbol{q}_i, \dot{\boldsymbol{q}}_i, t)$ denotes a vector having dimensions n_b that identifies the generalized inertia quadratic velocity force vector of the generic rigid body i obtained assuming that the body-fixed reference point $\bar{O}_i$ coincides with the body centroid G_i. Note that the inertia quadratic velocity force vector of the generic rigid body i assumes the simplified form given in Equation (133) because of the use of the set of Euler parameters as rotational coordinates. On the other hand, the external control force F_c is applied on the geometric point A_{i_c} considered as a material point belonging to the rigid body $i_c = 6$, that is, the front bottom roller. Thus, the virtual work produced by the external control action can be written as:

$$\delta W_c = \boldsymbol{F}_c^T \delta \boldsymbol{r}_{i_c} = \boldsymbol{F}_c^T \boldsymbol{L}_{i_c} \boldsymbol{B}_{i_c} \delta \boldsymbol{q} \tag{134}$$

where:

$$\boldsymbol{F}_c = \begin{bmatrix} F_c \\ 0 \\ 0 \end{bmatrix}, \quad \delta \boldsymbol{r}_{i_c} = \boldsymbol{L}_{i_c} \boldsymbol{B}_{i_c} \delta \boldsymbol{q} \tag{135}$$

where $\delta W_c \equiv \delta W_c(\boldsymbol{q}_{i_c}, \dot{\boldsymbol{q}}_{i_c}, \delta \boldsymbol{q}_{i_c}, t)$ denotes the virtual work of the external control action, $\boldsymbol{F}_c \equiv \boldsymbol{F}_c(t)$ is a time-dependent vector of dimension d representing the control force, $\delta \boldsymbol{r}_{i_c} \equiv \delta \boldsymbol{r}_{i_c}(A_{i_c}, \boldsymbol{q}_{i_c}, \delta \boldsymbol{q}_{i_c}, t)$ represents a vector having dimension d that identifies the virtual displacement of the geometric point A_{i_c} on which the external control force is applied, $\boldsymbol{L}_{i_c} \equiv \boldsymbol{L}_{i_c}(A_{i_c}, \boldsymbol{q}_{i_c}, t)$ is a matrix having dimensions $d \times n_b$ representing the Jacobian matrix of the position field of the rigid body i_c, and $\boldsymbol{B}_{i_c}$ is constant Boolean matrix having dimensions $n_b \times n_q$ that allows for recovering the generalized coordinate vector of the rigid body i_c from the vector of the system Lagrangian coordinates. Consequently, the generalized force vector associated with the control action can be readily obtained as:

$$\boldsymbol{Q}_{\mathrm{c}} = \left(\frac{\delta W_c}{\delta \boldsymbol{q}} \right)^T = \boldsymbol{B}_{i_c}^T \boldsymbol{L}_{i_c}^T \boldsymbol{F}_c \tag{136}$$

where $\boldsymbol{Q}_{\mathrm{c}} \equiv \boldsymbol{Q}_{\mathrm{c}}(\boldsymbol{q}, \dot{\boldsymbol{q}}, t)$ denotes a vector of dimension n_q that identifies the system generalized control force vector. Finally, one can determine the total generalized force vector acting on the multibody system as follows:

$$\boldsymbol{Q}_{\mathrm{b}} = \boldsymbol{Q}_{\mathrm{v}} + \boldsymbol{Q}_{\mathrm{e}} \tag{137}$$

where $\boldsymbol{Q}_{\mathrm{b}} \equiv \boldsymbol{Q}_{\mathrm{b}}(\boldsymbol{q}, \dot{\boldsymbol{q}}, t)$ is a strongly nonlinear vector of dimension n_q representing the system total body generalized force vector that takes into account all the inertia and external generalized forces describing the redundant coordinate multibody model of the pantograph scissor lift mechanism. The description of the dynamic quantities that appear in the differential part of the system equations of motion completes the dynamic formulation of the redundant coordinate multibody model.

5.4 Constraints formulation

The redundant coordinate multibody model of the pantograph scissor lift mechanism involves the presence of a nonlinear set of algebraic equations. The proper formulation of this relatively large set of algebraic equations is necessary for modeling two categories of constraint equations, namely, the set of intrinsic constraints, composed of $N_{c,\Phi}$ groups of nonlinear algebraic equations, and the set of extrinsic constraints, composed of $N_{c,\Psi}$ groups of nonlinear algebraic equations. While the set of intrinsic constraints is necessary for mathematically modeling the normalization conditions of the Euler parameters employed for describing without kinematic singularities the orientation in the space of each rigid body labeled with the integer i, the set of extrinsic constraints serves for the analytical description of the motion limitations imposed on each kinematic pair k of rigid bodies by the particular mechanical joint that connects them. Therefore, these two sets of algebraic constraints form two vectors of nonlinear algebraic equations which are respectively given by:

$$\boldsymbol{\Phi}_i = \boldsymbol{0}, \quad i = 1, 2, \ldots, N_{c,\Phi} \tag{138}$$

and

$$\boldsymbol{\Psi}_k = \boldsymbol{0}, \quad k = 1, 2, \ldots, N_{c,\Psi} \tag{139}$$

where $\boldsymbol{\Phi}_i \equiv \boldsymbol{\Phi}_i(\boldsymbol{q}_i, t)$ is a vector of dimension n_{c,Φ_i} representing the set of the generic intrinsic constraints associated with the rigid body i and $\boldsymbol{\Psi}_k \equiv \boldsymbol{\Psi}_k(\boldsymbol{q}_{i_k}, \boldsymbol{q}_{j_k}, t)$ is a vector of dimension n_{c,Ψ_k} representing the set of the generic extrinsic constraints associated

with the kinematic pair k. In fact, each set of Euler parameters requires only $n_{c,\Phi_i} = 1$ normalization condition which can be readily written as:

$$\boldsymbol{\Phi}_i = \boldsymbol{\theta}_i^T \boldsymbol{\theta}_i - 1, \quad i = 1, 2, \ldots, N_{c,\Phi} \tag{140}$$

Moreover, the set of extrinsic constraints has a composite dimension denoted with n_{c,Ψ_k}, which depends on the particular type of kinematic pair labeled with the integer k involved in the multibody model. In the case of the pantograph scissor lift mechanism analyzed in this paper as the case study, as mentioned before, only revolute joints and prismatic joints characterize the mechanical limitations of the relative motion between the rigid bodies that form the multibody mechanical system. Consequently, in this particular case, the redundant coordinate multibody model of the articulated mechanical system under study encompasses $n_{c,\Psi_k} = 5$ nonlinear algebraic equations for each kinematic pair k. Detailed information regarding the type and the collocation of the kinematic pairs employed for modeling the system mechanical joints is reported in Table 6.

In Table 6, the number k of each kinematic pair is specified together with its physical structure. The two bodies connected by the generic kinematic pair k are also identified in Table 6 using the integer numbers i_k and j_k, the ground body is identified with the integer 0, whereas the local position vectors having dimension d relative to the collocation points P_{i_k} and P_{j_k} are respectively indicated with $\bar{\boldsymbol{u}}_{i_k} \equiv \bar{\boldsymbol{u}}_{i_k}(P_{i_k})$ and $\bar{\boldsymbol{u}}_{j_k} \equiv \bar{\boldsymbol{u}}_{j_k}(P_{j_k})$. Also, the local direction vectors $\bar{\boldsymbol{v}}_{i_k} \equiv \bar{\boldsymbol{v}}_{i_k}(P_{i_k})$ and $\bar{\boldsymbol{v}}_{j_k} \equiv \bar{\boldsymbol{v}}_{j_k}(P_{j_k})$ reported in Table 6 identify the direction vectors having dimension d associated with the axis belonging to the generic mechanical joint k as seen by the two rigid bodies i_k and j_k involved in the kinematic pair k. Furthermore, as already introduced above, only two types of kinematic joints constrain the motion of the rigid bodies of the pantograph scissor lift mechanism, that is, revolute joints and prismatic joints. To systematically construct the nonlinear algebraic equations representing these two types of mechanical constraints, massive use of the kinematic model of the multibody system is made. Additionally, the following computational procedure is employed. First, for each kinematic pair k, the direction of the joint axis is identified leading to the following equations:

$$\bar{\boldsymbol{v}}_{1,i_k} = \bar{\boldsymbol{v}}_{i_k} = \begin{bmatrix} \bar{v}_{x,i_k} \\ \bar{v}_{y,i_k} \\ \bar{v}_{z,i_k} \end{bmatrix}, \quad \bar{\boldsymbol{v}}_{1,j_k} = \bar{\boldsymbol{v}}_{j_k} = \begin{bmatrix} \bar{v}_{x,j_k} \\ \bar{v}_{y,j_k} \\ \bar{v}_{z,j_k} \end{bmatrix}, \quad k = 1, 2, \ldots, N_{c,\Psi} \tag{141}$$

where $\bar{\boldsymbol{v}}_{1,i_k} \equiv \bar{\boldsymbol{v}}_{1,i_k}(P_{i_k})$ and $\bar{\boldsymbol{v}}_{1,j_k} \equiv \bar{\boldsymbol{v}}_{1,j_k}(P_{j_k})$ identify two direction vectors of dimension d associated with the axis belonging to the generic mechanical joint k as seen by the two rigid bodies i_k and j_k involved in the kinematic pair k, while $\bar{v}_{x,i_k} \equiv \bar{v}_{x,i_k}(P_{i_k})$, $\bar{v}_{y,i_k} \equiv \bar{v}_{y,i_k}(P_{i_k})$, and $\bar{v}_{z,i_k} \equiv \bar{v}_{z,i_k}(P_{i_k})$ are the Cartesian components of the local direction vector $\bar{\boldsymbol{v}}_{i_k}$, whereas $\bar{v}_{x,j_k} \equiv \bar{v}_{x,j_k}(P_{j_k})$, $\bar{v}_{y,j_k} \equiv \bar{v}_{y,j_k}(P_{j_k})$, and $\bar{v}_{z,j_k} \equiv \bar{v}_{z,j_k}(P_{j_k})$ are the Cartesian components of the local direction vector $\bar{\boldsymbol{v}}_{j_k}$. Subsequently, the following geometric quantities are explicitly computed:

$$\bar{w}_{i_k} = \sqrt{\bar{v}_{x,i_k}^2 + \bar{v}_{z,i_k}^2}, \quad \bar{w}_{j_k} = \sqrt{\bar{v}_{x,j_k}^2 + \bar{v}_{z,j_k}^2}, \quad k = 1, 2, \ldots, N_{c,\Psi} \tag{142}$$

where $\bar{w}_{i_k} \equiv \bar{w}_{i_k}(P_{i_k})$ and $\bar{w}_{j_k} \equiv \bar{w}_{j_k}(P_{j_k})$ are two constant geometric quantities associated with the kinematic pair k. Then, the following procedure is used for deriving an additional set of direction vectors in order to form two right-hand orthogonal triads associated with the kinematic pair k as seen from the two rigid bodies i_k and j_k:

$$\bar{w}_{i_k} \neq 0 \quad \Rightarrow \quad \begin{cases} \bar{\boldsymbol{v}}_{2,i_k} = \begin{bmatrix} -\frac{\bar{v}_{x,i_k}\bar{v}_{y,i_k}}{\bar{w}_{i_k}} \\ \bar{w}_{i_k} \\ -\frac{\bar{v}_{y,i_k}\bar{v}_{z,i_k}}{\bar{w}_{i_k}} \end{bmatrix} \\ \bar{\boldsymbol{v}}_{3,i_k} = \begin{bmatrix} -\frac{\bar{v}_{z,i_k}}{\bar{w}_{i_k}} \\ 0 \\ \frac{\bar{v}_{x,i_k}}{\bar{w}_{i_k}} \end{bmatrix} \end{cases}, \quad k = 1, 2, \ldots, N_{c,\Psi} \tag{143}$$

and

$$\bar{w}_{j_k} \neq 0 \quad \Rightarrow \quad \begin{cases} \bar{\boldsymbol{v}}_{2,j_k} = \begin{bmatrix} -\frac{\bar{v}_{x,j_k}\bar{v}_{y,j_k}}{\bar{w}_{j_k}} \\ \bar{w}_{j_k} \\ -\frac{\bar{v}_{y,j_k}\bar{v}_{z,j_k}}{\bar{w}_{j_k}} \end{bmatrix} \\ \bar{\boldsymbol{v}}_{3,j_k} = \begin{bmatrix} -\frac{\bar{v}_{z,j_k}}{\bar{w}_{j_k}} \\ 0 \\ \frac{\bar{v}_{x,j_k}}{\bar{w}_{j_k}} \end{bmatrix} \end{cases}, \quad k = 1, 2, \ldots, N_{c,\Psi} \tag{144}$$

or

$$\bar{w}_{i_k} = 0 \quad \Rightarrow \quad \begin{cases} \bar{\boldsymbol{v}}_{2,i_k} = \begin{bmatrix} 0 \\ 0 \\ \bar{v}_{y,i_k} \end{bmatrix} \\ \bar{\boldsymbol{v}}_{3,i_k} = \begin{bmatrix} \bar{v}_{y,i_k} \\ 0 \\ 0 \end{bmatrix} \end{cases}, \quad k = 1, 2, \ldots, N_{c,\Psi} \tag{145}$$

Table 6. Type and collocation of the kinematic joints.

Kinematic pair number	Kinematic pair type	First body number	Second body number	First body location point and joint axis	Second body location point and joint axis
k	Name	i_k	j_k	$\begin{cases} \bar{\boldsymbol{u}}_{i_k} = \begin{bmatrix} \bar{x}_{i_k} & \bar{y}_{i_k} & \bar{z}_{i_k} \end{bmatrix}^T \\ \bar{\boldsymbol{v}}_{i_k} = \begin{bmatrix} \bar{v}_{x,i_k} & \bar{v}_{y,i_k} & \bar{v}_{z,i_k} \end{bmatrix}^T \end{cases}$	$\begin{cases} \bar{\boldsymbol{u}}_{j_k} = \begin{bmatrix} \bar{x}_{j_k} & \bar{y}_{j_k} & \bar{z}_{j_k} \end{bmatrix}^T \\ \bar{\boldsymbol{v}}_{j_k} = \begin{bmatrix} \bar{v}_{x,j_k} & \bar{v}_{y,j_k} & \bar{v}_{z,j_k} \end{bmatrix}^T \end{cases}$
1	Revolute	1	0	$\begin{cases} \bar{\boldsymbol{u}}_1 = \begin{bmatrix} -\frac{L_1}{2} & 0 & 0 \end{bmatrix}^T \\ \bar{\boldsymbol{v}}_1 = \begin{bmatrix} 0 & 0 & 1 \end{bmatrix}^T \end{cases}$	$\begin{cases} \bar{\boldsymbol{u}}_0 = \begin{bmatrix} 0 & 0 & 0 \end{bmatrix}^T \\ \bar{\boldsymbol{v}}_0 = \begin{bmatrix} 0 & 1 & 0 \end{bmatrix}^T \end{cases}$
2	Revolute	2	6	$\begin{cases} \bar{\boldsymbol{u}}_2 = \begin{bmatrix} \frac{L_2}{2} & 0 & 0 \end{bmatrix}^T \\ \bar{\boldsymbol{v}}_2 = \begin{bmatrix} 0 & 0 & 1 \end{bmatrix}^T \end{cases}$	$\begin{cases} \bar{\boldsymbol{u}}_6 = \begin{bmatrix} 0 & 0 & 0 \end{bmatrix}^T \\ \bar{\boldsymbol{v}}_6 = \begin{bmatrix} 1 & 0 & 0 \end{bmatrix}^T \end{cases}$
3	Prismatic	6	0	$\begin{cases} \bar{\boldsymbol{u}}_6 = \begin{bmatrix} 0 & 0 & 0 \end{bmatrix}^T \\ \bar{\boldsymbol{v}}_6 = \begin{bmatrix} 0 & 0 & 1 \end{bmatrix}^T \end{cases}$	$\begin{cases} \bar{\boldsymbol{u}}_0 = \begin{bmatrix} L & 0 & 0 \end{bmatrix}^T \\ \bar{\boldsymbol{v}}_0 = \begin{bmatrix} 1 & 0 & 0 \end{bmatrix}^T \end{cases}$
4	Revolute	1	7	$\begin{cases} \bar{\boldsymbol{u}}_1 = \begin{bmatrix} \frac{L_1}{2} & 0 & 0 \end{bmatrix}^T \\ \bar{\boldsymbol{v}}_1 = \begin{bmatrix} 0 & 0 & 1 \end{bmatrix}^T \end{cases}$	$\begin{cases} \bar{\boldsymbol{u}}_7 = \begin{bmatrix} 0 & 0 & 0 \end{bmatrix}^T \\ \bar{\boldsymbol{v}}_7 = \begin{bmatrix} 1 & 0 & 0 \end{bmatrix}^T \end{cases}$
5	Prismatic	7	5	$\begin{cases} \bar{\boldsymbol{u}}_7 = \begin{bmatrix} 0 & 0 & 0 \end{bmatrix}^T \\ \bar{\boldsymbol{v}}_7 = \begin{bmatrix} 0 & 0 & 1 \end{bmatrix}^T \end{cases}$	$\begin{cases} \bar{\boldsymbol{u}}_5 = \begin{bmatrix} \frac{L_5}{2} & 0 & \frac{W_5}{2} \end{bmatrix}^T \\ \bar{\boldsymbol{v}}_5 = \begin{bmatrix} 1 & 0 & 0 \end{bmatrix}^T \end{cases}$
6	Revolute	2	5	$\begin{cases} \bar{\boldsymbol{u}}_2 = \begin{bmatrix} -\frac{L_2}{2} & 0 & 0 \end{bmatrix}^T \\ \bar{\boldsymbol{v}}_2 = \begin{bmatrix} 0 & 0 & 1 \end{bmatrix}^T \end{cases}$	$\begin{cases} \bar{\boldsymbol{u}}_5 = \begin{bmatrix} -\frac{L}{2} & 0 & \frac{W_5}{2} \end{bmatrix}^T \\ \bar{\boldsymbol{v}}_5 = \begin{bmatrix} 0 & 0 & 1 \end{bmatrix}^T \end{cases}$
7	Revolute	1	2	$\begin{cases} \bar{\boldsymbol{u}}_1 = \begin{bmatrix} 0 & 0 & 0 \end{bmatrix}^T \\ \bar{\boldsymbol{v}}_1 = \begin{bmatrix} 0 & 0 & 1 \end{bmatrix}^T \end{cases}$	$\begin{cases} \bar{\boldsymbol{u}}_2 = \begin{bmatrix} 0 & 0 & 0 \end{bmatrix}^T \\ \bar{\boldsymbol{v}}_2 = \begin{bmatrix} 0 & 0 & 1 \end{bmatrix}^T \end{cases}$
8	Revolute	3	0	$\begin{cases} \bar{\boldsymbol{u}}_3 = \begin{bmatrix} -\frac{L_3}{2} & 0 & 0 \end{bmatrix}^T \\ \bar{\boldsymbol{v}}_3 = \begin{bmatrix} 0 & 0 & 1 \end{bmatrix}^T \end{cases}$	$\begin{cases} \bar{\boldsymbol{u}}_0 = \begin{bmatrix} 0 & W & 0 \end{bmatrix}^T \\ \bar{\boldsymbol{v}}_0 = \begin{bmatrix} 0 & 1 & 0 \end{bmatrix}^T \end{cases}$
9	Revolute	4	8	$\begin{cases} \bar{\boldsymbol{u}}_4 = \begin{bmatrix} \frac{L_4}{2} & 0 & 0 \end{bmatrix}^T \\ \bar{\boldsymbol{v}}_4 = \begin{bmatrix} 0 & 0 & 1 \end{bmatrix}^T \end{cases}$	$\begin{cases} \bar{\boldsymbol{u}}_8 = \begin{bmatrix} 0 & 0 & 0 \end{bmatrix}^T \\ \bar{\boldsymbol{v}}_8 = \begin{bmatrix} 1 & 0 & 0 \end{bmatrix}^T \end{cases}$
10	Prismatic	8	0	$\begin{cases} \bar{\boldsymbol{u}}_8 = \begin{bmatrix} 0 & 0 & 0 \end{bmatrix}^T \\ \bar{\boldsymbol{v}}_8 = \begin{bmatrix} 0 & 0 & 1 \end{bmatrix}^T \end{cases}$	$\begin{cases} \bar{\boldsymbol{u}}_0 = \begin{bmatrix} L & W & 0 \end{bmatrix}^T \\ \bar{\boldsymbol{v}}_0 = \begin{bmatrix} 1 & 0 & 0 \end{bmatrix}^T \end{cases}$
11	Revolute	3	9	$\begin{cases} \bar{\boldsymbol{u}}_3 = \begin{bmatrix} \frac{L_3}{2} & 0 & 0 \end{bmatrix}^T \\ \bar{\boldsymbol{v}}_3 = \begin{bmatrix} 0 & 0 & 1 \end{bmatrix}^T \end{cases}$	$\begin{cases} \bar{\boldsymbol{u}}_9 = \begin{bmatrix} 0 & 0 & 0 \end{bmatrix}^T \\ \bar{\boldsymbol{v}}_9 = \begin{bmatrix} 1 & 0 & 0 \end{bmatrix}^T \end{cases}$
12	Prismatic	9	5	$\begin{cases} \bar{\boldsymbol{u}}_9 = \begin{bmatrix} 0 & 0 & 0 \end{bmatrix}^T \\ \bar{\boldsymbol{v}}_9 = \begin{bmatrix} 0 & 0 & 1 \end{bmatrix}^T \end{cases}$	$\begin{cases} \bar{\boldsymbol{u}}_5 = \begin{bmatrix} \frac{L_5}{2} & 0 & -\frac{W_5}{2} \end{bmatrix}^T \\ \bar{\boldsymbol{v}}_5 = \begin{bmatrix} 1 & 0 & 0 \end{bmatrix}^T \end{cases}$
13	Revolute	4	5	$\begin{cases} \bar{\boldsymbol{u}}_4 = \begin{bmatrix} -\frac{L_4}{2} & 0 & 0 \end{bmatrix}^T \\ \bar{\boldsymbol{v}}_4 = \begin{bmatrix} 0 & 0 & 1 \end{bmatrix}^T \end{cases}$	$\begin{cases} \bar{\boldsymbol{u}}_5 = \begin{bmatrix} -\frac{L}{2} & 0 & -\frac{W_5}{2} \end{bmatrix}^T \\ \bar{\boldsymbol{v}}_5 = \begin{bmatrix} 0 & 0 & 1 \end{bmatrix}^T \end{cases}$
14	Revolute	3	4	$\begin{cases} \bar{\boldsymbol{u}}_3 = \begin{bmatrix} 0 & 0 & 0 \end{bmatrix}^T \\ \bar{\boldsymbol{v}}_3 = \begin{bmatrix} 0 & 0 & 1 \end{bmatrix}^T \end{cases}$	$\begin{cases} \bar{\boldsymbol{u}}_4 = \begin{bmatrix} 0 & 0 & 0 \end{bmatrix}^T \\ \bar{\boldsymbol{v}}_4 = \begin{bmatrix} 0 & 0 & 1 \end{bmatrix}^T \end{cases}$

and

$$\bar{w}_{j_k} = 0 \quad \Rightarrow \quad \begin{cases} \bar{\boldsymbol{v}}_{2,j_k} = \begin{bmatrix} 0 \\ 0 \\ \bar{v}_{y,j_k} \end{bmatrix} \\ \bar{\boldsymbol{v}}_{3,j_k} = \begin{bmatrix} \bar{v}_{y,j_k} \\ 0 \\ 0 \end{bmatrix} \end{cases} , \quad k = 1, 2, \ldots, N_{c,\Psi} \tag{146}$$

where $\bar{\boldsymbol{v}}_{1,i_k} \equiv \bar{\boldsymbol{v}}_{1,i_k}(P_{i_k})$, $\bar{\boldsymbol{v}}_{2,i_k} \equiv \bar{\boldsymbol{v}}_{2,i_k}(P_{i_k})$, and $\bar{\boldsymbol{v}}_{3,i_k} \equiv \bar{\boldsymbol{v}}_{3,i_k}(P_{i_k})$ form a right-hand orthogonal triad of local directions vectors having dimension d associated with the joint axis of the rigid body i_k, while $\bar{\boldsymbol{v}}_{1,j_k} \equiv \bar{\boldsymbol{v}}_{1,j_k}(P_{j_k})$, $\bar{\boldsymbol{v}}_{2,j_k} \equiv \bar{\boldsymbol{v}}_{2,j_k}(P_{j_k})$, and $\bar{\boldsymbol{v}}_{3,j_k} \equiv \bar{\boldsymbol{v}}_{3,j_k}(P_{j_k})$ form a right-hand orthogonal triad of local directions vectors having dimension d associated with the joint axis of the rigid body j_k. These local direction vectors can be readily transformed in their global counterparts by using the rotation matrices respectively associated with the rigid bodies i_k and j_k involved in the kinematic pair k and respectively denoted with $\boldsymbol{A}_{i_k}$ and $\boldsymbol{A}_{j_k}$ as follows:

$$\begin{cases} \boldsymbol{v}_{1,i_k} = \boldsymbol{A}_{i_k} \bar{\boldsymbol{v}}_{1,i_k} \\ \boldsymbol{v}_{2,i_k} = \boldsymbol{A}_{i_k} \bar{\boldsymbol{v}}_{2,i_k} \\ \boldsymbol{v}_{3,i_k} = \boldsymbol{A}_{i_k} \bar{\boldsymbol{v}}_{3,i_k} \end{cases} , \quad \begin{cases} \boldsymbol{v}_{1,j_k} = \boldsymbol{A}_{j_k} \bar{\boldsymbol{v}}_{1,j_k} \\ \boldsymbol{v}_{2,j_k} = \boldsymbol{A}_{j_k} \bar{\boldsymbol{v}}_{2,j_k} \\ \boldsymbol{v}_{3,j_k} = \boldsymbol{A}_{j_k} \bar{\boldsymbol{v}}_{3,j_k} \end{cases} , \quad k = 1, 2, \ldots, N_{c,\Psi} \tag{147}$$

where the direction vectors $\boldsymbol{v}_{1,i_k} \equiv \boldsymbol{v}_{1,i_k}(P_{i_k})$, $\boldsymbol{v}_{2,i_k} \equiv \boldsymbol{v}_{2,i_k}(P_{i_k})$, and $\boldsymbol{v}_{3,i_k} \equiv \boldsymbol{v}_{3,i_k}(P_{i_k})$ of dimension d respectively represent the global counterpart of the local direction vectors $\bar{\boldsymbol{v}}_{1,i_k}$, $\bar{\boldsymbol{v}}_{2,i_k}$, and $\bar{\boldsymbol{v}}_{3,i_k}$, while the direction vectors $\boldsymbol{v}_{1,j_k} \equiv \boldsymbol{v}_{1,j_k}(P_{j_k})$, $\boldsymbol{v}_{2,j_k} \equiv \boldsymbol{v}_{2,j_k}(P_{j_k})$, and $\boldsymbol{v}_{3,j_k} \equiv \boldsymbol{v}_{3,j_k}(P_{j_k})$ of dimension d respectively represent the global counterpart of the local direction vectors $\bar{\boldsymbol{v}}_{1,j_k}$, $\bar{\boldsymbol{v}}_{2,j_k}$, and $\bar{\boldsymbol{v}}_{3,j_k}$. Once the right-hand orthogonal triads of each body involved in the generic kinematic pair k of each joint are defined, one can go ahead with the computation of the following geometric vector representing the distance between two material points P_{i_k} and P_{j_k} collocated on the same joint axis k:

$$\boldsymbol{d}_k = \boldsymbol{r}_{i_k} - \boldsymbol{r}_{j_k} = \boldsymbol{R}_{i_k} + \boldsymbol{A}_{i_k} \bar{\boldsymbol{u}}_{i_k} - \boldsymbol{R}_{j_k} - \boldsymbol{A}_{j_k} \bar{\boldsymbol{u}}_{j_k}, \quad k = 1, 2, \ldots, N_{c,\Psi} \tag{148}$$

where $\boldsymbol{d}_k \equiv \boldsymbol{d}_k(P_{i_k}, P_{j_k}, \boldsymbol{q}_{i_k}, \boldsymbol{q}_{j_k}, t)$ is a vector of dimension d representing the distance vector between the two material points P_{i_k} and P_{j_k} collocated on the joint axis k, while $\boldsymbol{r}_{i_k} \equiv \boldsymbol{r}_{i_k}(P_{i_k}, \boldsymbol{q}_{i_k}, t)$ and $\boldsymbol{r}_{j_k} \equiv \boldsymbol{r}_{j_k}(P_{j_k}, \boldsymbol{q}_{j_k}, t)$ are two vector having dimension d respectively representing the global position vectors of the points P_{i_k} and P_{j_k} as seen be the rigid bodies i_k and j_k involved in the kinematic pair k. By knowing the analytical form of the right-hand orthogonal triads of each body involved in the generic kinematic pair k of each mechanical joint, as well as the distance vector between the two material points P_{i_k} and P_{j_k} collocated on the joint axis k, one can systematically formulate the algebraic equations of the kinematic joints of interest. For this purpose, in the case of a generic revolute joint, one can construct the following vector of extrinsic constraints:

$$\boldsymbol{\Psi}_k = \begin{bmatrix} \boldsymbol{d}_k \\ \boldsymbol{v}_{2,i_k}^T \boldsymbol{v}_{1,j_k} \\ \boldsymbol{v}_{3,i_k}^T \boldsymbol{v}_{1,j_k} \end{bmatrix} \tag{149}$$

Similarly, in the case of a generic prismatic joint, one can construct the following vector of extrinsic constraints:

$$\boldsymbol{\Psi}_k = \begin{bmatrix} \boldsymbol{v}_{2,i_k}^T \boldsymbol{d}_k \\ \boldsymbol{v}_{3,i_k}^T \boldsymbol{d}_k \\ \boldsymbol{v}_{1,i_k}^T \boldsymbol{v}_{2,j_k} \\ \boldsymbol{v}_{1,i_k}^T \boldsymbol{v}_{3,j_k} \\ \boldsymbol{w}_{i_k}^T \boldsymbol{w}_{j_k} - c_{0,k} \end{bmatrix} \tag{150}$$

where $\boldsymbol{w}_{i_k} \equiv \boldsymbol{w}_{i_k}(P_{i_k}, \boldsymbol{q}_{i_k}, t)$ and $\boldsymbol{w}_{j_k} \equiv \boldsymbol{w}_{j_k}(P_{j_k}, \boldsymbol{q}_{j_k}, t)$ are two nonparallel vectors of dimension d respectively belonging to the rigid bodies i_k and j_k, whereas $c_{0,k}$ is a constant scalar quantity representing the initial numerical value of the dot product between the geometric vectors $\boldsymbol{w}_{i_k}$ and $\boldsymbol{w}_{j_k}$. For instance, one can readily determine the geometric direction vectors denoted with $\boldsymbol{w}_{i_k}$ and $\boldsymbol{w}_{j_k}$ as follows:

$$\begin{cases} \boldsymbol{w}_{i_k} = a_{i_k} \boldsymbol{v}_{2,i_k} + b_{i_k} \boldsymbol{v}_{3,i_k} \\ \boldsymbol{w}_{j_k} = a_{j_k} \boldsymbol{v}_{2,j_k} + b_{j_k} \boldsymbol{v}_{3,j_k} \end{cases} , \quad k = 1, 2, \ldots, N_{c,\Psi} \tag{151}$$

where a_{i_k}, b_{i_k}, a_{j_k}, and b_{j_k} are constant coefficients that must be properly prescribed for each kinematic pair k. At this stage, as an intermediate step, one can directly assemble the complete vector of intrinsic constraints as follows:

$$\boldsymbol{\Phi} = \sum_{i=1}^{N_{c,\Phi}} \boldsymbol{B}_{\Phi_i}^T \boldsymbol{\Phi}_i \tag{152}$$

where $\boldsymbol{\Phi} \equiv \boldsymbol{\Phi}(\boldsymbol{q}, t)$ is a nonlinear vector of algebraic equations containing the entire set of intrinsic constraints having dimension $n_{c,\Phi}$ given by:

$$n_{c,\Phi} = \sum_{i=1}^{N_{c,\Phi}} n_{c,\Phi_i} = 9 \tag{153}$$

The constant rectangular matrix denoted with $\boldsymbol{B}_{\Phi_i}$ is a Boolean matrix of dimensions $n_{c,\Phi_i} \times n_{c,\Phi}$ that allows for recovering the generic set of intrinsic constraints associated with the rigid body i from the complete set of intrinsic constraints as follows:

$$\boldsymbol{\Phi}_i = \boldsymbol{B}_{\Phi_i} \boldsymbol{\Phi}, \quad i = 1, 2, \ldots, N_{c,\Phi} \tag{154}$$

Adopting a similar procedure, one can directly assemble the complete vector of extrinsic constraints as follows:

$$\boldsymbol{\Psi} = \sum_{k=1}^{N_{c,\Psi}} \boldsymbol{B}_{\Psi_k}^T \boldsymbol{\Psi}_k \tag{155}$$

where $\boldsymbol{\Psi} \equiv \boldsymbol{\Psi}(\boldsymbol{q}, t)$ is a nonlinear vector of algebraic equations containing the entire set of extrinsic constraints having dimension $n_{c,\Psi}$ given by:

$$n_{c,\Psi} = \sum_{k=1}^{N_{c,\Psi}} n_{c,\Psi_k} = 70 \tag{156}$$

The constant rectangular matrix denoted with $\boldsymbol{B}_{\Psi_k}$ is a Boolean matrix of dimensions $n_{c,\Psi_k} \times n_{c,\Psi}$ that allows for recovering the generic set of extrinsic constraints associated with the kinematic pair k from the complete set of extrinsic constraints as follows:

$$\boldsymbol{\Psi}_k = \boldsymbol{B}_{\Psi_k} \boldsymbol{\Psi}, \quad i = 1, 2, \ldots, N_{c,\Psi} \tag{157}$$

The last fundamental step in the formulation of the constraint equations is the following assembly process relative to the total vector of algebraic constraints:

$$\boldsymbol{C} = \begin{bmatrix} \boldsymbol{\Phi} \\ \boldsymbol{\Psi} \end{bmatrix} \tag{158}$$

where $\boldsymbol{C} \equiv \boldsymbol{C}(\boldsymbol{q}, t)$ is a nonlinear vector of algebraic constraints having dimension n_c defined as:

$$n_c = n_{c,\Phi} + n_{c,\Psi} = 79 \tag{159}$$

From the analytical definition of the total vector of algebraic constraints, one can readily determine the constraint Jacobian matrix and the constraint quadratic velocity vector as follows:

$$\boldsymbol{C}_{\boldsymbol{q}} = \frac{\partial \boldsymbol{C}}{\partial \boldsymbol{q}} = \begin{bmatrix} \boldsymbol{\Phi}_{\boldsymbol{q}} \\ \boldsymbol{\Psi}_{\boldsymbol{q}} \end{bmatrix}, \quad \boldsymbol{Q}_{\mathrm{d}} = \boldsymbol{C}_{\boldsymbol{q}} \ddot{\boldsymbol{q}} - \ddot{\boldsymbol{C}} = \begin{bmatrix} \boldsymbol{Q}_{\mathrm{d},\Phi} \\ \boldsymbol{Q}_{\mathrm{d},\Psi} \end{bmatrix} \tag{160}$$

where $\boldsymbol{C}_{\boldsymbol{q}} \equiv \boldsymbol{C}_{\boldsymbol{q}}(\boldsymbol{q}, t)$ is a rectangular matrix of dimensions $n_c \times n_q$ representing the system constraint Jacobian matrix, $\boldsymbol{\Phi}_{\boldsymbol{q}} \equiv \boldsymbol{\Phi}_{\boldsymbol{q}}(\boldsymbol{q}, t)$ is a rectangular matrix of dimensions $n_{c,\Phi} \times n_q$ representing the system intrinsic constraint Jacobian matrix, $\boldsymbol{\Psi}_{\boldsymbol{q}} \equiv \boldsymbol{\Psi}_{\boldsymbol{q}}(\boldsymbol{q}, t)$ is a rectangular matrix of dimensions $n_{c,\Psi} \times n_q$ representing the system extrinsic constraint Jacobian matrix, $\boldsymbol{Q}_{\mathrm{d}} \equiv \boldsymbol{Q}_{\mathrm{d}}(\boldsymbol{q}, \dot{\boldsymbol{q}}, t)$ is vector of dimension n_c representing the system constraint quadratic velocity vector, $\boldsymbol{Q}_{\mathrm{d},\Phi} \equiv \boldsymbol{Q}_{\mathrm{d},\Phi}(\boldsymbol{q}, \dot{\boldsymbol{q}}, t)$ is vector of dimension $n_{c,\Phi}$ representing the system intrinsic constraint quadratic velocity vector, and $\boldsymbol{Q}_{\mathrm{d},\Psi} \equiv \boldsymbol{Q}_{\mathrm{d},\Psi}(\boldsymbol{q}, \dot{\boldsymbol{q}}, t)$ is vector of dimension $n_{c,\Psi}$ representing the system extrinsic constraint quadratic velocity vector. As a final remark, it is important to note that the constraint Jacobian matrix plays a fundamental role in the dynamic analysis of rigid multibody mechanical systems based on a redundant coordinate modeling approach. By respectively denoting with r_c and r_q the row rank and the column rank of the rectangular matrix $\boldsymbol{C}_{\boldsymbol{q}}$ representing the total constraint Jacobian matrix, always equal in virtue of a fundamental result of linear algebra, insights and fundamental geometric properties of the articulated mechanical system of interest can be deduced. In fact, the row rank of the constraint Jacobian matrix allows for determining the number of independent constraint equations denoted with $n_{\bar{c}}$, that is, to identify the algebraic equations that are kinematically redundant. Similarly, the column rank of the constraint Jacobian matrix is necessary for the systematic calculation of the system degrees of freedom denoted with n_f, namely, for the partition of the Lagrangian coordinates of the multibody system into two subsets of independent and dependent generalized coordinates. In summary, one can write the following two fundamental equations:

$$n_{\bar{c}} = r_c = r, \quad n_f = n_q - r_q = n_q - r \tag{161}$$

where the important result of linear algebra stating the fact that the row rank r_c and the column rank r_q of a general rectangular matrix are equal and denoted with r was used. More specifically, a matrix factorization technique of numerical linear algebra, such as the Gaussian elimination process with partial or full pivoting, can be applied to the constraint Jacobian matrix considered row-wise or column-wise. The former process is necessary for identifying the r independent constraint equations, whereas the latter process leads to the definition of the r dependent generalized coordinates. In particular, by applying row-wise a proper matrix factorization to the constraint Jacobian matrix, one can readily find the subset of $m_{i_{np}} = r$ independent constraint equations associated with the non-pivot rows and the subset of $m_{i_p} = n_c - r$ dependent constraint equations associated with the pivot rows. Similarly, by performing column-wise the same numerical process to the constraint Jacobian matrix, one can easily find the subset of $m_{j_{np}} = n_q - r$ independent generalized coordinates associated with the non-pivot columns and the subset of $m_{j_p} = r$ dependent generalized coordinates associated with the pivot columns. Since the constraint Jacobian matrix $\boldsymbol{C}_{\boldsymbol{q}}$ depend on configuration vector $\boldsymbol{q}$, in theory, the two identification processes mentioned before should be repeated several times at different time intervals. In practice, it is sufficient to perform these tasks only at the beginning of the dynamical simulation, considering the initial value of the configuration vector denoted with $\boldsymbol{q}_0$. For instance, in the case of the pantograph scissor lift mechanism assumed in this paper as the case study, by implementing the two numerical procedures mentioned before, since the rank of the constraint Jacobian matrix is equal to $r = 62$ and the total number of the system generalized coordinates is equal to $n_q = 63$, one can readily identify $n_{\bar{c}} = 62$ independent constraint equations and only $n_f = 1$ degree of freedom. By doing so, in order to be able to adopt a standard multibody procedure for the numerical solution of the differential-algebraic dynamic equations, one can define the independent constraint vector denoted with $\bar{\boldsymbol{C}} \equiv \bar{\boldsymbol{C}}(\boldsymbol{q}, t)$ having dimension $n_{\bar{c}}$, the independent constraint Jacobian matrix denoted with $\bar{\boldsymbol{C}}_{\boldsymbol{q}} \equiv \bar{\boldsymbol{C}}_{\boldsymbol{q}}(\boldsymbol{q}, t)$ having dimensions $n_{\bar{c}} \times n_q$, and the independent constraint quadratic velocity vector denoted with $\bar{\boldsymbol{Q}}_{\mathrm{d}} \equiv \bar{\boldsymbol{Q}}_{\mathrm{d}}(\boldsymbol{q}, \dot{\boldsymbol{q}}, t)$ having dimension $n_{\bar{c}}$. By employing the fundamental principles of classical mechanics in conjunction with the mathematical technique of analytical dynamics based

on the introduction of the Lagrange multipliers, the differential-algebraic equations of motion of the multibody system under study assume the following final form represented in the configuration space:

$$\left\{ \begin{array}{l} \boldsymbol{M}\ddot{\boldsymbol{q}} = \boldsymbol{Q}_{\mathrm{b}} + \boldsymbol{Q}_{\mathrm{c}} - \boldsymbol{C}_{\boldsymbol{q}}^{T}\boldsymbol{\lambda} \\ \\ \boldsymbol{C} = \boldsymbol{0} \end{array} \right. \Rightarrow \left\{ \begin{array}{l} \boldsymbol{M}\ddot{\boldsymbol{q}} = \boldsymbol{Q}_{\mathrm{b}} + \boldsymbol{Q}_{\mathrm{c}} - \bar{\boldsymbol{C}}_{\boldsymbol{q}}^{T}\bar{\boldsymbol{\lambda}} \\ \\ \bar{\boldsymbol{C}} = \boldsymbol{0} \end{array} \right. \tag{162}$$

where $\boldsymbol{\lambda} \equiv \boldsymbol{\lambda}(t)$ is a vector of dimension n_c containing the total number of Lagrange multipliers associated with the entire set of algebraic constraint equations and $\bar{\boldsymbol{\lambda}} \equiv \bar{\boldsymbol{\lambda}}(t)$ is a vector of dimension $n_{\bar{c}}$ containing the independent Lagrange multipliers associated with the independent set of algebraic constraint equations. The system equations of motion given by Equation (162) represent a set of index-3 differential-algebraic equations, which can be mathematically transformed in the following equivalent form:

$$\left\{ \begin{array}{l} \boldsymbol{M}\ddot{\boldsymbol{q}} = \boldsymbol{Q}_{\mathrm{b}} + \boldsymbol{Q}_{\mathrm{c}} - \bar{\boldsymbol{C}}_{\boldsymbol{q}}^{T}\bar{\boldsymbol{\lambda}} \\ \\ \bar{\boldsymbol{C}}_{\boldsymbol{q}}\ddot{\boldsymbol{q}} = \bar{\boldsymbol{Q}}_{\mathrm{d}} \end{array} \right. \tag{163}$$

where Equation (163) represents a set of index-1 differential-algebraic equations of motion, containing only the independent subset of kinematic constraints meaningful for the dynamic analysis, that require in their computer implementation the use of an appropriate constraint stabilization technique [148, 149]. As discussed below, the differential-algebraic equations encountered in the dynamic analysis of multibody mechanical systems are characterized by a mathematical property called the differential index, which can be interpreted as a degree of difficulty in properly solving them using a numerical integration procedure [150]. Roughly speaking, the differential index of a system of differential-algebraic equations corresponds to the number of time derivatives to be applied to the set of constraint equations in order to transform them into an equivalent explicit set of ordinary differential equations [151]. Therefore, by performing a proper number of differentiations in time onto the constraint equations that appear in the original set of differential-algebraic equations, one can eliminate the Lagrange multipliers and obtain an equivalent set of ordinary differential equations. From a numerical standpoint, however, the implementation of any index reduction process, employed for transforming the differential-algebraic equations into their equivalent ordinary form, comes with the price of requiring the use of an additional constraint stabilization technique, which is necessary for satisfying the algebraic equations at both the position and velocity levels [152, 153]. This issue is further discussed in the numerical results section of the paper.

5.5 State-space representation

The last step necessary for the computer implementation of the redundant coordinate multibody model of the pantograph scissor lift mechanism is the transformation of the system equations of motion from the configuration space to the state space. However, before doing that, one should be able to analytically determine the system generalized acceleration vector. This calculation can be readily performed by using the index-1 form of the differential-algebraic equations of motion and employing a standard multibody computational procedure such as the augmented formulation or the embedding technique. Considering Equation (163), the multibody procedure based on the augmented formulation is selected, since it can be readily written as:

$$\left[\begin{array}{cc} \boldsymbol{M} & \bar{\boldsymbol{C}}_{\boldsymbol{q}}^{T} \\ \bar{\boldsymbol{C}}_{\boldsymbol{q}} & \boldsymbol{O} \end{array} \right] \left[\begin{array}{c} \ddot{\boldsymbol{q}} \\ \bar{\boldsymbol{\lambda}} \end{array} \right] = \left[\begin{array}{c} \boldsymbol{Q}_{\mathrm{b}} + \boldsymbol{Q}_{\mathrm{c}} \\ \bar{\boldsymbol{Q}}_{\mathrm{d}} \end{array} \right] \quad \Leftrightarrow \quad \boldsymbol{M}_{\mathrm{a}}\boldsymbol{q}_{\mathrm{a}} = \boldsymbol{Q}_{\mathrm{a}} \tag{164}$$

where:

$$\boldsymbol{q}_{\mathrm{a}} = \left[\begin{array}{c} \ddot{\boldsymbol{q}} \\ \bar{\boldsymbol{\lambda}} \end{array} \right], \quad \boldsymbol{M}_{\mathrm{a}} = \left[\begin{array}{cc} \boldsymbol{M} & \bar{\boldsymbol{C}}_{\boldsymbol{q}}^{T} \\ \bar{\boldsymbol{C}}_{\boldsymbol{q}} & \boldsymbol{O} \end{array} \right], \quad \boldsymbol{Q}_{\mathrm{a}} = \left[\begin{array}{c} \boldsymbol{Q}_{\mathrm{b}} + \boldsymbol{Q}_{\mathrm{c}} \\ \bar{\boldsymbol{Q}}_{\mathrm{d}} \end{array} \right] \tag{165}$$

where $n_a = n_q + n_{\bar{c}} = 125$ is the characteristic dimension of the multibody problem at hand, $\boldsymbol{q}_{\mathrm{a}} \equiv \boldsymbol{q}_{\mathrm{a}}(t)$ is a vector of dimension n_a representing the system augmented coordinate vector including the system generalized coordinates and the independent Lagrange multipliers, $\boldsymbol{M}_{\mathrm{a}} \equiv \boldsymbol{M}_{\mathrm{a}}(\boldsymbol{q}, t)$ is a square matrix having dimensions $n_a \times n_a$ that identifies the system augmented mass matrix including the system mass matrix and the total independent constraint Jacobian matrix, and $\boldsymbol{Q}_{\mathrm{a}} \equiv \boldsymbol{Q}_{\mathrm{a}}(\boldsymbol{q}, \dot{\boldsymbol{q}}, t)$ is a vector of dimension n_a which describes the system augmented generalized force vector containing the total body generalized force vector and the independent constraint quadratic velocity vector. More importantly, Equation (164) forms a linear system of algebraic equations that can be numerically solved by using a conventional Gaussian procedure, leading to the determination at each time step of the numerical simulation of the system generalized acceleration vector and of the vector of independent Lagrange multipliers. By doing so, one can carry out the transformation of the system dynamic equations from the configuration space to the state space in order to allow for the use of standard numerical integration procedures for the numerical solution of the equations of motion, like the explicit Runge-Kutta methods or the explicit linear multistep methods. For this purpose, define the following vector of state variables:

$$\boldsymbol{z} = \left[\begin{array}{c} \boldsymbol{z}_1 \\ \boldsymbol{z}_2 \end{array} \right] = \left[\begin{array}{c} \boldsymbol{q} \\ \dot{\boldsymbol{q}} \end{array} \right] \tag{166}$$

where $n_z = 2n_q = 126$ is the dimension of the state space and $\boldsymbol{z} \equiv \boldsymbol{z}(t)$ is a vector of dimension n_z representing the system state vector. Consequently, the state function associated with the introduction of the state vector defined above is given by:

$$\boldsymbol{f} = \left[\begin{array}{c} \boldsymbol{f}_1 \\ \boldsymbol{f}_2 \end{array} \right] = \left[\begin{array}{c} \dot{\boldsymbol{q}} \\ \ddot{\boldsymbol{q}} \end{array} \right] \tag{167}$$

where $\boldsymbol{f} \equiv \boldsymbol{f}(\boldsymbol{z}, t)$ is a nonlinear vector function of dimension n_z that identifies the system state function in which the system generalized acceleration vector is obtained from the computer implementation of the augmented formulation. At this stage, it is noteworthy to emphasize the point that the explicit definition of the system state function is made possible by the use of a proper multibody solution procedure such as, for example, the augmented formulation method mentioned before, which requires the computer implementation of a constraint stabilization procedure. Finally, the state-space representation of the redundant coordinate multibody model of the pantograph scissor lift mechanism assumes the following canonical form:

$$\left\{ \begin{array}{l} \dot{\boldsymbol{z}} = \boldsymbol{f} \\ \boldsymbol{z}(t = 0) = \boldsymbol{z}_0 \end{array} \right. \tag{168}$$

where $\boldsymbol{z}_0$ denotes a constant vector having dimension n_z including the state-space set of initial conditions, which, for the problem at hand, assumes the following simple form:

$$\boldsymbol{z}_0 = \begin{bmatrix} \boldsymbol{q}_0 \\ \boldsymbol{0} \end{bmatrix} \tag{169}$$

where $\boldsymbol{q}_0$ denotes a constant vector having dimension n_q including the configuration-space set of initial conditions. The state-space dynamic model of the mechanical system under study is amenable to be treated with several families of numerical integration schemes for the computer implementation and the numerical solution of the equations of motion [154]. Additionally, since the system dynamical model was obtained considering an index-1 form of the differential-algebraic equations, it is necessary to include in the numerical integration scheme an additional computational step in which the drift of the algebraic equations is counteracted through the use of a robust constraint stabilization procedure, such as the generalized coordinate partitioning approach, the direct correction algorithm, and the Baumgarte method [155–157]. In this paper, the generalized coordinate partitioning method is used for enforcing the fulfillment of the constraint equations at both the position and velocity levels, thereby leading to accurate numerical solutions of the system equations of motion, which allow for testing several control policies in realistic scenarios in which the pantograph scissor lift mechanism operates.

6. Numerical results and discussion

6.1 Description of the numerical experiments

In order to demonstrate the effectiveness of the control strategy devised in this investigation, the two mechanical models of the pantograph scissor lift mechanism proposed in this work were implemented in a virtual simulation environment. More specifically, both the minimal coordinate multibody model and the redundant coordinate multibody model were implemented by coding two computer programs developed using the numerical computing environment based on MATLAB. In the first case, that is, in the case of the minimal coordinate multibody model, a special-purpose computer program was developed for simulating the pantograph scissor lift mechanism. On the other hand, in the second case, that is, in the case of the redundant coordinate multibody model, a general-purpose computer program was developed for simulating the pantograph scissor lift mechanism. Furthermore, in order to perform an additional comparison with the numerical results obtained using another software, the redundant coordinate multibody model was also implemented employing SIMSCAPE MULTIBODY, which is a MATLAB-based graphical modeling and programming environment. By doing so, several dynamical simulations were performed to validate the control strategy developed herein, as well as the proposed mechanical models of the pantograph scissor lift mechanism, which reproduce the behavior of the articulated mechanical system of interest in different operational scenarios. For this purpose, the computational procedure utilized for performing the numerical simulations of both the minimal and the redundant coordinate multibody models is the ODE15s solver, which is implemented in MATLAB and in SIMSCAPE MULTIBODY for obtaining accurate numerical solutions of highly nonlinear sets of ordinary differential equations. The numerical scheme followed by the ODE15s solver is a variable-step variable-order computational procedure, based on the numerical differentiation formulas of orders from one to five, which is particularly suitable for solving stiff problems, such as those arising from the index reduction of differential-algebraic equations [158]. The numerical results obtained by using this powerful and effective computer subroutine are then interpolated in a post-processing phase to find a numerical solution that is evenly spaced on the discretized time grid. The fundamental parameters of the numerical solver employed in this paper are reported in Table 7.

Table 7. Fundamental parameters of the numerical solver used in MATLAB and in SIMSCAPE MULTIBODY.

Descriptions	Symbols	Data (units)
Dynamical simulation time span	T_s	10 (s)
Dynamical simulation time step	Δt	10^{-3} (s)
Solver relative error tolerance	ε_r	10^{-8} (m) or (rad)
Solver absolute error tolerance	ε_a	10^{-10} (m) or (rad)

In Table 7, T_s and Δt respectively indicate the time span and the time step of the dynamical simulation, while ε_r and ε_a respectively identify the relative error tolerance and the absolute error tolerance of the numerical solver. On the other hand, since the redundant coordinate multibody model of the mechanical system under study is described by a nonlinear set of index-1 differential-algebraic equations, the generalized coordinate partitioning method was employed in conjunction with the numerical solver as a constraint stabilization technique to avoid the drift phenomenon associated with the violations of the algebraic equations [159,160]. To this end, the system approximate solution, which is obtained at each time step from the numerical solver by performing the time marching of the equations of motion, is partitioned first into two subsets of dependent and independent generalized coordinates, and the same process is repeated for the generalized velocities. Subsequently, the algebraic constraint equations are numerically enforced at both the position and velocity levels by exploiting the partition into dependent and independent variables. Therefore, the generalized coordinate partitioning method, which is necessary for the computer implementation of general multibody models based on a redundant set of generalized coordinates for enforcing the satisfaction of the constraint equations at both the position and velocity levels, was used in the multibody models constructed by using MATLAB and SIMSCAPE MULTIBODY. Consequently, the computational methods employed in this paper for solving both the nonlinear ordinary differential equations and the nonlinear differential-algebraic equations lead to approximate solutions of the dynamic equations describing the motion of the pantograph scissor lift mechanism that are physically consistent and numerically stable. In this vein, the main goal of the numerical experiments carried out by using the two mechanical models of the pantograph scissor lift mechanism is to find the best combination of the control parameters that define both the feedforward controller and the feedback controller. The fundamental parameters associated with the control strategy proposed in this work are the feedforward controller actuation time denoted with T_a, as well as the feedback controller proportional and derivative coefficients respectively indicated as k_c and σ_c. As discussed in detail below, this process aimed at tuning the control parameters is iteratively performed starting from the default parameters used as references that are reported in Table 3.

6.2 Computer implementation of the minimal coordinate multibody model using MATLAB

In this subsection, the numerical results obtained from the computer implementation in MATLAB of the minimal coordinate multibody model of the pantograph scissor lift mechanism developed in Section 4. are presented and discussed. The numerical experiments carried out and described in this subsection are meant to qualitatively and quantitatively refine the actuation time

denoted with T_a that characterizes the analytical law designed for the feedforward controller. For this purpose, three cases are considered. In Case A1 (reference), $T_a = 2.5$ (s) is assumed; in Case A2 (first feedforward parameters test), $T_a = 5$ (s) is assumed; in Case A3 (second feedforward parameters test), $T_a = 7.5$ (s) is assumed. While Case A1 is identical to the default configuration of the system control parameters reported in Table 3, Case A2 and Case A3 represent two trials for establishing the influence of the feedforward controller actuation time T_a on the system time response and its dynamic behavior in general. In Figure 4, the time laws representing the motion of the bar in correspondence to the three case studies A1, A2, and A3 considered are shown. In particular, Figure 4a represents the angular displacement of the bar, while Figure 4b represents its angular velocity computed using the minimal coordinate multibody model implemented in MATLAB.

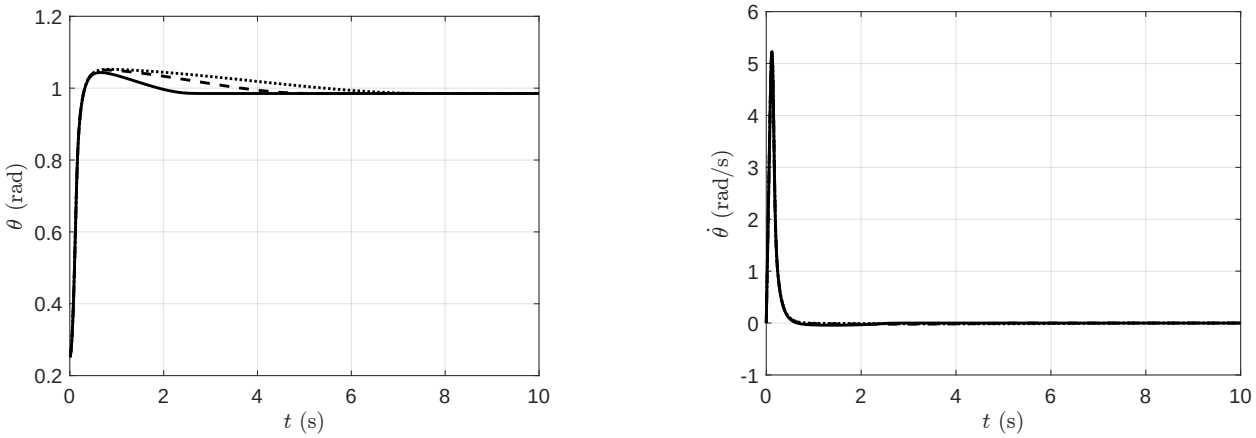

(a) *Angular displacement* θ. **(b)** *Angular velocity* $\dot{\theta}$.

Figure 4. *Angular displacement* θ *and angular velocity* $\dot{\theta}$ *of the bar obtained using the minimal coordinate multibody model implemented in MATLAB. The solid line (——) corresponds to Case A1; the dashed line (- - -) corresponds to Case A2; the dotted line (·····) corresponds to Case A3.*

In Figure 5, the time laws representing the motion of the platform in correspondence to the three case studies A1, A2, and A3 considered are shown. In particular, Figure 5a represents the vertical displacement of the platform, while Figure 5b represents its vertical velocity computed using the minimal coordinate multibody model implemented in MATLAB.

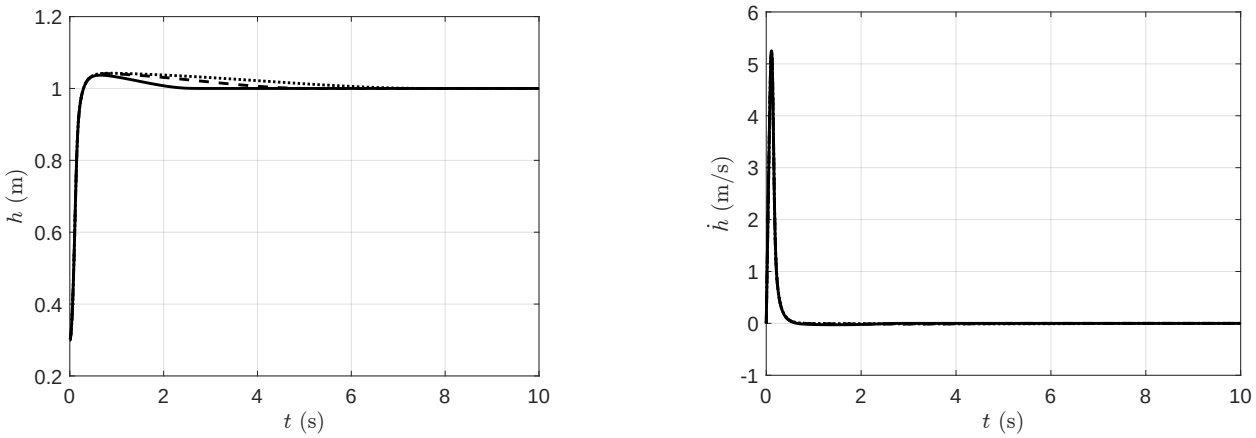

(a) *Vertical displacement* h. **(b)** *Vertical velocity* $\dot{h}$.

Figure 5. *Vertical displacement* h *and vertical velocity* $\dot{h}$ *of the platform obtained using the minimal coordinate multibody model implemented in MATLAB. The solid line (——) corresponds to Case A1; the dashed line (- - -) corresponds to Case A2; the dotted line (·····) corresponds to Case A3.*

In Figure 6, the time laws representing the motion of the roller in correspondence to the three case studies A1, A2, and A3 considered are shown. In particular, Figure 6a represents the horizontal displacement of the roller, while Figure 6b represents its horizontal velocity computed using the minimal coordinate multibody model implemented in MATLAB.

In Figure 7, the time laws representing the implementation of the proposed control strategy in correspondence to the three case studies A1, A2, and A3 considered are shown. In particular, Figure 7a and Figure 7b respectively represent the feedforward and feedback control forces, while Figure 7c represents the total control force applied to the mechanical system computed using the minimal coordinate multibody model implemented in MATLAB.

The numerical results presented in this subsection demonstrate that the control strategy devised in this work is effective and efficient. More importantly, by observing the controller performance metrics reported in Table 8, it is apparent that the parameter choice corresponding to Case A1, namely $T_a = 2.5$ (s), leads to the best time response of the articulated mechanical system at hand in terms of the classic control performance metrics like the rise time, the maximum overshoot, the settling time, and the steady-state error.

This conclusion is confirmed by the controller performance metrics obtained using the minimal coordinate multibody model implemented in MATLAB and shown in Table 8, which are computed for the vertical displacement of the lift table denoted with h in the three cases of interest labeled as A1, A2, and A3. For convenience, the computational time of the numerical simulations carried out using the minimal coordinate multibody model implemented in MATLAB is also reported in Table 8.

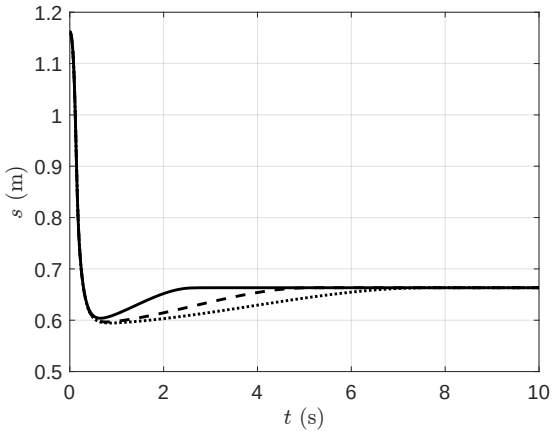

(a) *Horizontal displacement s.*

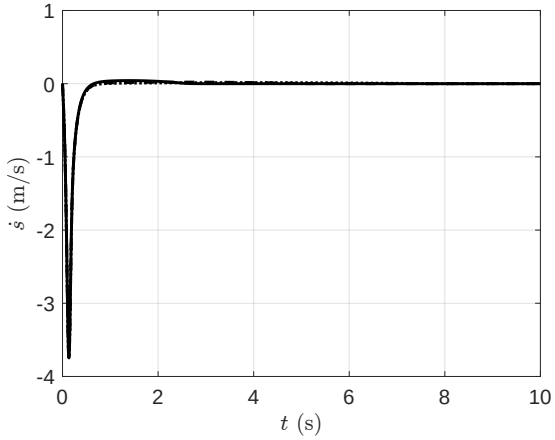

(b) *Horizontal velocity $\dot{s}$.*

Figure 6. *Horizontal displacement s and horizontal velocity $\dot{s}$ of the roller obtained using the minimal coordinate multibody model implemented in MATLAB. The solid line (——) corresponds to Case A1; the dashed line (- - -) corresponds to Case A2; the dotted line (·····) corresponds to Case A3.*

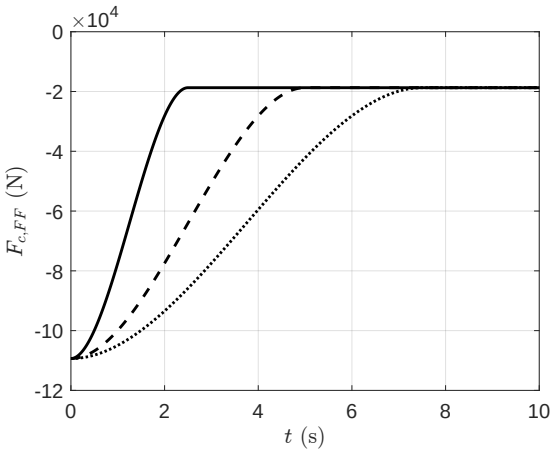

(a) *Feedforward control force $F_{c,FF}$.*

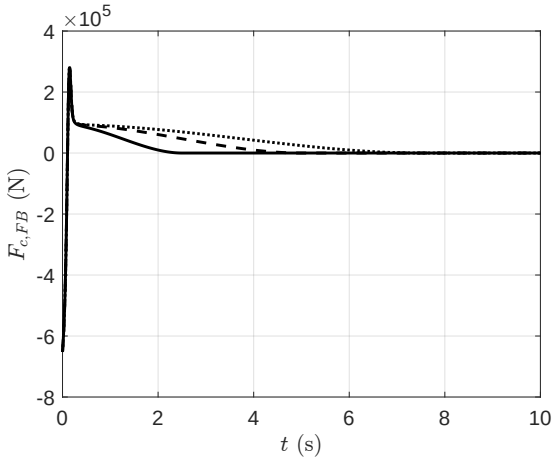

(b) *Feedback control force $F_{c,FB}$.*

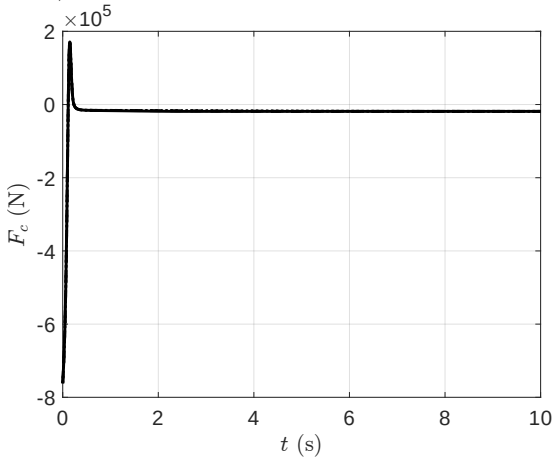

(c) *Total control force F_c.*

Figure 7. *Feedforward control force $F_{c,FF}$, feedback control force $F_{c,FB}$, and total control force F_c applied to the mechanical system obtained using the minimal coordinate multibody model implemented in MATLAB. The solid line (——) corresponds to Case A1; the dashed line (- - -) corresponds to Case A2; the dotted line (·····) corresponds to Case A3.*

Table 8. Controller performance metrics for the platform vertical displacement h computed by using the minimal coordinate multibody model implemented in MATLAB.

Case	Rise time	Maximum overshoot	Settling time	Steady-state error	Computational time
A1	0.178 (s)	3.699 (%)	0.213 (s)	3.997×10^{-15} (m)	2.935 (s)
A2	0.178 (s)	4.118 (%)	0.213 (s)	3.997×10^{-15} (m)	2.889 (s)
A3	0.178 (s)	4.235 (%)	0.213 (s)	5.418×10^{-14} (m)	2.915 (s)

6.3 Computer implementation of the redundant coordinate multibody model using MATLAB

In this subsection, the numerical results obtained from the computer implementation in MATLAB of the redundant coordinate multibody model of the pantograph scissor lift mechanism developed in Section 5. are presented and discussed. The numerical experiments carried out and described in this subsection are meant to qualitatively and quantitatively refine the proportional and derivative coefficients respectively denoted with k_c and σ_c that characterize the analytical law designed for the feedback controller. For this purpose, three cases are considered. In Case B1 (reference), $k_c = 1.308 \cdot 10^6$ (N/m) and $\sigma_c = 1.610 \cdot 10^5$ (N $\times$ s/m) are assumed; in Case B2 (first feedback parameters test), $k_c = 6.541 \cdot 10^5$ (N/m) and $\sigma_c = 8.049 \cdot 10^4$ (N $\times$ s/m) are assumed; in Case B3 (second feedback parameters test), $k_c = 3.924 \cdot 10^6$ (N/m) and $\sigma_c = 6.439 \cdot 10^5$ (N $\times$ s/m) are assumed. While Case B1 is identical to the default configuration of the system control parameters reported in Table 3, Case B2 and Case B3 represent two trials for establishing the influence of the feedback controller proportional and derivative coefficients k_c and σ_c on the system time response and its dynamic behavior in general. In Figure 8, the time laws representing the motion of the bar in correspondence to the three case studies B1, B2, and B3 considered are shown. In particular, Figure 8a represents the angular displacement of the bar, while Figure 8b represents its angular velocity computed using the redundant coordinate multibody model implemented in MATLAB.

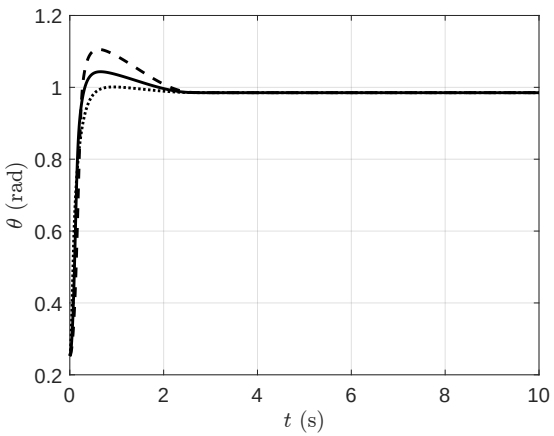

(a) *Angular displacement θ.*

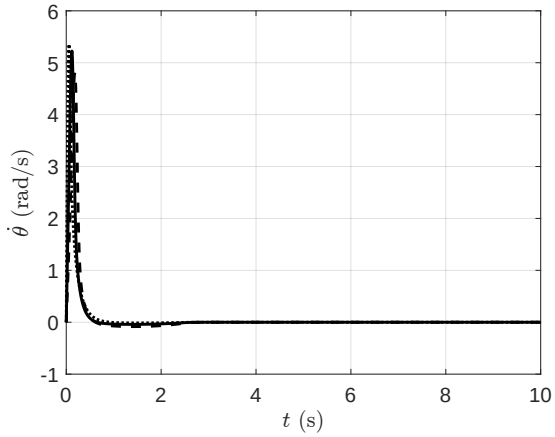

(b) *Angular velocity $\dot{\theta}$.*

Figure 8. *Angular displacement θ and angular velocity $\dot{\theta}$ of the bar obtained using the redundant coordinate multibody model implemented in MATLAB. The solid line (——) corresponds to Case B1; the dashed line (- - -) corresponds to Case B2; the dotted line (·····) corresponds to Case B3.*

In Figure 9, the time laws representing the motion of the platform in correspondence to the three case studies B1, B2, and B3 considered are shown. In particular, Figure 9a represents the vertical displacement of the platform, while Figure 9b represents its vertical velocity computed using the redundant coordinate multibody model implemented in MATLAB.

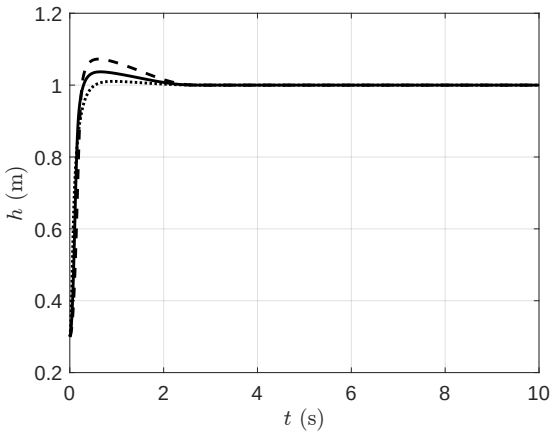

(a) *Vertical displacement h.*

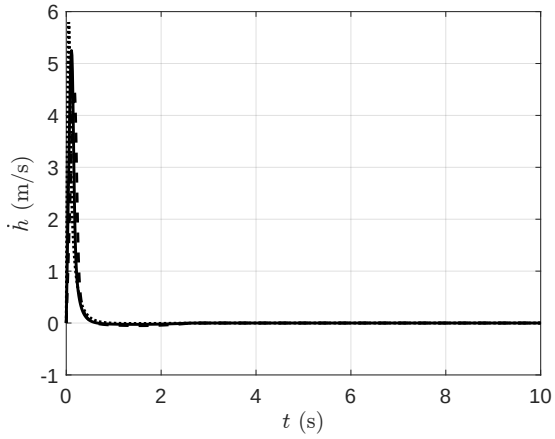

(b) *Vertical velocity $\dot{h}$.*

Figure 9. *Vertical displacement h and vertical velocity $\dot{h}$ of the platform obtained using the redundant coordinate multibody model implemented in MATLAB. The solid line (——) corresponds to Case B1; the dashed line (- - -) corresponds to Case B2; the dotted line (·····) corresponds to Case B3.*

In Figure 10, the time laws representing the motion of the roller in correspondence to the three case studies B1, B2, and B3 considered are shown. In particular, Figure 10a represents the horizontal displacement of the roller, while Figure 10b represents its horizontal velocity computed using the redundant coordinate multibody model implemented in MATLAB.

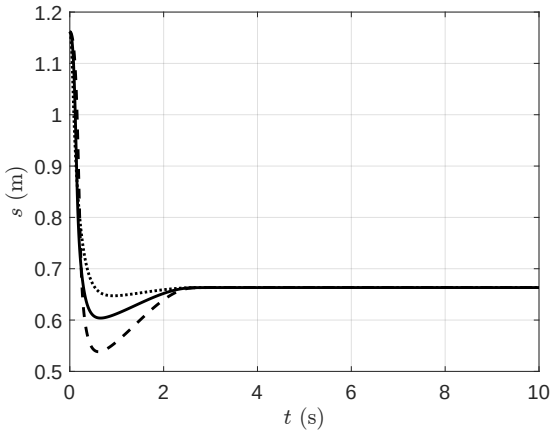

(a) *Horizontal displacement s.*

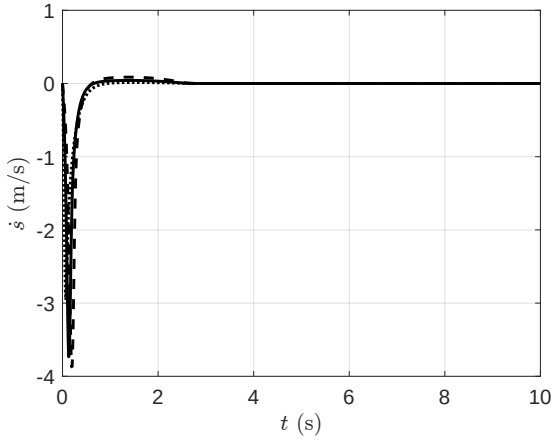

(b) *Horizontal velocity $\dot{s}$.*

Figure 10. *Horizontal displacement s and horizontal velocity $\dot{s}$ of the roller obtained using the redundant coordinate multibody model implemented in MATLAB. The solid line (——) corresponds to Case B1; the dashed line (- - -) corresponds to Case B2; the dotted line (·····) corresponds to Case B3.*

In Figure 11, the time laws representing the implementation of the proposed control strategy in correspondence to the three case studies B1, B2, and B3 considered are shown. In particular, Figure 11a and Figure 11b respectively represent the feedforward and feedback control forces, while Figure 11c represents the total control force applied to the mechanical system computed using the redundant coordinate multibody model implemented in MATLAB.

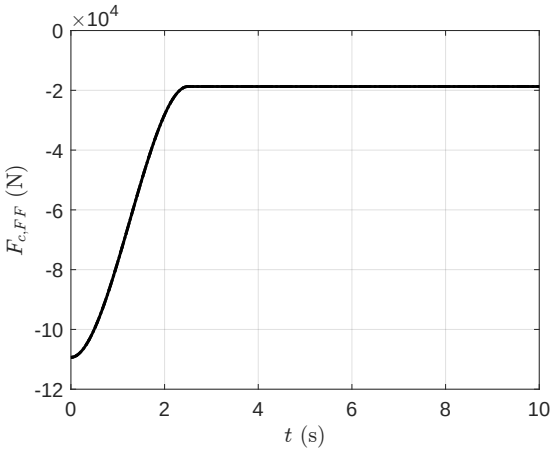

(a) *Feedforward control force $F_{c,FF}$.*

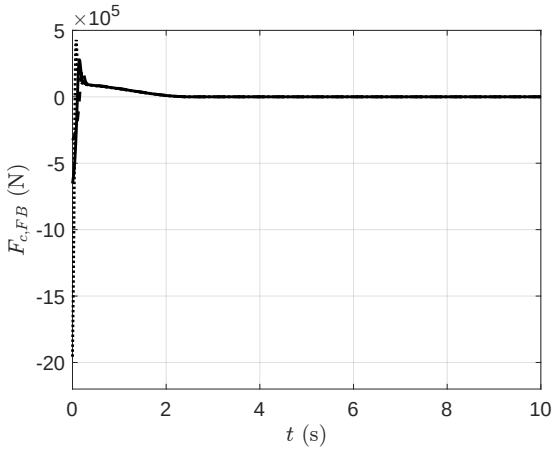

(b) *Feedback control force $F_{c,FB}$.*

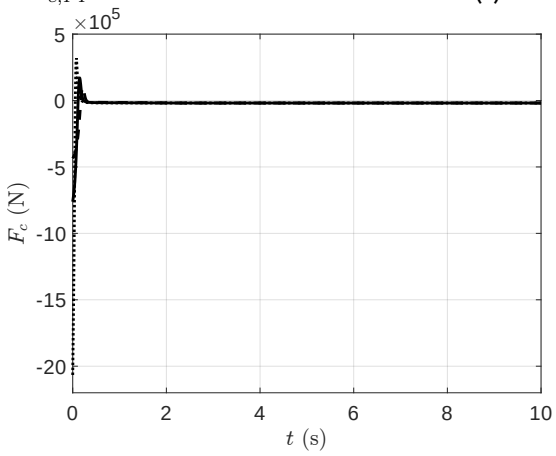

(c) *Total control force F_c.*

Figure 11. *Feedforward control force $F_{c,FF}$, feedback control force $F_{c,FB}$, and total control force F_c applied to the mechanical system obtained using the redundant coordinate multibody model implemented in MATLAB. The solid line (——) corresponds to Case B1; the dashed line (- - -) corresponds to Case B2; the dotted line (·····) corresponds to Case B3.*

The numerical results presented in this subsection demonstrate that the control strategy devised in this work is effective and efficient. More importantly, by observing the controller performance metrics reported in Table 9, it is apparent that the parameter choice corresponding to Case B3, namely $k_c = 3.924 \cdot 10^6$ (N/m) and $\sigma_c = 6.439 \cdot 10^5$ (N $\times$ s/m), leads to the best time response of the articulated mechanical system at hand in terms of the classic control performance metrics like the rise time, the maximum overshoot, the settling time, and the steady-state error.

Table 9. Controller performance metrics for the platform vertical displacement h computed by using the redundant coordinate multibody model implemented in MATLAB.

Case	Rise time	Maximum overshoot	Settling time	Steady-state error	Computational time
B1	0.170 (s)	3.698 (%)	0.210 (s)	4.999×10^{-12} (m)	29.647 (s)
B2	0.210 (s)	7.249 (%)	1.270 (s)	9.780×10^{-15} (m)	30.193 (s)
B3	0.210 (s)	1.044 (%)	0.290 (s)	7.283×10^{-14} (m)	37.846 (s)

This conclusion is confirmed by the controller performance metrics obtained using the redundant coordinate multibody model implemented in MATLAB and shown in Table 9, which are computed for the vertical displacement of the lift table denoted with h in the three cases of interest labeled as B1, B2, and B3. For convenience, the computational time of the numerical simulations carried out using the redundant coordinate multibody model implemented in MATLAB is also reported in Table 9.

6.4 General discussion and final remarks

In this section, the numerical results obtained from the computer implementation of the mechanical models of the pantograph scissor lift mechanism analyzed in this work were presented. As expected, the effectiveness of the control strategy devised in this paper was demonstrated through several numerical experiments. To this end, the numerical results proposed in this section are divided into two groups. First and foremost, the system dynamic response and the corresponding control performance found by implementing the minimal coordinate multibody model in MATLAB were shown. Subsequently, the analogous set of numerical results arising from the computer implementation of the redundant coordinate multibody model in MATLAB was presented. The two mechanical models were numerically solved using the same computational scheme based on the ODE15s subroutine coded in the MATLAB simulation environment. Furthermore, the differential-algebraic equations of motion pertaining to the redundant coordinate multibody model were numerically solved including the generalized coordinate partitioning method as an additional numerical procedure for the stabilization of the algebraic constraints. In both cases, the feasibility of the computer implementation of the vector and matrix quantities involved in the definition of the system multibody models, necessary for performing the static and dynamic simulations of interest for this investigation, was demonstrated. Despite the presence of fundamental differences in the formulation approaches employed for the analytical derivation of the equations of motion corresponding to the same articulated mechanical system, the numerical results of the dynamic analysis of the pantograph scissor lift mechanism considered as the case study are identical, thereby validating the viability of the control technique proposed in this work.

As mentioned before, MATLAB was employed as the fundamental computational environment for performing numerical experiments on the control strategy developed in this work, which was applied to the mechanical models of the pantograph scissor lift mechanism considered as the case study, modeled using both a minimal coordinate multibody approach and a redundant coordinate multibody approach. To this end, in the former case, a special-purpose multibody program was developed in MATLAB to describe the mechanism at hand as a minimal coordinate multibody model, whereas, in the latter case, a general-purpose multibody program was developed in MATLAB to describe the mechanism at hand as a redundant coordinate multibody model. Additionally, in order to perform a further comparison by means of numerical experiments, the pantograph scissor lift mechanism was also modeled by employing a redundant coordinate multibody approach implemented using the SIMSCAPE MULTIBODY software. A block diagram summarizing the computer implementation in SIMSCAPE MULTIBODY of the system redundant coordinate multibody model is represented in Figure 12.

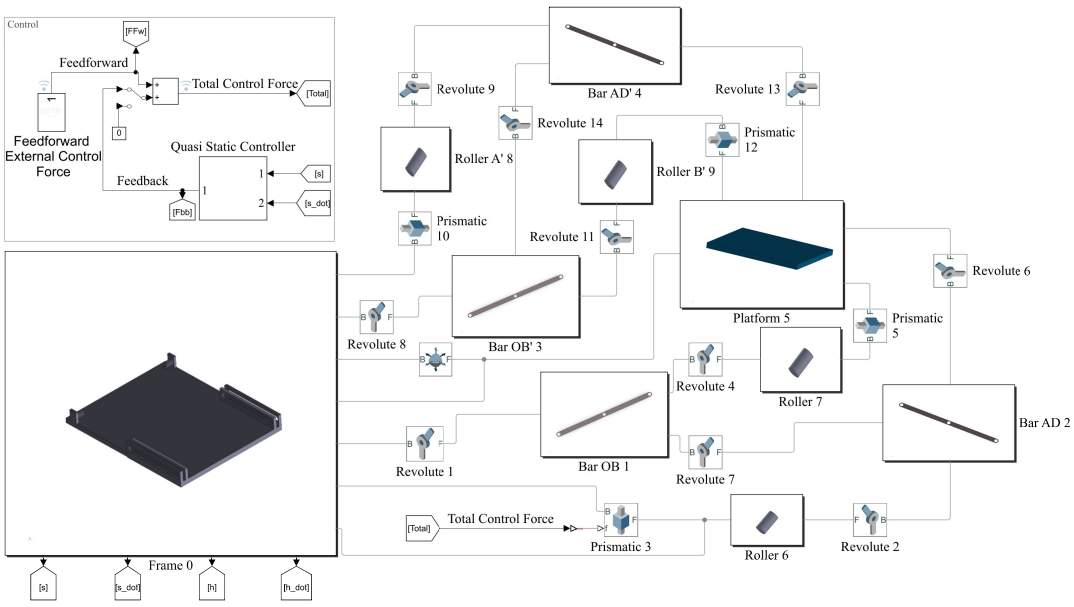

Figure 12. *Redundant coordinate multibody model of the pantograph scissor lift mechanism implemented in SIMSCAPE MULTIBODY.*

In Figure 12, the fundamental elements that characterize the redundant coordinate multibody model are shown. These are

the rigid bodies (ground, bars, rollers, and platform), the kinematic joints (revolute joints and prismatic joints), the force elements (dampers), the force fields (gravity force), and the control actuators (feedforward plus feedback controller). On the other hand, both the minimal coordinate multibody model and the redundant coordinate multibody model were implemented in MATLAB through the use of a conventional procedural programming approach, which is based on the development of the fundamental subroutines necessary for the analytical formulation of the system equations of motion and their subsequent numerical solution. In order to demonstrate that both the computer models provide consistent numerical results when operating in the same conditions, a preliminary static test and a preliminary dynamic test were carried out first. This preliminary analysis is meant for comparing the numerical results of the two multibody models devised in the paper and implemented in MATLAB with those calculated using SIMSCAPE MULTIBODY. In the preliminary test for statics, the controller is switched off and set on its constant equilibrium force value, while the pantograph scissor lift mechanism is positioned in the final equilibrium configuration. In the preliminary test for dynamics, on the other hand, the controller is switched on and the default values for its control parameters are set, while the pantograph scissor lift mechanism is positioned in the initial equilibrium configuration. In Figure 13, the numerical results of the preliminary static and dynamic analyses performed on the multibody models of the pantograph scissor lift mechanism are shown. In particular, Figure 13a represents the numerical results of the preliminary static analysis found using MATLAB and SIMSCAPE MULTIBODY, whereas Figure 13b represents the numerical results of the preliminary dynamic analysis found using MATLAB and SIMSCAPE MULTIBODY.

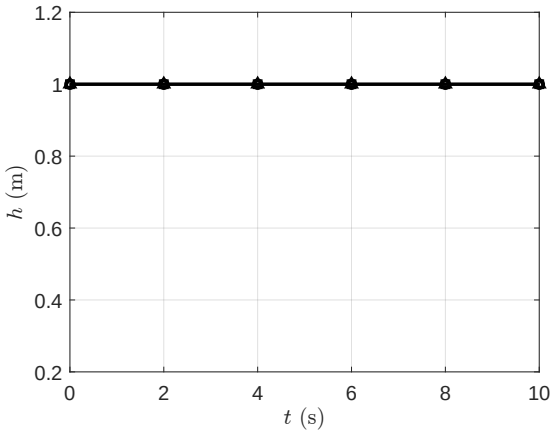

(a) *Static vertical displacement h.*

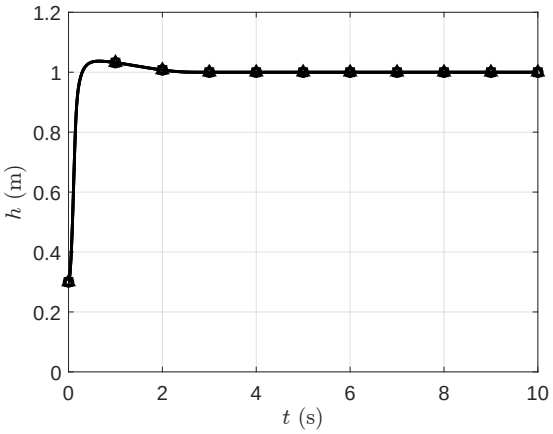

(b) *Dynamic vertical displacement h.*

Figure 13. *Vertical displacement h of the platform obtained in static and dynamic conditions. The solid line (——) with the triangle markers (△) corresponds to the numerical results obtained using the minimal coordinate multibody model implemented in MATLAB; the solid line (——) with the square markers (□) corresponds to the numerical results obtained using the redundant coordinate multibody model implemented in MATLAB; the solid line (——) with the circle markers (○) corresponds to the numerical results obtained using the redundant coordinate multibody model implemented in SIMSCAPE MULTIBODY.*

As represented in Figure 13, although the numerical results presented in this section arise from three completely different multibody models of the same articulated mechanical system, the outcomes of the preliminary analysis obtained in MATLAB and in SIMSCAPE MULTIBODY for the mechanical system under study are fully consistent.

As a final remark, the campaign of numerical experiments realized in this work led to the identification of the best combination of parameters to be used for tuning both the controllers having feedforward and feedback architectures. In particular, the control parameters considered in this analysis were the feedforward controller actuation time indicated as T_a, the feedback controller proportional coefficient denoted with k_c, and the feedback controller derivative coefficient denoted with σ_c. While the feedforward controller actuation time was refined using the MATLAB simulation environment by using the minimal coordinate multibody model, the feedback controller proportional and derivative coefficients were refined in the MATLAB simulation environment by using the redundant coordinate multibody model. This iterative refinement process returned the parameter set composed of $T_a = 2.5$ (s), $k_c = 3.924 \cdot 10^6$ (N/m), and $\sigma_c = 6.439 \cdot 10^5$ (N $\times$ s/m). In fact, as it is clearly apparent from the numerical results presented in this section, as well as by observing the controller performance metrics reported in Table 8 and in Table 9, this set of control parameters produced the best time response of the mechanical system at hand in terms of the classic control performance metrics, such as the rise time, the maximum overshoot, the settling time, and the residual steady-state error. A summary of the numerical experiments performed for gradually refining the actual values of the control parameters is reported in Table 10.

Table 10. Numerical values of the controller parameters employed in all the configurations of the numerical experiments.

Case	Actuation time	Proportional coefficient	Derivative coefficient
A1 (reference)	$T_a = 2.5$ (s)	$k_c = 1.308 \cdot 10^6$ (N/m)	$\sigma_c = 1.610 \cdot 10^5$ (N $\times$ s/m)
A2	$T_a = 5.0$ (s)	$k_c = 1.308 \cdot 10^6$ (N/m)	$\sigma_c = 1.610 \cdot 10^5$ (N $\times$ s/m)
A3	$T_a = 7.5$ (s)	$k_c = 1.308 \cdot 10^6$ (N/m)	$\sigma_c = 1.610 \cdot 10^5$ (N $\times$ s/m)
B1 (reference)	$T_a = 2.5$ (s)	$k_c = 1.308 \cdot 10^6$ (N/m)	$\sigma_c = 1.610 \cdot 10^5$ (N $\times$ s/m)
B2	$T_a = 2.5$ (s)	$k_c = 6.541 \cdot 10^5$ (N/m)	$\sigma_c = 8.049 \cdot 10^4$ (N $\times$ s/m)
B3 (refined)	$T_a = 2.5$ (s)	$k_c = 3.924 \cdot 10^6$ (N/m)	$\sigma_c = 6.439 \cdot 10^5$ (N $\times$ s/m)

In conclusion, by iteratively determining the refined values of the control parameters k_c and σ_c, and considering the performance metrics mentioned above, the system response was further improved. To this end, the original results for the control parameters obtained from the linearization of the system dynamic model were modified by doubling, tripling, and quadrupling their original magnitudes. In the transition from the initial values of the control parameters to the doubled ones, it was observed a consistent reduction of the maximum overshoot of the platform vertical displacement, while this reduction was instead of a minor entity in

the transition from the doubled to the tripled values of the control parameters, as well as from the tripled to the quadrupled values. However, the maximum value of the control force also increases significantly with each gain in the magnitude of the control parameters, leading to a global reduction of efficiency of the control system. Observing this behavior, and also taking into account the peak of the control force, a new value of the parameter k_c was defined using the value for which an improvement of the vertical displacement of the platform was manifested. It was found then that the refined value of the control parameter k_c is three times the original value calculated by employing the linearized dynamical model. Subsequently, by gradually increasing and testing the various system responses corresponding to the iterative tuning of the feedback control system, the control parameter σ_c was modified as well. After appropriate evaluations, the control parameter σ_c was set equal to four times its original value considered in the standard controller design, leading to the results reported in Table 9. By doing so, the final performance parameters are considerably improved compared to those originally obtained and reported in Table 8. More importantly, this was not the only improvement achieved by implementing the iterative procedure described above, since the magnitude of the control force also decreased significantly, thereby leading to the determination of the refined set of control parameters shown in Table 10.

As expected, the dynamical simulations of the minimal coordinate multibody model run faster than those of the redundant coordinate multibody model, as respectively shown by the computational times reported in Table 8 and in Table 9. While the former dynamical model has a computational time of about 3 seconds, the latter dynamical model has a computational time of about 30 seconds, that is, its simulation time is about 10 times larger than the one of the first mathematical model. It is worth mentioning that the simulation time depends on several factors, which are only partially related to the presence of the nonlinear control strategy proposed in this work. The most important factor affecting the computational time is, evidently, the dimension of the dynamical model to be simulated. Furthermore, in the case of the use of a redundant coordinate multibody formulation approach, the computer implementation of a constraint stabilization technique in conjunction with the numerical solver is also of fundamental importance, thereby negatively affecting the efficiency of the dynamical simulations. The use of this additional numerical procedure, however, is aimed at drastically improving the accuracy of the numerical results. While in the minimal coordinate multibody model only 1 nonlinear differential equation is numerically solved, in the redundant coordinate multibody model, on the other hand, 63 nonlinear differential equations are numerically solved. This process is carried out in conjunction with the application, at each time step of the dynamical simulation, of the generalized coordinate partitioning method, implemented at both the position and velocity levels, to the 62 independent algebraic equations describing the kinematic constraints. Therefore, the computational efficiency of the proposed control method is generally consistent with all the observations reported above.

7. Summary, conclusions, and future directions of research

In this study, a new control strategy suitable for performing the tracking control of fully-actuated multibody mechanical systems is proposed and its use is demonstrated by means of numerical experiments considering as the case study a pantograph scissor lift mechanism. In particular, two mathematical models of the articulated mechanical system considered in the paper are analytically derived in this work, that is, a minimal coordinate multibody model and a redundant coordinate multibody model. Both the multibody models of the pantograph scissor lift mechanism were implemented in special-purpose and general-purpose computer codes developed in the MATLAB computational environment. Additionally, the redundant coordinate multibody model was also implemented in a virtual environment using the SIMSCAPE MULTIBODY software, thereby leading to three computer models of the same articulated mechanical system, which served as the fundamental computational tools for performing numerical experiments on the effectiveness of the new control strategy proposed in this investigation.

By adopting a nonlinear feedforward plus feedback control architecture, the present investigation proposes the systematic development within the multibody framework of a new control methodology capable of controlling the motion of articulated mechanical systems and its subsequent computational testing through numerical experiments. More precisely, one of the main contributions of the present work is the development of a new nonlinear control strategy that leverages a combined control architecture based on a quasi-static feedforward controller, serving as the modulating controller, in conjunction with an error-based proportional-derivative feedback controller, representing the compensating controller. In particular, employing both the minimal coordinate and the redundant coordinate multibody approaches for modeling articulated mechanical systems formed by only rigid components, this investigation is focused on the systematic construction of two mechanical models of a pantograph scissor lift mechanism that represents the case study considered in this work. To this end, a minimal coordinate multibody model and a redundant coordinate multibody model are systematically derived in this paper. While the minimal coordinate multibody model serves as the basic analytical tool for the design of the control law to be applied to the pantograph scissor lift mechanism, the redundant coordinate multibody model is used in the paper for testing the effectiveness of the proposed control strategy. Numerous computational experiments described in the manuscript demonstrate and discuss the effectiveness of the control approach proposed in this investigation. It is shown in the paper that the fundamental mechanical parameters of both the feedforward and the feedback controllers can be readily refined through simple computer simulations to obtain enhanced performance of the system dynamic response evaluated in terms of the conventional metrics employed in the classical control theory, such as the rise time, the maximum overshoot, the settling time, and the residual steady-state error.

In the description of the proposed control method, it is assumed that it is necessary to deal with a fully actuated mechanical system to be controlled. This is a basic assumption behind all the analytical developments presented in the paper. The articulated mechanical system to be controlled can have an arbitrary number of degrees of freedom and could also be a rigid-flexible multibody system. Therefore, an interesting issue to be addressed in future investigations is the extension of the proposed method to underactuated mechanical systems, such as flexible multibody systems, in which is challenging, if not impossible, to have a control action associated with each generalized coordinate. Moreover, to further develop the multibody modeling approach and the nonlinear control methodology employed in this paper, several directions of research could be followed in future investigations. For instance, two possible paths of future research work that could be immediately covered are the following. First, the modeling and control techniques proposed in this paper could be readily applied to robotic mechanical systems having serial or parallel architectures in order to find a solution to the trajectory tracking problem of the robot end-effector. This family of mechanical systems is particularly suitable for the application of the control method proposed in the paper because, in this case, the control problem is typically formulated by assuming a fully actuated structure of the array of control inputs. Second, the approach devised in this paper could also be extended to space systems like rigid satellites with flexible appendages in order to solve the attitude control problem. In this interesting scenario, the control system should be designed to guide the satellite motion and, at the same time, reduce the mechanical vibrations induced by the excitation of the resonant mode shapes associated with its deformable components. Also, the systematic comparison of the effectiveness and the efficiency of the control method proposed in this work with the performance of the nonlinear control techniques available in the literature could be the object of future research works. Another challenging domain of topics that could be addressed in future works is the improvement of the analytical and numerical background used in the paper for achieving the multibody modeling and the nonlinear control of articulated mechanical systems in general, leading to more advanced, effective, and efficient solution strategies. All the interesting topics mentioned above will be considered in future

investigations.

Author Contributions

This research paper was principally devised and developed by the first author (Carmine Maria Pappalardo). Great support in the development of the paper was provided by the second author (Rosario La Regina). The detailed review carried out by the third author (Domenico Guida) considerably improved the quality of the work. The manuscript was written with the contribution of all authors. All authors discussed the results, reviewed the methodology, and approved the final version of the manuscript.

Acknowledgments

None.

Conflict of Interest

The authors declared no potential conflicts of interest with respect to the research, authorship, and publication of this article.

Funding

The authors received no financial support for the research, authorship, and publication of this article.

Data Availability Statements

The datasets generated and/or analyzed during the current study are available from the corresponding author on reasonable request.

References

[1] Haug, E.J., *Computer aided kinematics and dynamics of mechanical systems. Vol. 1: basic methods*, Allyn & Bacon, Inc., 1989.
[2] Shabana, A.A., Zaazaa, K.E., Sugiyama, H., *Railroad vehicle dynamics: a computational approach*, CRC press, 2007.
[3] Schiehlen, W., Multibody system dynamics: roots and perspectives, *Multibody system dynamics*, 1997, 1(2), 149–188.
[4] Eberhard, P., Schiehlen, W., Computational dynamics of multibody systems: history, formalisms, and applications, *Journal of computational and nonlinear dynamics*, 2006, 1(1), 3–12.
[5] Bruni, S., Meijaard, J., Rill, G., Schwab, A., State-of-the-art and challenges of railway and road vehicle dynamics with multibody dynamics approaches, *Multibody System Dynamics*, 2020, 49(1), 1–32.
[6] Jain, A., *Robot and multibody dynamics: analysis and algorithms*, Springer Science & Business Media, 2010.
[7] Song, Y., Rønnquist, A., Jiang, T., Nåvik, P., Identification of short-wavelength contact wire irregularities in electrified railway pantograph–catenary system, *Mechanism and Machine Theory*, 2021, 162, 104338.
[8] Zheng, Y., Shabana, A.A., A two-dimensional shear deformable ancf consistent rotation-based formulation beam element, *Nonlinear Dynamics*, 2017, 87(2), 1031–1043.
[9] Marques, F., Flores, P., Claro, J., Lankarani, H.M., Modeling and analysis of friction including rolling effects in multibody dynamics: a review, *Multibody System Dynamics*, 2019, 45(2), 223–244.
[10] Flores, P., Lankarani, H.M., *Contact force models for multibody dynamics*, vol. 226, Springer, 2016.
[11] Pennestrì, E., Rossi, V., Salvini, P., Valentini, P.P., Review and comparison of dry friction force models, *Nonlinear dynamics*, 2016, 83(4), 1785–1801.
[12] Pennestri, E., Valentini, P., Vita, L., Multibody dynamics simulation of planar linkages with dahl friction, *Multibody System Dynamics*, 2007, 17(4), 321–347.
[13] Villecco, F., Pellegrino, A., Entropic measure of epistemic uncertainties in multibody system models by axiomatic design, *Entropy*, 2017, 19(7), 291.
[14] Villecco, F., On the evaluation of errors in the virtual design of mechanical systems, *Machines*, 2018, 6(3), 36.
[15] Shabana, A., *Dynamics of multibody systems*, Cambridge university press, 2020.
[16] Shabana, A.A., *Computational dynamics*, John Wiley & Sons, 2009.
[17] Sugiyama, H., Shabana, A.A., Omar, M.A., Loh, W.Y., Development of nonlinear elastic leaf spring model for multibody vehicle systems, *Computer methods in applied mechanics and engineering*, 2006, 195(50-51), 6925–6941.
[18] Cajić M., Lazarević M.P., Fractional order spring/spring-pot/actuator element in a multibody system: Application of an expansion formula, *Mechanics Research Communications*, 2014, 62, 44–56.
[19] Hua, G., Jingyu, Z., Hao, Z., Qingkai, H., Jinguo, L., Dynamic investigation of a spatial multi-body mechanism considering joint clearance and friction based on coordinate partitioning method, *Proceedings of the Institution of Mechanical Engineers, Part C: Journal of Mechanical Engineering Science*, 2021, 235(24), 7569–7587.
[20] Berbyuk, V., Boström, A., Optimization problems of controlled multibody systems having spring-damper actuators, *International applied mechanics*, 2001, 37(7), 935–940.
[21] Schiehlen, W., et al., *Multibody systems handbook*, vol. 6, Springer, 1990.
[22] Nemov, A.S., Matikainen, M.K., Wang, T., Mikkola, A., Analysis of electromechanical systems based on the absolute nodal coordinate formulation, *Acta Mechanica*, 2022, 1–12.
[23] Rakhsha, M., Yang, L., Hu, W., Negrut, D., On the use of multibody dynamics techniques to simulate fluid dynamics and fluid–solid interaction problems, *Multibody System Dynamics*, 2021, 53(1), 29–57.
[24] Omar, M.A., Shabana, A.A., Mikkola, A., Loh, W.Y., Basch, R., Multibody system modeling of leaf springs, *Journal of Vibration and Control*, 2004, 10(11), 1601–1638.
[25] Pappalardo, C.M., Guida, D., A comparative study of the principal methods for the analytical formulation and the numerical solution of the equations of motion of rigid multibody systems, *Archive of Applied Mechanics*, 2018, 88(12), 2153–2177.
[26] Pennestrì, E., Vita, L., Multibody dynamics in advanced education, *Advances in computational multibody systems*, Springer, 2005, 345–370.
[27] Inkol, K.A., Brown, C., McNally, W., Jansen, C., McPhee, J., Muscle torque generators in multibody dynamic simulations of optimal sports performance, *Multibody System Dynamics*, 2020, 50(4), 435–452.
[28] Amirouche, F.M., Amirouche, F.M., *Fundamentals of multibody dynamics: theory and applications*, Springer, 2006.
[29] Roberson, R.E., Schwertassek, R., *Dynamics of multibody systems*, Springer Science & Business Media, 2012.
[30] Nikravesh, P.E., *Planar multibody dynamics: formulation, programming and applications*, CRC press, 2007.
[31] Nikravesh, P.E., *Computer-aided analysis of mechanical systems*, Prentice-Hall, Inc., 1988.
[32] Bauchau, O.A., *Flexible multibody dynamics*, vol. 176, Springer, 2011.
[33] Shabana, A.A., *Computational continuum mechanics*, John Wiley & Sons, 2018.
[34] Flores, P., *Concepts and formulations for spatial multibody dynamics*, Springer, 2015.
[35] Nikravesh, P.E., An overview of several formulations for multibody dynamics, *Product Engineering*, 2004, 189–226.
[36] de Jalón, J.G., Twenty-five years of natural coordinates, *Multibody System Dynamics*, 2007, 18(1), 15–33.

[37] Pappalardo, C.M., Guida, D., On the lagrange multipliers of the intrinsic constraint equations of rigid multibody mechanical systems, *Archive of Applied Mechanics*, 2018, 88(3), 419–451.
[38] Gerstmayr, J., Schöberl, J., A 3d finite element method for flexible multibody systems, *Multibody System Dynamics*, 2006, 15(4), 305–320.
[39] Bathe, K.J., Finite element procedures for solids and structures linearanalysis, *Finite Element Procedures*, 1982, 148–214.
[40] Orzechowski, G., Matikainen, M.K., Mikkola, A.M., Inertia forces and shape integrals in the floating frame of reference formulation, *Nonlinear Dynamics*, 2017, 88(3), 1953–1968.
[41] Shabana, A.A., Definition of ancf finite elements, *Journal of Computational and Nonlinear Dynamics*, 2015, 10(5).
[42] Sanborn, G.G., Shabana, A.A., A rational finite element method based on the absolute nodal coordinate formulation, *Nonlinear Dynamics*, 2009, 58(3), 565–572.
[43] Shabana, A.A., Ancf consistent rotation-based finite element formulation, *Journal of Computational and Nonlinear Dynamics*, 2016, 11(1).
[44] Cottrell, J.A., Hughes, T.J., Bazilevs, Y., *Isogeometric analysis: toward integration of CAD and FEA*, John Wiley & Sons, 2009.
[45] Betsch, P., Steinmann, P., Frame-indifferent beam finite elements based upon the geometrically exact beam theory, *International journal for numerical methods in engineering*, 2002, 54(12), 1775–1788.
[46] Campanelli, M., Berzeri, M., Shabana, A.A., Performance of the incremental and non-incremental finite element formulations in flexible multibody problems, *J. Mech. Des.*, 2000, 122(4), 498–507.
[47] Ding, J., Wallin, M., Wei, C., Recuero, A.M., Shabana, A.A., Use of independent rotation field in the large displacement analysis of beams, *Nonlinear Dynamics*, 2014, 76(3), 1829–1843.
[48] Koganti, P.B., Udwadia, F.E., Unified approach to modeling and control of rigid multibody systems, *Journal of Guidance, Control, and Dynamics*, 2016, 39(12), 2683–2698.
[49] Bai, Q., Shehata, M., Review study of using euler angles and euler parameters in multibody modeling of spatial holonomic and non-holonomic systems, *International Journal of Dynamics and Control*, 2022, 1–19.
[50] Meirovitch, L., *Methods of analytical dynamics*, Courier Corporation, 2010.
[51] Ling, H., Shabana, A.A., Euler angles and numerical representation of the railroad track geometry, *Acta Mechanica*, 2021, 232(8), 3121–3139.
[52] Spring, K.W., Euler parameters and the use of quaternion algebra in the manipulation of finite rotations: a review, *Mechanism and machine theory*, 1986, 21(5), 365–373.
[53] Flores, P., Euler angles, bryant angles and euler parameters, *Concepts and formulations for spatial multibody dynamics*, Springer, 2015, 15–22.
[54] Shabana, A.A., Euler parameters kinetic singularity, *Proceedings of the Institution of Mechanical Engineers, Part K: Journal of Multi-body Dynamics*, 2014, 228(3), 307–313.
[55] Pappalardo, C.M., Guida, D., On the use of two-dimensional euler parameters for the dynamic simulation of planar rigid multibody systems, *Archive of Applied Mechanics*, 2017, 87(10), 1647–1665.
[56] Bauchau, O.A., Trainelli, L., The vectorial parameterization of rotation, *Nonlinear dynamics*, 2003, 32(1), 71–92.
[57] Haghshenas-Jaryani, M., Bowling, A., A new switching strategy for addressing euler parameters in dynamic modeling and simulation of rigid multibody systems, *Multibody System Dynamics*, 2013, 30(2), 185–197.
[58] Wittenburg, J., *General Multibody Systems*, Springer, 2008.
[59] Xu, X., Luo, J., Feng, X., Peng, H., Wu, Z., A generalized inertia representation for rigid multibody systems in terms of natural coordinates, *Mechanism and Machine Theory*, 2021, 157, 104174.
[60] De Jalon, J.G., Unda, J., Avello, A., Natural coordinates for the computer analysis of multibody systems, *Computer Methods in Applied Mechanics and Engineering*, 1986, 56(3), 309–327.
[61] Saura, M., Segado, P., Dopico, D., Computational kinematics of multibody systems: Two formulations for a modular approach based on natural coordinates, *Mechanism and Machine Theory*, 2019, 142, 103602.
[62] De Jalon, J.G., Bayo, E., *Kinematic and dynamic simulation of multibody systems: the real-time challenge*, Springer Science & Business Media, 2012.
[63] Garcia-Vallejo, D., Mayo, J., Escalona, J., Domínguez, J., Three-dimensional formulation of rigid-flexible multibody systems with flexible beam elements, *Multibody System Dynamics*, 2008, 20(1), 1–28.
[64] Shabana, A.A., Ancf reference node for multibody system analysis, *Proceedings of the Institution of Mechanical Engineers, Part K: Journal of Multi-body Dynamics*, 2015, 229(1), 109–112.
[65] Pappalardo, C.M., A natural absolute coordinate formulation for the kinematic and dynamic analysis of rigid multibody systems, *Nonlinear Dynamics*, 2015, 81(4), 1841–1869.
[66] Pappalardo, C.M., Guida, D., Dynamic analysis of planar rigid multibody systems modeled using natural absolute coordinates, *Applied and Computational Mechanics*, 2018, 12(1).
[67] Bestle, D., Eberhard, P., Analyzing and optimizing multibody systems, *Mechanics of structures and machines*, 1992, 20(1), 67–92.
[68] Pappalardo, C.M., Guida, D., On the computational methods for solving the differential-algebraic equations of motion of multibody systems, *Machines*, 2018, 6(2), 20.
[69] Vaculín, O., Krüger, W.R., Valášek, M., Overview of coupling of multibody and control engineering tools, *Vehicle System Dynamics*, 2004, 41(5), 415–429.
[70] Pogorelov, D., Differential–algebraic equations in multibody system modeling, *Numerical algorithms*, 1998, 19(1), 183–194.
[71] Slotine, J.J.E., Li, W., et al., *Applied nonlinear control*, vol. 199, Prentice hall Englewood Cliffs, NJ, 1991.
[72] Strogatz, S.H., *Nonlinear dynamics and chaos: with applications to physics, biology, chemistry, and engineering*, CRC press, 2018.
[73] Vaidyanathan, S., Volos, C., et al., *Advances and applications in nonlinear control systems*, vol. 635, Springer, 2016.
[74] Cheli, F., Diana, G., *Advanced dynamics of mechanical systems*, vol. 2020, Springer, 2015.
[75] Krysinski, T., Malburet, F., *Mechanical vibrations: Active and passive control*, vol. 103, John Wiley & Sons, 2010.
[76] Laulusa, A., Bauchau, O.A., Review of classical approaches for constraint enforcement in multibody systems, *Journal of computational and nonlinear dynamics*, 2008, 3(1).
[77] Bauchau, O.A., Laulusa, A., Review of contemporary approaches for constraint enforcement in multibody systems, *Journal of Computational and Nonlinear Dynamics*, 2008, 3(1).
[78] Shabana, A.A., Flexible multibody dynamics: review of past and recent developments, *Multibody system dynamics*, 1997, 1(2), 189–222.
[79] Mikkola, A.M., Shabana, A.A., A non-incremental finite element procedure for the analysis of large deformation of plates and shells in mechanical system applications, *Multibody System Dynamics*, 2003, 9(3), 283–309.
[80] Khalil, H.K., *Nonlinear systems third edition*, vol. 115, 2002.
[81] Valášek, M., Design of nonlinear control of nonlinear multibody systems, *Virtual Nonlinear Multibody Systems*, Springer, 2003, 263–278.
[82] Kwatny, H.G., Blankenship, *Nonlinear Control and Analytical Mechanics: a computational approach*, Birkhauser, 2000.
[83] Wasfy, T.M., Noor, A.K., Computational strategies for flexible multibody systems, *Appl. Mech. Rev.*, 2003, 56(6), 553–613.
[84] Dabiri, A., Poursina, M., Machado, J., Dynamics and optimal control of multibody systems using fractional generalized divide-and-conquer algorithm, *Nonlinear Dynamics*, 2020, 102(3), 1611–1626.
[85] Peterson, D.L., Gede, G., Hubbard, M., Symbolic linearization of equations of motion of constrained multibody systems, *Multibody System Dynamics*, 2015, 33(2), 143–161.
[86] Seifried, R., *Dynamics of underactuated multibody systems*, Springer, 2014.
[87] Udwadia, F.E., Schutte, A.D., Equations of motion for general constrained systems in lagrangian mechanics, *Acta mechanica*, 2010, 213(1), 111–129.
[88] Udwadia, F., Equations of motion for constrained multibody systems and their control, *Journal of Optimization Theory and Applications*, 2005, 127(3), 627–638.
[89] Udwadia, F.E., Wanichanon, T., On general nonlinear constrained mechanical systems, *Numerical Algebra, Control & Optimization*, 2013, 3(3), 425.
[90] Koganti, P.B., Udwadia, F.E., Dynamics and precision control of uncertain tumbling multibody systems, *Journal of Guidance, Control, and Dynamics*, 2017, 40(5), 1176–1190.
[91] Nachbagauer, K., Oberpeilsteiner, S., Sherif, K., Steiner, W., The use of the adjoint method for solving typical optimization problems in multibody dynamics, *Journal of Computational and Nonlinear Dynamics*, 2015, 10(6).
[92] Dopico, D., Zhu, Y., Sandu, A., Sandu, C., Direct and adjoint sensitivity analysis of ordinary differential equation multibody formulations, *Journal of Computational and Nonlinear Dynamics*, 2015, 10(1).

[93] Callejo, A., Sonneville, V., Bauchau, O.A., Discrete adjoint method for the sensitivity analysis of flexible multibody systems, *Journal of Computational and Nonlinear Dynamics*, 2019, 14(2).
[94] Ebrahimi, M., Butscher, A., Cheong, H., Iorio, F., Design optimization of dynamic flexible multibody systems using the discrete adjoint variable method, *Computers & Structures*, 2019, 213, 82–99.
[95] Kirk, D.E., *Optimal control theory: an introduction*, Courier Corporation, 2004.
[96] Lauß, T., Oberpeilsteiner, S., Steiner, W., Nachbagauer, K., The discrete adjoint method for parameter identification in multibody system dynamics, *Multibody system dynamics*, 2018, 42(4), 397–410.
[97] Nejat, A.A., Moghadasi, A., Held, A., Adjoint sensitivity analysis of flexible multibody systems in differential-algebraic form, *Computers & Structures*, 2020, 228, 106148.
[98] Angeli, A., Desmet, W., Naets, F., Deep learning for model order reduction of multibody systems to minimal coordinates, *Computer Methods in Applied Mechanics and Engineering*, 2021, 373, 113517.
[99] Kubat, M., Kubat, *An introduction to machine learning*, vol. 2, Springer, 2017.
[100] Choi, H.S., An, J., Han, S., Kim, J.G., Jung, J.Y., Choi, J., Orzechowski, G., Mikkola, A., Choi, J.H., Data-driven simulation for general-purpose multibody dynamics using deep neural networks, *Multibody System Dynamics*, 2021, 51(4), 419–454.
[101] Ye, Y., Huang, P., Sun, Y., Shi, D., Mbsnet: A deep learning model for multibody dynamics simulation and its application to a vehicle-track system, *Mechanical Systems and Signal Processing*, 2021, 157, 107716.
[102] Lewis, F.L., Vrabie, D., Syrmos, V.L., *Optimal control*, John Wiley & Sons, 2012.
[103] Kurinov, I., Orzechowski, G., Hämäläinen, P., Mikkola, A., Automated excavator based on reinforcement learning and multibody system dynamics, *IEEE Access*, 2020, 8, 213998–214006.
[104] Manrique Escobar, C.A., Pappalardo, C.M., Guida, D., A parametric study of a deep reinforcement learning control system applied to the swing-up problem of the cart-pole, *Applied Sciences*, 2020, 10(24), 9013.
[105] Momin, G.G., Hatti, R., Dalvi, K., Bargi, F., Devare, R., Design, manufacturing & analysis of hydraulic scissor lift, *International Journal of Engineering Research and General Science*, 2015, 3(2), 733–740.
[106] Ismael, O.Y., Almaged, M., Mahmood, A., et al., Quantitative design analysis of an electric scissor lift, *American Academic Scientific Research Journal for Engineering, Technology, and Sciences*, 2019, 59(1), 128–141.
[107] Hongyu, T., Ziyi, Z., Design and simulation based on pro/e for a hydraulic lift platform in scissors type, *Procedia Engineering*, 2011, 16, 772–781.
[108] Akgün, Y., Gantes, C.J., Sobek, W., Korkmaz, K., Kalochairetis, K., A novel adaptive spatial scissor-hinge structural mechanism for convertible roofs, *Engineering Structures*, 2011, 33(4), 1365–1376.
[109] Mohan, S., Zech, W.C., Characteristics of worker accidents on nysdot construction projects, *Journal of Safety Research*, 2005, 36(4), 353–360.
[110] Liu, T., Sun, J., Simulative calculation and optimal design of scissor lifting mechanism, *2009 Chinese Control and Decision Conference*, IEEE, 2079–2082.
[111] Olenin, G., Design of hydraulic scissors lifting platform, 2016.
[112] Li, B., Wang, S.M., Yuan, R., Xue, X.Z., Zhi, C.J., Dynamic characteristics of planar linear array deployable structure based on scissor-like element with joint clearance using a new mixed contact force model, *Proceedings of the Institution of Mechanical Engineers, Part C: Journal of Mechanical Engineering Science*, 2016, 230(18), 3161–3174.
[113] Ciupan, C., Ciupan, E., Pop, E., Algorithm for designing a hydraulic scissor lifting platform, *MATEC Web of Conferences*, vol. 299, EDP Sciences, 03012.
[114] Khatib, M.I., Shaikh, S., Ullah, M.A., Rehan, M.M., Shoeb, M., Rameez, M.A., Uddin, M.S., Fabrication of hydraulic scissor lift, 2020.
[115] Stawinski, L., Kosucki, A., Morawiec, A., Sikora, M., A new approach for control the velocity of the hydrostatic system for scissor lift with fixed displacement pump, *Archives of Civil and Mechanical Engineering*, 2019, 19(4), 1104–1115.
[116] Islam, M., Yin, C., Jian, S., Rolland, L., Dynamic analysis of scissor lift mechanism through bond graph modeling, 1393–1399.
[117] Jain, A., Unified formulation of dynamics for serial rigid multibody systems, *Journal of Guidance, Control, and Dynamics*, 1991, 14(3), 531–542.
[118] Sherif, K., Nachbagauer, K., Steiner, W., On the rotational equations of motion in rigid body dynamics when using euler parameters, *Nonlinear Dynamics*, 2015, 81(1), 343–352.
[119] Wang, Y.P., Chen, W.Q., Structure analysis and control optimization on high speed lift platform, *Journal of Donghua University: English Edition*, 2012, 29(6), 501–505.
[120] Takesue, N., Komoda, Y., Murayama, H., Fujiwara, K., Fujimoto, H., Scissor lift with real-time self-adjustment ability based on variable gravity compensation mechanism, *Advanced Robotics*, 2016, 30(15), 1014–1026.
[121] Zhang, Y., Li, S., Liao, L., Near-optimal control of nonlinear dynamical systems: A brief survey, *Annual Reviews in Control*, 2019, 47, 71–80.
[122] Iqbal, J., Ullah, M., Khan, S.G., Khelifa, B., Cˇ ukovic´ S., Nonlinear control systems-a brief overview of historical and recent advances, *Nonlinear Engineering*, 2017, 6(4), 301–312.
[123] Nersesov, S., Haddad, W., On the stability and control of nonlinear dynamical systems via vector lyapunov functions, *IEEE Transactions on Automatic Control*, 2006, 51(2), 203–215.
[124] Koshkouei, A.J., Burnham, K.J., Zinober, A.S., Dynamic sliding mode control design, *IEE Proceedings-Control Theory and Applications*, 2005, 152(4), 392–396.
[125] Wu, J., Wang, J., Wang, L., Li, T., Dynamics and control of a planar 3-dof parallel manipulator with actuation redundancy, *Mechanism and Machine Theory*, 2009, 44(4), 835–849.
[126] Tang, K., Huang, S., Tan, K., Lee, T., Combined pid and adaptive nonlinear control for servo mechanical systems, *Mechatronics*, 2004, 14(6), 701–714.
[127] Resende, C.Z., Carelli, R., Sarcinelli-Filho, M., A nonlinear trajectory tracking controller for mobile robots with velocity limitation via fuzzy gains, *Control Engineering Practice*, 2013, 21(10), 1302–1309.
[128] Primbs, J.A., Nevistic V., Doyle, J.C., Nonlinear optimal control: A control lyapunov function and receding horizon perspective, *Asian Journal of Control*, 1999, 1(1), 14–24.
[129] Khansari-Zadeh, S.M., Billard, A., Learning control lyapunov function to ensure stability of dynamical system-based robot reaching motions, *Robotics and Autonomous Systems*, 2014, 62(6), 752–765.
[130] Toulabi, M., Dobakhshari, A.S., Ranjbar, A.M., An adaptive feedback linearization approach to inertial frequency response of wind turbines, *IEEE Transactions on Sustainable Energy*, 2016, 8(3), 916–926.
[131] Abdul-Adheem, W.R., Ibraheem, I.K., Humaidi, A.J., Azar, A.T., Model-free active input–output feedback linearization of a single-link flexible joint manipulator: an improved active disturbance rejection control approach, *Measurement and Control*, 2021, 54(5-6), 856–871.
[132] Thivagar, M.L., Hamad, A.A., Topological geometry analysis for complex dynamic systems based on adaptive control method, *Periodicals of Engineering and Natural Sciences*, 2019, 7(3), 1345–1353.
[133] Nicol, C., Macnab, C., Ramirez-Serrano, A., Robust adaptive control of a quadrotor helicopter, *Mechatronics*, 2011, 21(6), 927–938.
[134] Ashrafiuon, H., Erwin, R.S., Sliding mode control of underactuated multibody systems and its application to shape change control, *International Journal of Control*, 2008, 81(12), 1849–1858.
[135] Strano, S., Terzo, M., A multi-purpose seismic test rig control via a sliding mode approach, *Structural Control and Health Monitoring*, 2014, 21(8), 1193–1207.
[136] Kwan, C., Lewis, F.L., Robust backstepping control of nonlinear systems using neural networks, *IEEE Transactions on Systems, Man, and Cybernetics-Part A: Systems and Humans*, 2000, 30(6), 753–766.
[137] Yagiz, N., Hacioglu, Y., Backstepping control of a vehicle with active suspensions, *Control Engineering Practice*, 2008, 16(12), 1457–1467.
[138] Çimen, T., State-dependent riccati equation (sdre) control: a survey, *IFAC Proceedings Volumes*, 2008, 41(2), 3761–3775.
[139] Strano, S., Terzo, M., A sdre-based tracking control for a hydraulic actuation system, *Mechanical Systems and Signal Processing*, 2015, 60, 715–726.
[140] Hendricks, E., Jannerup, O., Sørensen, P.H., *Linear systems control: deterministic and stochastic methods*, Springer, 2008.
[141] Zhang, W., Zhang, C., Zhao, J., Du, C., A study on the static stability of scissor lift, *The Open Mechanical Engineering Journal*, 2015, 9(1).
[142] Manrique-Escobar, C.A., Pappalardo, C.M., Guida, D., A multibody system approach for the systematic development of a closed-chain kinematic model for two-wheeled vehicles, *Machines*, 2021, 9(11), 245.
[143] Rivera, Z.B., De Simone, M.C., Guida, D., Unmanned ground vehicle modelling in gazebo/ros-based environments, *Machines*, 2019, 7(2), 42.
[144] Pappalardo, C.M., De Simone, M.C., Guida, D., Multibody modeling and nonlinear control of the pantograph/catenary system, *Archive of Applied Mechanics*, 2019, 89(8), 1589–1626.

[145] De, S., Guida, D., Control design for an under-actuated uav model, *FME Transactions*, 2018, 46(4), 443–452.
[146] Pappalardo, C.M., Lettieri, A., Guida, D., Identification of a dynamical model of the latching mechanism of an aircraft hatch door using the numerical algorithms for subspace state-space system identification., *IAENG International Journal of Applied Mathematics*, 2021, 51(2).
[147] De Simone, M.C., Guida, D., Identification and control of a unmanned ground vehicle by using arduino, *UPB Sci. Bull. Ser. D*, 2018, 80, 141–154.
[148] Mariti, L., Belfiore, N.P., Pennestrì, E., Valentini, P.P., Comparison of solution strategies for multibody dynamics equations, *International Journal for Numerical Methods in Engineering*, 2011, 88(7), 637–656.
[149] Park, K., Chiou, J., Stabilization of computational procedures for constrained dynamical systems, *Journal of Guidance, Control, and Dynamics*, 1988, 11(4), 365–370.
[150] Wang, X., Haug, E., Pan, W., Implicit numerical integration for design sensitivity analysis of rigid multibody systems, *Mechanics based design of structures and machines*, 2005, 33(1), 1–30.
[151] Negrut, D., Haug, E.J., German, H.C., An implicit runge–kutta method for integration of differential algebraic equations of multibody dynamics, *Multibody system dynamics*, 2003, 9(2), 121–142.
[152] Shabana, A.A., Hussein, B.A., A two-loop sparse matrix numerical integration procedure for the solution of differential/algebraic equations: Application to multibody systems, *Journal of Sound and Vibration*, 2009, 327(3-5), 557–563.
[153] Hussein, B.A., Shabana, A.A., Sparse matrix implicit numerical integration of the stiff differential/algebraic equations: implementation, *Nonlinear Dynamics*, 2011, 65(4), 369–382.
[154] Eich-Soellner, E., Führer, C., *Numerical methods in multibody dynamics*, vol. 45, Springer, 1998.
[155] Flores, P., Machado, M., Seabra, E., Tavares da Silva, M., A parametric study on the baumgarte stabilization method for forward dynamics of constrained multibody systems, *Journal of computational and nonlinear dynamics*, 2011, 6(1).
[156] Pennestrı, E., Valentini, P., Coordinate reduction strategies in multibody dynamics: A review, *Proceedings of the Conference on Multibody System Dynamics*.
[157] Marques, F., Souto, A.P., Flores, P., On the constraints violation in forward dynamics of multibody systems, *Multibody System Dynamics*, 2017, 39(4), 385–419.
[158] Shampine, L.F., Reichelt, M.W., The matlab ode suite, *SIAM journal on scientific computing*, 1997, 18(1), 1–22.
[159] Wehage, R.A., Haug, E.J., Generalized coordinate partitioning for dimension reduction in analysis of constrained dynamic systems, 1982.
[160] Wehage, K.T., Wehage, R.A., Ravani, B., Generalized coordinate partitioning for complex mechanisms based on kinematic substructuring, *Mechanism and Machine Theory*, 2015, 92, 464–483.

ORCID iD

Carmine Maria Pappalardo https://orcid.org/0000-0003-3763-7104
Rosario La Regina https://orcid.org/0000-0003-4934-5678
Domenico Guida https://orcid.org/0000-0002-2870-9199

© 2022 Shahid Chamran University of Ahvaz, Ahvaz, Iran. This article is an open access article distributed under the terms and conditions of the Creative Commons Attribution-NonCommercial 4.0 International (CC BY-NC 4.0 license) (http://creativecommons.org/licenses/by-nc/4.0/)

How to cite this article: Carmine Maria Pappalardo, Rosario La Regina, Domenico Guida. Multibody Modeling and Nonlinear Control of a Pantograph Scissor Lift Mechanism, J. Appl. Comput. Mech., 9(1), 2023, 129-167. https://doi.org/10.22055/jacm.2022.40537.3605

Publisher's Note: Shahid Chamran University of Ahvaz remains neutral with regard to jurisdictional claims in published maps and institutional affiliations.